SENSITIVITY STUDIES OF FILTER FUNCTIONS IN COMPUTERIZED TOMOGRAPHY

A Thesis Submitted
In Partial Fulfilment of the Requirements
for the Degree of

MASTER OF TECHNOLOGY

by
PANKAJ ARORA

to the

NUCLEAR ENGINEERING AND TECHNOLOGY PROGRAMME

INDIAN INSTITUTE OF TECHNOLOGY, KANPUR

APRIL, 1987

TH
621.3815324
A867S

-2 DEC 1987
CENTRAL LIBRARY
I. I. T. Kanpur.
Acc. No. A 98979

NETP-1987-M-PRO-SEN

DEDICATED TO

MY

PARENTS

CERTIFICATE

This is to certify that this work on "SENSITIVITY STUDIES OF FILTER FUNCTIONS IN COMPUTERIZED TOMOGRAPHY" by Mr. Pankaj Arora has been carried out under our supervision and has not been submitted elsewhere for the award of a degree.

(P. MUNSHI)
Lecturer
Nuclear Engineering and
Technology Programme
I.I.T. Kanpur

(R.K.S. RATHORE)
Assistant Professor
Mathematics Department
I.I.T. Kanpur

April, 1987.

ACKNOWLEDGEMENTS

I express my deep sense of gratitude to Mr. Prabhat Munshi and Dr. R.K.S. Rathore for suggesting and supervising the work. I am deeply indebted to them for the building up my interest in this fascinating field of CAT, their inspiring guidance, meticulous attention, and for their untiring devotion throughout the tenure of this work.

I am grateful to Professor K. SRI RAM, Professor A. SENGUPTA, Dr. M.S. KALRA, Dr. I.D. DHARIYAL for their valuable advices and suggestions.

I am also thankful to all my friends, Ashwin, Partha Ashim, and particularly to . Manoj K. Jain for helping me in the last stages of my thesis. I wish to thank all the members of our 'SCORPIO GANG' for the fruitful (often unending) discussions (disputes?).

Finally, many many thanks are for my parents, Baldev, Taruna, Mickey and Ginni for their love and encouragement during my stay away from home, that kept me going.

April, 1987. -PANKAJ ARORA

CONTENTS

		Page
	LIST OF TABLES	v)
	LIST OF FIGURES	vi)
	ABSTRACT	xii)
CHAPTER 1	INTRODUCTION	1
CHAPTER 2	PRELIMINARIES	3
	2.1 Data Collection	3
	2.2 Image Reconstruction by Convolution and Backprojection	6
	2.3 Image Display	14
CHAPTER 3	RESULTS	18
	3.1 Results with Existing Filters	18
	3.2 Testing of the Higher Order Filters	20
CHAPTER 4	DISCUSSION AND SUGGESTIONS	71
APPENDICES	A Simulated Data Used For Reconstruction	
	B Results with Various Filters and their Corresponding Higher Order Filters	
	Results with Lewitt's Filter for Different Epsilon Values	
	C Air-water Flow Data	
	D Higher Order Filters	
REFERENCES		

LIST OF TABLES

TABLE	TITLE
1	Data used for the reconstruction algorithm
2	Data used for the reconstruction algorithm
3	Results with Lewitt's I, II, and III order filters ($\varepsilon = 0.0$)
4	Results with Lewitt's I, II, and III order filters ($\varepsilon = 1.0$)
5	Results with Sinc I, II, and III order filters
6	Results with Sincsquare I, II, and III order filters
7	Results with Lewitt's filter for different epsilon values.

LIST OF FIGURES

FIGURE	TITLE	PAGE
2.1	Parallel beam geometry	5
2.2	Direct inverse geometry	12
2.3	Hidden line 3-dimensional representation of reconstructed function $\mu(r) = \begin{cases} 1 & 0 \leq r < 0.55 \\ 0 & 0.55 \leq r \leq 1.0 \end{cases}$ with Lewitt's filter	15
2.4	Representation of reconstructed function $\mu(r) = \begin{cases} 1 & 0 \leq r < 0.2 \\ 0 & 0.2 \leq r < 0.4 \\ 1 & 0.4 \leq r \leq 1.0 \end{cases}$ with a grid of 1681 cells	16
2.5	Representation of reconstructed function $\mu(r) = \begin{cases} 0 & 0 \leq r < 0.55 \\ 1 & 0.55 \leq r \leq 1.0 \end{cases}$ with a grid of 441 cells.	17
3.1	Results with simulated data	21
3.2(a)	Results with simulated data for Lewitt's filter with different epsilon values	22
3.2(b)	Results with simulated data for Lewitt's filter with different epsilon values	23
3.3	Results with simulated data for $\mu(r) = \delta(0)$ for Lewitt's filter with different epsilon values	24

FIGURE	TITLE	PAGE
3.4	Results with simulated data	25
3.5	Reconstructed density profile (radial) for air-water flow data	26
3.6	Results for various data sets (cross-sectionally averaged density)	27
3.7	The spatial domain representation of the convolving function with Lewitt's filter ($\varepsilon = 0.0$)	28
3.8	The spatial domain representation of the convolving function with Lewitt's filter ($\varepsilon = 1.0$)	29
3.9	The spatial domain representation of the convolving function with Sinc filter	30
3.10	The spatial domain representation of the convolving function with Sincsquare filter	31
3.11	Results with simulated data for $\mu(r) = 1.0$ for Lewitt's I, II and III order filters ($\varepsilon = 0.0$)	32
3.12	Results with simulated data for $\mu(r) = 1.0$ for Sinc I, II and III order filters	33
3.13	Results with simulated data for $\mu(r) = 1.0$ for Sincsquare I, II and III order filters	34
3.14	Results with simulated data for $\mu(r) = \delta(0)$ for Lewitt's I, II and III order filters with $\varepsilon = 1.0$	35

FIGURE	TITLE	PAGE
3.15	Results with simulated data for $\mu(r) = \delta(0)$ for Sinc I, II and III order filters	36
3.16	Results with simulated data for $\mu(r) = \delta(0)$ for Sincsquare I, II and III order filters	37
3.17	Results with simulated data for Lewitt's I, II and III order filters with $\varepsilon = 0.0$	38
3.18	Results with simulated data for Lewitt's I, II and III order filters with $\varepsilon = 0.0$	39
3.19	Results with simulated data for Sinc I, II and III order filters	40
3.20	Results with simulated data for Sinc I, II and III order filters	41
3.21	Results with simulated data for Sincsquare I, II and III order filters	42
3.22	Results with simulated data for Sincsquare I, II and III order filters	43
3.23	Results with simulated data for $\mu(r) = r$ for Lewitt's I, II and III order filters with $\varepsilon = 0.0$	44
3.24	Results with simulated data for $\mu(r) = r$ for Sinc I, II and III order filters	45
3.25	Results with simulated data for $\mu(r) = r$ for Sincsquare I, II and III order filters	46

FIGURE	TITLE	PAGE
3.26	Results with simulated data for $\mu(r)$ = exp (+r) for Lewitt's I, II and III order filters with $\varepsilon = 0.0$	47
3.27	Results with simulated data for $\mu(r)$ = exp(+r) for Sinc I, II and III order filters	48
3.28	Results with simulated data for $\mu(r)$ = exp(+r) for Sincsquare I, II and III order filters	49
3.29	Results with simulated data for $\mu(r)$ = exp(-r) for (a) Lewitt's ($\varepsilon = 0.0$), (b) Sinc, (c) Sincsquare I, II and III order filters	50
3.30	Results with simulated data for $\mu(r) = 1-r$ for (a) Lewitt's ($\varepsilon=0.0$), (b) Sinc, (c) Sincsquare I, II and III order filters	51
3.31	Results with simulated data for $\mu(r) = r^2$ for (a) Lewitt's ($\varepsilon = 0.0$), (b) Sinc, (c) Sincsquare I, II and III order filters	52
3.32	Results with simulated data for $\mu(r) = 1-r^2$ for (a) Lewitt's ($\varepsilon = 0.0$), (b) Sinc, (c) Sincsquare I, II and III order filters	53
3.33	Results with simulated data for $\mu(r) = 1.0$ for Lewitt's I, II and III order filters with $\varepsilon = 1.0$	54

FIGURE		TITLE	PAGE
	3.34	Results with simulated data for $\mu(r) = r$ for Lewitt's I, II and III order filters with $\varepsilon = 1.0$	55
	3.35	Results with simulated data for $\mu(r) = r^2$ for Lewitt's I, II and III order filters with $\varepsilon = 1.0$	56
	3.36	Results with simulated data for $\mu(r) = 1-r$ for Lewitt's I, II and III order filters with $\varepsilon = 1.0$	57
	3.37	Results with simulated data for $\mu(r) = 1-r^2$ for Lewitt's I, II and III order filters with $\varepsilon = 1.0$	58
	3.38	Results with simulated data for Lewitt's I, II and III order filters with $\varepsilon = 1.0$	59
	3.39	Results with simulated data for Lewitt's I, II and III order filters with $\varepsilon = 1.0$	60
	3.40	Results with simulated data for (r) = exp(+r) for Lewitt's I, II and III order filters with = 1.0	61
	3.41	Results with simulated data for $\mu(r)$ = exp(-r) for Lewitt's I, II and III order filters with $\varepsilon = 1.0$	62
	3.42	Results with simulated data for $\mu(r) = \delta(0)$ for Lewitt's I, II and III order filters with $\varepsilon = 1.0$	63

FIGURE	TITLE	PAGE
3.43	The hidden line 3-dimensional representation of reconstructed function $\mu(r) = 1.0$ with Lewitt's filter ($\varepsilon=0.0$)	64
3.44	The hidden line 3-dimensional representation of reconstructed function $\mu(r) = \delta(0)$ with Lewitt's filter ($\varepsilon=0.0$)	65
3.45	The hidden line 3-dimensional representation of reconstructed function $\mu(r) = \exp(+r)$ with Lewitt's filter ($\varepsilon=0.0$)	66
3.46	The hidden line 3-dimensional representation of reconstructed function $\mu(r) = \exp(-r)$ with Lewitt's filter ($\varepsilon=0.0$)	67
3.47	The hidden line 3-dimensional representation of reconstructed function $\mu(r) = r$ with Lewitt's filter ($\varepsilon= 0.0$)	68
3.48	The hidden line 3-dimensional representation of reconstructed function $\mu(r) = \begin{cases} 0 & 0 \leq r < 0.5 \\ 1 & 0.55 < r \leq 1.0 \end{cases}$	69

ABSTRACT

This work deals in evaluating the performance of various filters reported in literature and their corresponding higher order filters developed at IIT-Kanpur. Initially, a sensitivity analysis had been carried out for various filter parameters using fan-beam convolution-backprojection algorithm for various simulated bubbly and annular flow data. The projection data for air-water bubbly flow is also processed to obtain the density distribution. Finally, the parallel-beam convolution-backprojection algorithm has been tested for various simulated bubbly and annular flow data. A comparative study of the relative performance of the linear filters (and their corresponding higher order filters), has been carried out with the simulated data. The results indicate an increase in both accuracy and smoothness if the higher order filters are used.

CHAPTER 1

INTRODUCTION

The algorithms used in present day CAT scanners are generally based on the convolution-backprojection scheme suggested by Ramachandran and Lakshminarayanan [1]. This algorithm requires measured data in the form of line integrals of the spatial distribution of the physical property of interest Convolution-backprojection is so named because of the two basic steps involved in this algorithm: (a) measured data (called projection data), which has been collected by the scanner, is convolved with a filter function, and (b) the filtered data is backprojected to form the image. The choice of these filters depends upon the user. A class of linear filters (in frequency domain) for the parallel beam geometry has been suggested by Lewitt [2] . The accuracy of reconstruction depends on the judicious choice of filter appropriate for the function being investigated. This selection process (of appropriate filter) puts a severe limitation on the methodology which claims independence of a priori information regarding the nature of function being investigated.

The present study is an effort towards evaluating the performance of some existing filters, and their corresponding higher order filters developed at IIT Kanpur. The

algorithm was initially tested with simulated data representing bubbly and annular flows. The air-water flow data [3,4,5] was processed with linear filter to get density maps for the study of Ref. [3]. Reconstruction of the simulated data shows encouraging results for the higher order filters.

CHAPTER 2

PRELIMINARIES

In this chapter, we discuss the computational and mathematical procedures underlying the data collection, image reconstruction, and image display in the practice of computerized tomography.

2.1 DATA COLLECTION:

In computerized tomography the number of photons transmitted through an object is counted by an array of detectors. This array is rotated by a fixed angular increment between each set of measurements. From these measurements the total attenuation along each measurement path is derived, which can be written as:

$$N = N_o \exp\left[- \int_c \mu(r,\emptyset)\, ds \right] \qquad (2.1)$$

where,

N = detector reading (counts/second)

N_o = source strength (counts/second)

$\bar{s}$ = path of radiation (ray)

c = chord along which s is integrated

μ = absorption coefficient

$r,\emptyset$ = cylindrical co-ordinates.

From (2.1)

$$\int_{c} \mu(r,\phi)\, ds = \ln (N_o/N) = P(s,\theta) \qquad (2.2)$$

where,

$P(s,\theta)$ is called projection data and it is the line integral of function along the line specified by s and θ, see Fig. 2.1. In practical application of reconstruction from projections, the measured data corresponds to estimates of $P(s, \theta)$ for numerous discrete values of s and θ. Further, for the simplification of the reconstruction algorithm the projections are sampled uniformly in both s and θ. Therefore, projections are measured at N angles $\Delta\theta$ apart, with M equispaced rays Δs apart for each of the angle of view.

We choose,

$$\Delta\theta = \frac{\pi}{N}$$

$$\Delta s = \frac{1}{M}$$

In order to ensure that the collection of rays specified by

$$\{(m\Delta s,\ n\Delta\theta) \ : -M \leq m \leq +M,\ 1 \leq n \leq N\}$$

cover the whole object from a complete range of directions.

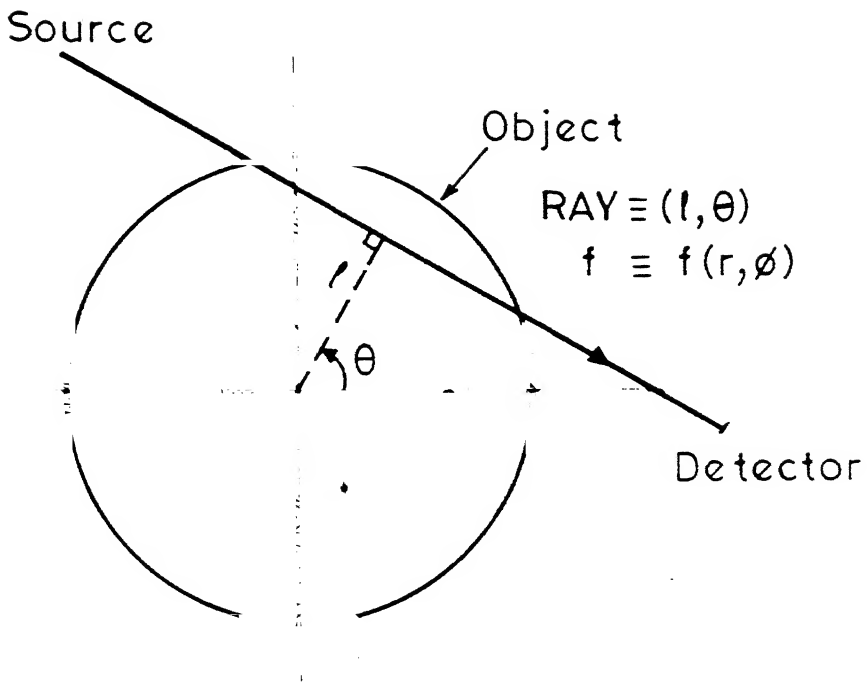

FIG. 2.1 PARALLEL-BEAM GEOMETRY.

We denote by $\hat{P}(R, \theta_n)$ the 1-D Fourier transform with respect to s of projection at angle θ_n, where, θ_n denotes the $n\Delta\theta$

$$\hat{P}(R, \theta_n) = \int_{-\infty}^{+\infty} P(s, \theta_n)\, e^{i2\pi Rs}\, ds \qquad (2.3)$$

2.2 IMAGE RECONSTRUCTION BY CONVOLUTION AND BACK-PROJECTION:

The starting point for the derivation of this method is the projection theorem for Fourier transform or sometimes called projection-slice theorem [6], which gives the result

$$\hat{P}(R, \theta) = \hat{\mu}(R\,\mathrm{Cos}\theta, R\,\mathrm{Sin}\theta) \qquad (2.4)$$

The physical interpretation of this result is as follows: Consider θ a fixed angle, then the theorem says that as R varies, the value of $\hat{P}(R, \theta_n)$ is the same as the value of $\hat{\mu}$ at R and angle θ in Fourier space.

Taking the inverse Fourier transform of (2.4)

$$\mu(x,y) = \int_{0}^{\pi} \int_{-\infty}^{\infty} \hat{P}(R,\theta)\; e^{i2\pi R(x\,\mathrm{Cos}\theta + y\,\mathrm{Sin}\theta)} |R|\, dR\, d\theta \qquad (2.5)$$

For the computation of the integral (involved in eqn.(2.5) , we need to make some approximation because the limits on R varies from $-\infty$ to $+\infty$ which introduces

divergence. Therefore, an appropriate cut-off of R is used to evaluate the integral, which otherwise diverges. So, a function W(R) is introduced in eqn.(2.5) called as window function or filter. Window function is chosen in such a way that

$$W(R) = \begin{cases} \text{Some function of } R, & |R| \leq R_c \\ 0, & |R| > R_c \end{cases}$$

where,

R_c = 1/2 Δs, Δs is distance between rays.

Window function of the above form causes abrupt truncation of the function in the Fourier domain, which leads to oscillations in the spatial domain. The amplitude of these oscillations may be reduced greatly by choosing a different window function whose value tapers less abruptly to zero at the cutoff frequency R_c.

To reduce the amplitude of oscillations in spatial domain, which arises because of abrupt truncation in Fourier domain we developed new family of filters here at IIT Kanpur.

The base filters used in this thesis are:

Lewitt's filter $W(R) = \begin{cases} 1 - \varepsilon|R|/R_c, & |R| \leq R_c \\ 0, & |R| > R_c \end{cases}$

$$\text{Sinc filter}, W(R) = \begin{cases} \dfrac{\text{Sin}(\pi R/R_c)}{\pi R/R_c}, & R \leq R_c \\ 0, & R > R_c \end{cases}$$

$$\text{Sinc square filter}, W(R) = \begin{cases} \left[\dfrac{\text{Sin}(\pi R/R_c)}{(\pi R/R_c)}\right]^2, & R \leq R_c \\ 0, & R > R_c \end{cases}$$

After introducing the window function in eqn.(2.5) we get

$$\mu(x,y) = \int_0^{\pi} \int_{-R_c}^{+R_c} \hat{P}(R,\theta).W(R)\, e^{i2\pi R(x\,\text{Cos}\theta + y\,\text{Sin}\theta)} |R|\, dR\, d\theta \qquad (2.6)$$

Substituting for $\hat{P}(R,\theta)$ from eqn.(2.3) and interchanging the order of integration over s and R we get

$$\mu(x,y) = \int_0^{\pi} \int_{-\infty}^{\infty} P(s,\theta)\, q(x\,\text{Cos}\theta + y\,\text{Sin}\theta - s)\, ds\, d\theta \qquad (2.7)$$

If we assume object to be of unit radius then limits on s will be from -1 to $+1$, so we get

$$\mu(x,y) = \int_0^{\pi} \int_{-1}^{1} P(s,\theta)\, q(x\,\text{Cos}\theta + y\,\text{Sin}\theta - s)\, ds\, d\theta \qquad (2.8)$$

where,

$$q(s) = \int_{-1/2\Delta s}^{+1/2\Delta s} |R|\, W(R)\, e^{i2\pi Rs}\, dR \qquad (2.9)$$

q(s) is called convolving function. To get the corresponding higher order filters [7] of the filter functions stated above we use the relation,

$$q^{[k+1]}(s) = \frac{2^{2k}\, q^{[k]}(s) - \frac{1}{4}\, q^{[k]}(s/2)}{2^{2k} - 1} \qquad (2.10)$$

The equations (2.8) and (2.9) form the basis of the method of convolution-back projection. To see how this name (convolution-backprojection) arises, we break eqn. (2.8) into two equations:

$$\tilde{P}(s',\theta) = \int_{-1}^{+1} P(s,\theta)\, q(s'-s)\, ds \qquad (2.11)$$

$$\mu(x,y) = \int_{0}^{\pi} \tilde{P}(x\,\mathrm{Cos}\theta + y\,\mathrm{Sin}\theta, \theta)\, d\theta \qquad (2.12)$$

The operation represented by (2.11) is convolution and P(s', θ) called convolved projection at angle θ is the result of the convolution over s of the projection at angle θ and the convolving function q(s).

The operation represented by (2.12) is known as backprojection and geometrical representation of this is that the argument of $\tilde{P}$ in eqn. (2.10) are parameters of ray through the point (x,y) at angle θ, so that μ(x,y)

is obtained by the integration of the values of the convolved projections associated with all rays passing through the point (x,y).

For the implementation of eqns.(2.11) and (2.12) we discretise these equations. The simplest way is to use trapezoidal rule and we get,

$$\mu(x,y) \simeq \Delta\theta \sum_{n=1}^{N} \tilde{P}(s', \theta_n) \qquad (2.13)$$

$$\tilde{P}(m'\Delta s, \theta_n) \simeq \Delta s \sum_{m=-M}^{+M} P(m\Delta s, \theta_n)\, q((m'-m)\Delta s) \qquad (2.14)$$

Up till now we were discussing about parallel-beam geometry and this algorithm can also be used for fan-beam geometry. In fan-beam geometry each ray is considered as one of a set of diverging rays (σ,β), where β determines the source position and σ is the angle of divergence of the ray from the source-to-center line and line integral or projection data is denoted by $g(\sigma,\beta)$. We assume that source is always outside the object to be reconstructed so that $g(\sigma,\beta)$ is zero for $|\sigma|$ greater than some acute angle δ.

From Fig. (2.2), we get the following relationships:

$$s = D \sin\sigma \qquad (2.15a)$$

$$\theta = \beta + \sigma \qquad (2.15b)$$

$$r\cos = (\theta - \phi) - s = U \sin(\sigma' - \sigma) \qquad (2.15c)$$

$$U^2 = [r\ \mathrm{Cos}(\beta - \phi)]^2 + [D + r\ \mathrm{Sin}(\beta - \phi)]^2 \qquad (2.15d)$$

$$\sigma' = \tan^{-1}\left[\frac{r\ \mathrm{Cos}(\beta - \phi)}{D + r\ \mathrm{Sin}(\beta - \phi)}\right] \qquad (2.15e)$$

where,

D is the radius of the circle on which source lies

U is the distance between any point (r, ϕ) and the source

σ' is the angle of the diverging ray which passes through the point (r, ϕ).

Writing equivalent of eqn. (2.5) in cylindrical co-ordinates

$$\mu(r,\phi) = \frac{1}{2} \int_0^{2\pi} \int_{-\infty}^{\infty} P(R,\theta)\ \exp[i\ 2\pi R\ r\ \mathrm{Cos}(\theta - \phi)]\ |R|\ dR\ d\theta \qquad (2.16)$$

Incorporating the window function in eqn. (2.16) and substituting $P(R, \theta)$ from eqn. (2.3)

$$\mu(r,\phi) = \frac{1}{2} \int_{-\infty}^{\infty} \int_{-\infty}^{\infty} \int_0^{2\pi} P(s,\theta)\ W(R)\ \exp[i2\pi R\ [r\ \mathrm{Cos}(\theta - \phi) - s]]\ d\theta\ ds\ dR \qquad (2.17)$$

Now changing variables from (s, θ) to (α, β) using transformations (2.15a,b,c,d,e) we obtain:

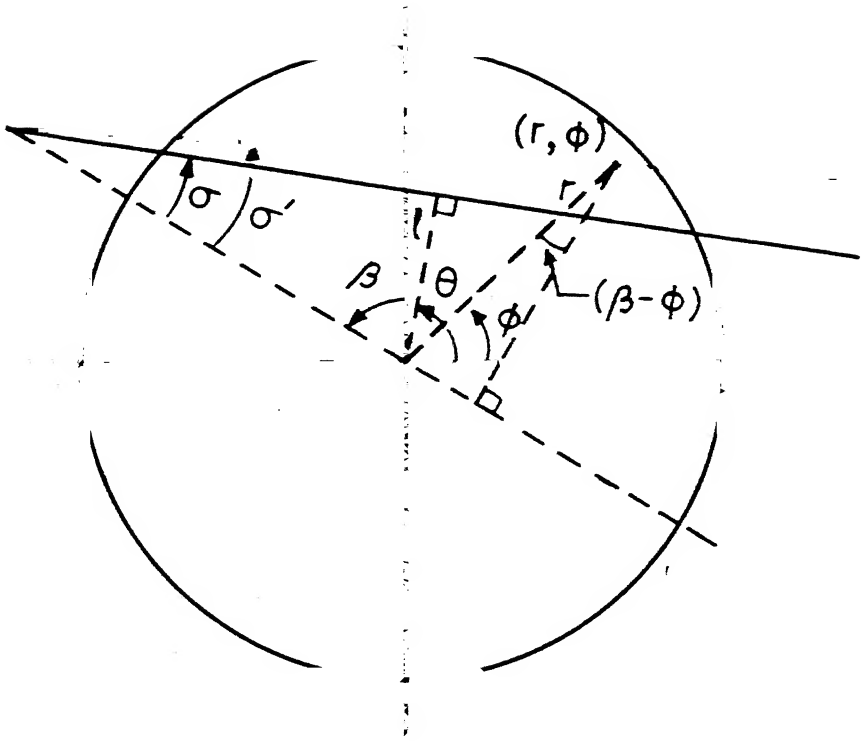

FIG. 2.2 DIRECT INVERSE GEOMETRY.

$$\mu(r,\phi) = \frac{D}{2} \int_{-R_c}^{+R_c} \int_{-\delta}^{+\delta} \int_{o}^{2\pi} g(\sigma,\beta)\, \mathrm{Cos}(\sigma)\, \exp[i2\pi RU\, \mathrm{Sin}(\sigma' - \sigma)\, W(R)\, |R|\, d\beta\, d\sigma\, dR \qquad (2.18)$$

In simple form we can write eqn. (2.18) as:

$$\mu(r,\phi) = \frac{D}{2} \int_{o}^{2\pi} \tilde{g}_c(\sigma',\beta)\, d\beta \qquad (2.19)$$

where,

$$\tilde{g}_c(\sigma',\beta) = \int_{-\delta}^{+\delta} g(\sigma,\beta)\, \mathrm{Cos}(\sigma)\, q(U\, \mathrm{Sin}(\sigma' - \sigma))\, d\sigma \qquad (2.20)$$

and

$$q(s) = \int_{-R_c}^{+R_c} |R| W(R) \exp(i\, 2\pi Rs)\, dR \qquad (2.21)$$

Discretised version of eqns. (2.19) and (2.20) using trapezoidal rule can be written as :

$$\mu(r,\phi) = \frac{D\alpha\Delta\beta}{2} \sum_{n=0}^{N-1} \frac{1}{L^2(\beta_m, r,\phi)}\, \tilde{g}_c(\sigma', m\Delta\beta) \qquad (2.22)$$

where ,

$$\ddot{\tilde{g}}_c(k\alpha, m\Delta\beta) = \sum_{i=-M}^{+M} \mathrm{Cos}(i\alpha)\, g(i\alpha, m\Delta\beta)\, q(\mathrm{Sin}(k-i)\alpha) \qquad (2.23)$$

So, for the implementation of algorithm we use eqns. (2.13) and (2.14) for parallel-beam geometry and eqns. (2.22) and (2.23) for fan-beam geometry.

2.3 IMAGE DISPLAY:

In general image is displayed in the form of a matrix. The elements of the matrix vary from 0 to 99 or from 0 to 33 and are called 'CT numbers'. At the bottom of the picture are indicated the maximum and minimum values of the parameter 'LITF'. 'LITF' is the reconstructed value and is related to point density values or it is the density of the unit cell if we divide the entire output matrix into nxn square grid (n can be 21 or 41). Since we are interested in cross-sectionally averaged density. Thus <LITF> is represented as cross sectional average density, and it is the sum of values of LITF over the entire cross-section of the object divided by the number of unit cells present (See Figs.2.4, 2.5).

We have also represented the reconstructed functions by the hidden line 3-dimensional graph using the graphics facility of DEC 1090 (See Fig. 2.3).

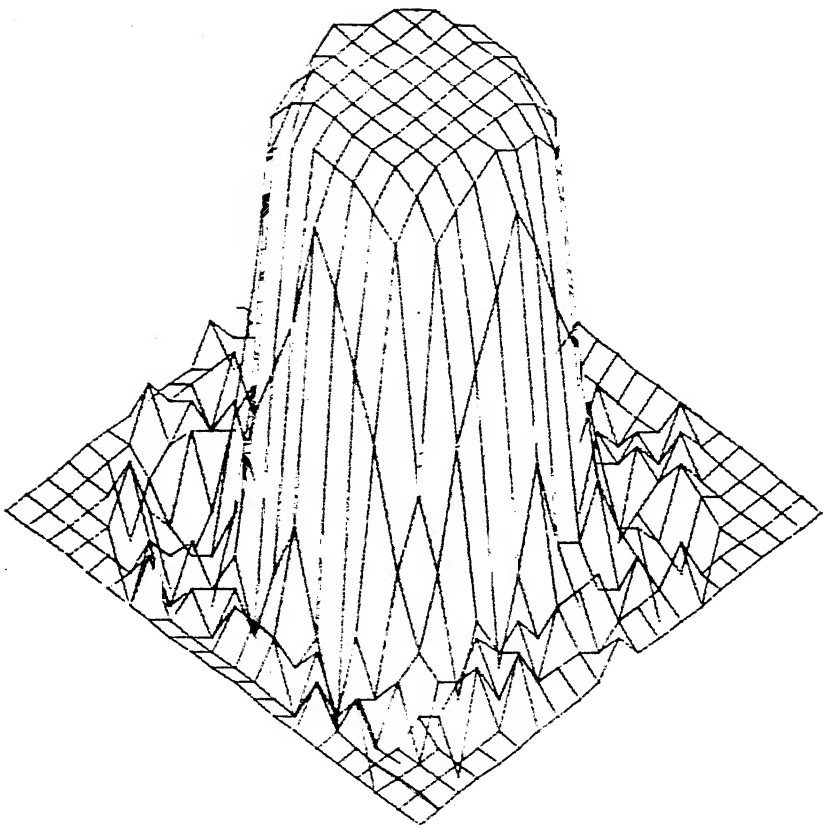

FIG. 2.3 HIDDEN LINE 3-DIMENSIONAL REPRESENTATION OF RECONSTRUCTED FUNCTION $\mu(r) = \begin{cases} 1 & 0 \leqslant r < 0.55 \\ 0 & 0.55 \leqslant r \leqslant 1.0 \end{cases}$ WITH LEWITT'S FILTER

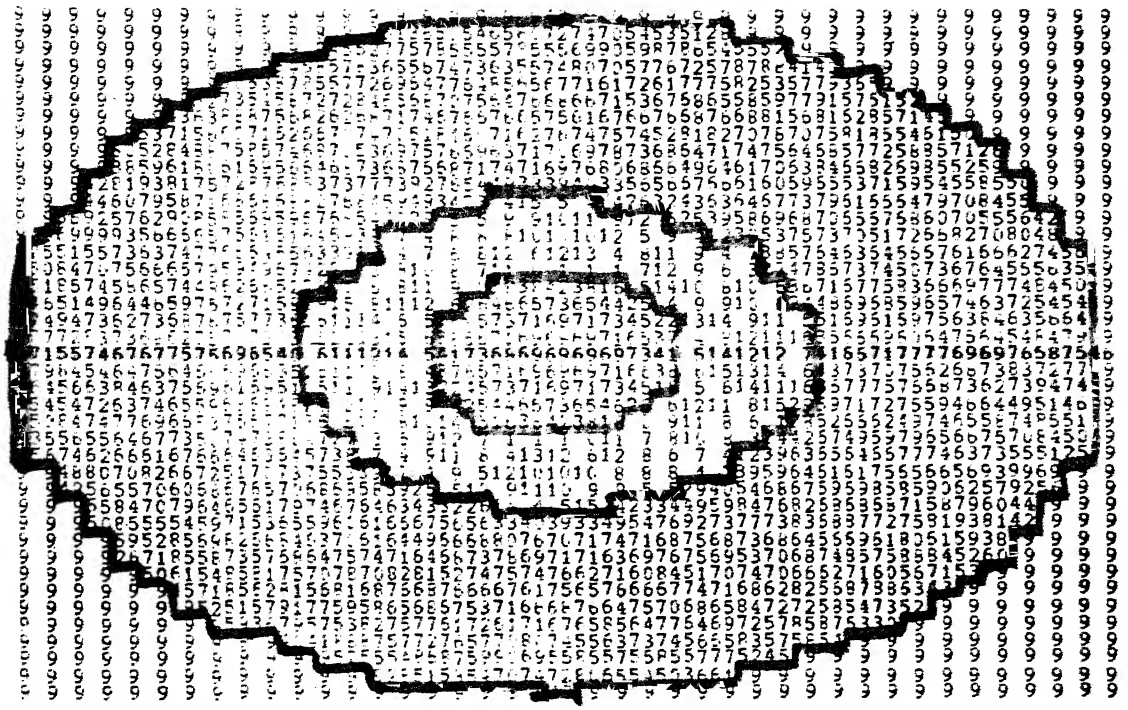

MINIMUM LITF=-0.16493[illegible]E+01 MAXIMUM LITF= 0.15698540E+01

ITF= 0.79586144E+[illegible]

FIG. 2.4 REPRESENTATION OF RECONSTRUCTED FUNCTION $\mu(r) = \begin{bmatrix} 1 & 0 \leqslant r < 0.2 \\ 0 & 0.2 \leqslant r < 0.4 \\ 1 & 0.4 \leqslant r \leqslant 1.0 \end{bmatrix}$ WITH A GRID OF 1681 CELLS.

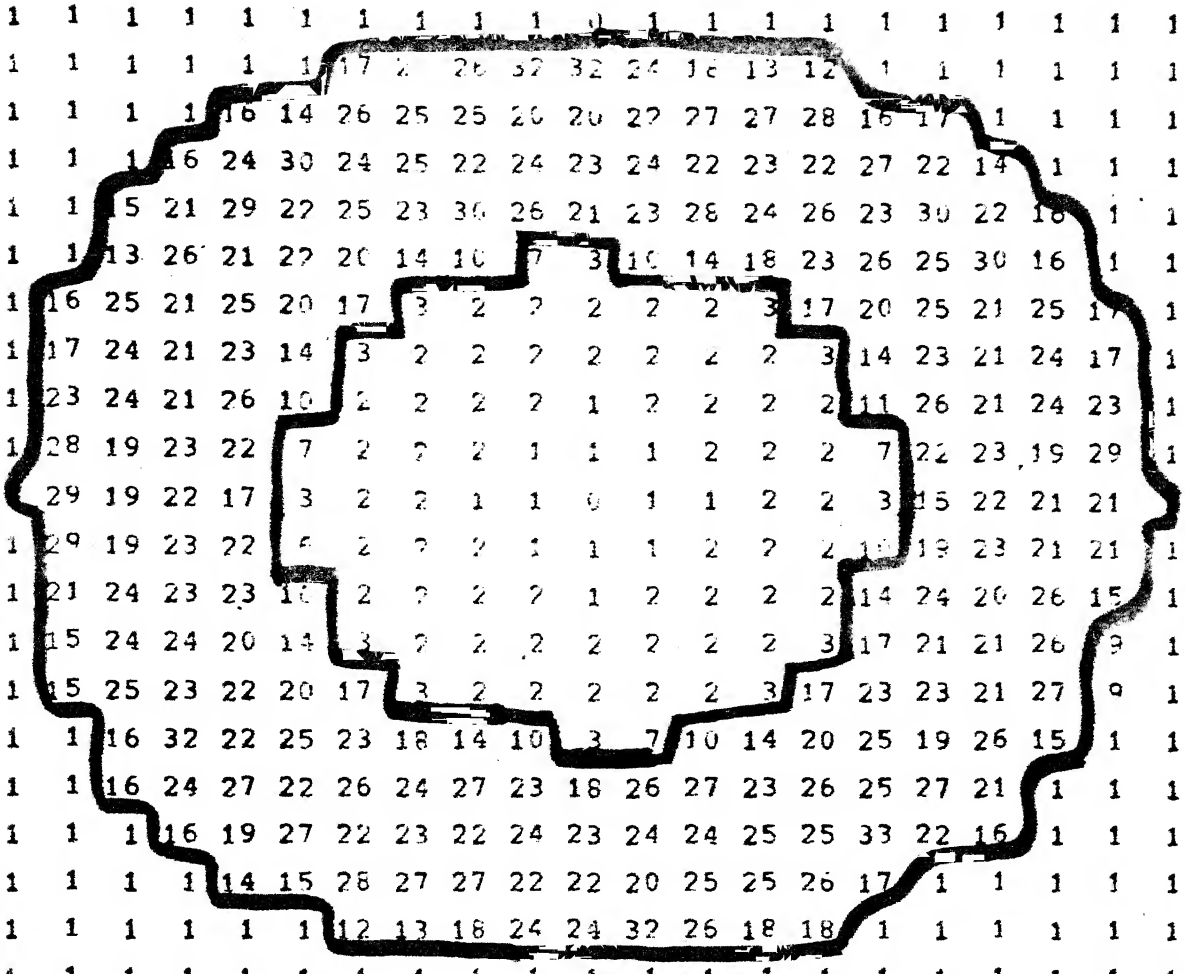

MINIMUM LITF=-0.53304010E-01 MAXIMUM LITF= 0.15371310E+01

LITF= 0.71056507E+00

FIG. 2.5 REPRESENTATION OF RECONSTRUCTED FUNCTION

$$\mu(r) = \begin{bmatrix} 0 & 0 \leq r < 0.55 \\ 1 & 0.55 \leq r \leq 1.0 \end{bmatrix}$$ WITH A GRID OF 441 CELLS

CHAPTER 3

RESULTS

The present study involved the following:

(a) Implementation and testing of the existing algorithms and their application in the point density measurement of air-water flow, and

(b) Implementation of the convolution-backprojection algorithm [1] with higher order filters and its eventual validation against simulated data for various assumed distributions.

3.1 RESULTS WITH EXISTING FILTERS:

The algorithm for fan-beam geometry written in FORTRAN was tested for simulated data sets for different known distributions. Reconstruction of the known distributions was done for different value of epsilon for the filter suggested by Lewitt [2] . The known distributions taken are:

$$\mu(r) = 1.0$$

$$\mu(r) = r$$

$$\mu(r) = 1-r$$

$$\mu(r) = r^2$$

$$\mu(r) = 1-r^2$$

$$\mu(r) = \exp(+r)$$

$$\mu(r) = \exp(-r)$$

$$\mu(r) = \delta(0)$$

$$\mu(r) = \begin{cases} 1.0 & 0.0 \leq r \leq 0.5 \\ 0.0 & 0.5 < r \leq 1.0 \end{cases}$$

$$\mu(r) = \begin{cases} 0.0 & 0.0 \leq r \leq 0.5 \\ 1.0 & 0.5 < r \leq 1.0 \end{cases}$$

$$\mu(r) = \begin{cases} 1.0 & 0.0 \leq r \leq 0.2 \\ 0.0 & 0.2 < r \leq 0.4 \\ 1.0 & 0.4 < r \leq 1.0 \end{cases}$$

The simulated projection data for the above cases is generated by taking object radius to be unity and ray spacing 1.25°. There are 41 rays in one scan and 41 different source positions. The reconstructed density distribution for above cases is shown in Figs. 3.1, 3.2a, 3.2b, 3.3, 3.4. The reconstructed values for all the cases are in good agreement, within $\pm$ 0.03 of the true values. It is seen that as the value of the epsilon goes from 0 to 1 the value of the average of the distribution function decreases by 0.01 to 0.03. This is expected because of the nature of W(R). The results are summarised in Table 5 in Appendix B.

The air-water flow data was processed and calibrated to get the density distribution for various cases of $\langle \rho \rangle$, the cross-sectionally averaged density. Figure 3.5 shows

the results for two extreme cases of epsilon values. In Fig. 3.6, we have compared the $<\rho_{CT}>$, the reconstructed density with $<\rho>$ for various sets (scans); the reconstructed density is within $\pm$ 0.03 g/cm^3 of the actual density values. These results are comparable with the results of two other methods [8, 9].

3.2 TESTING OF HIGHER ORDER FILTERS:

The algorithm for parallel beam geometry was tested for the same known distributions, which were used for fan-beam geometry. While generating the data ray spacing is taken as 0.1 and there are 21 rays in one scan and 21 source positions. The data generated is summarised in Table 1 and Table 2 of Appendix A.

Then, different filters and their corresponding higher order filters were taken and functions were reconstructed. The results are shown in the Fig. 3.11 to Fig. 3.48 for the known distribution functions mentioned in the previous page. It is seen that the reconstructed values are within $\pm$ 0.01 to $\pm$ 0.025 of the actual values for most of the cases.

It is seen in all the cases that higher order filters give more accurate results and degree of smoothness also increases. The results for all the filters and their corresponding higher order filters are summarised in Table 1-4 in Appendix B.

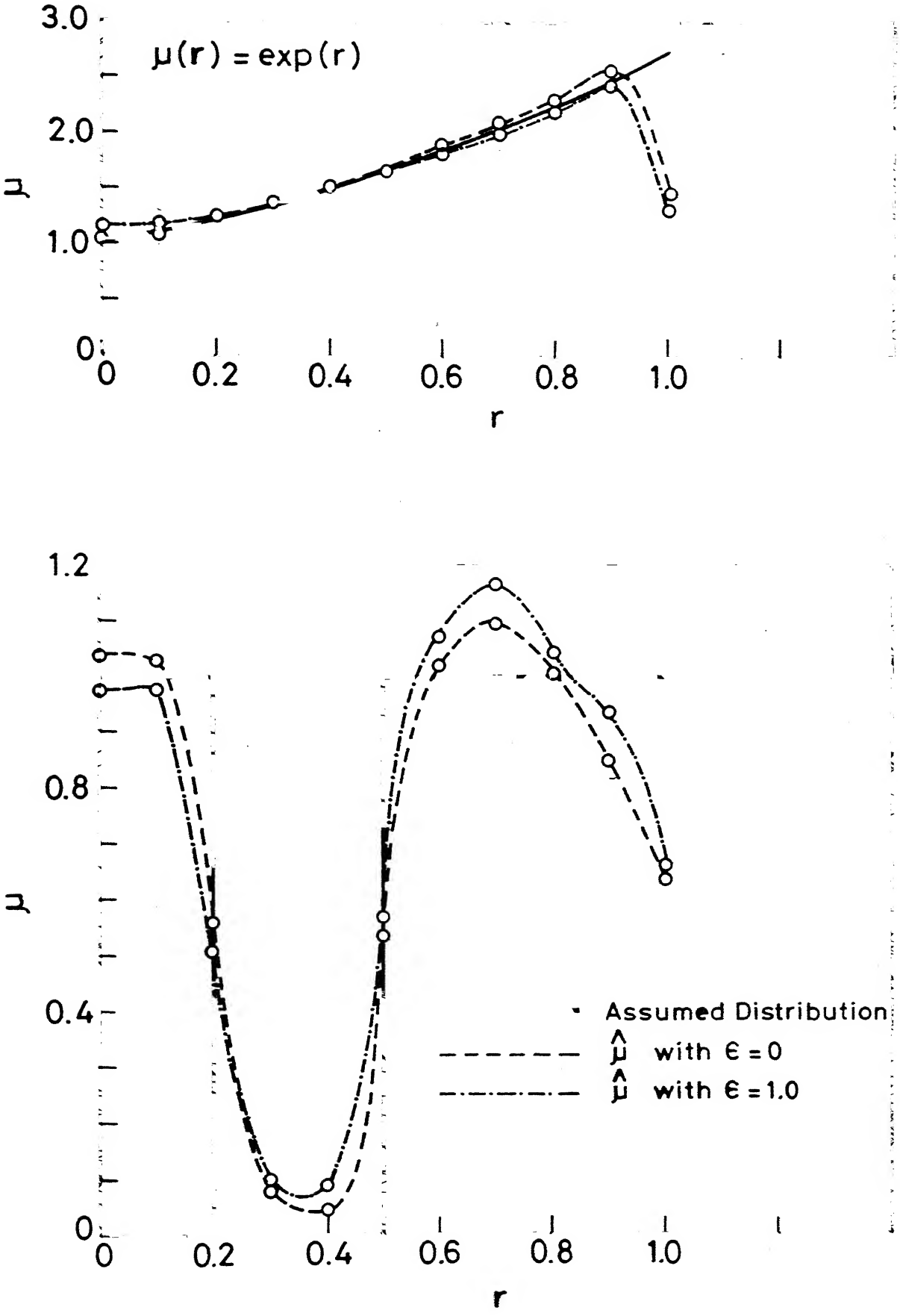

Fig. 3.1 RESULTS WITH SIMULATED DATA.

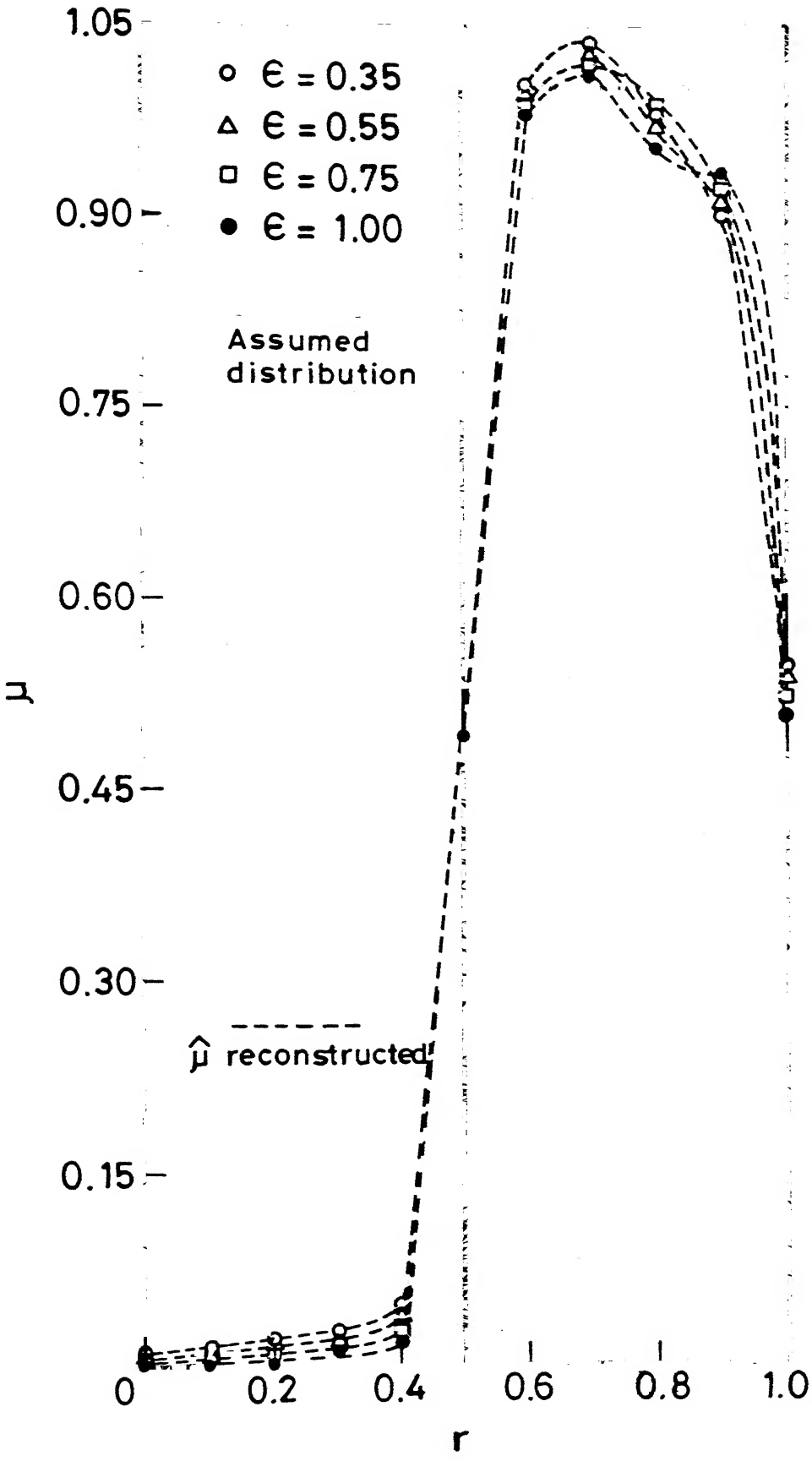

Fig. 3.2 (a) Results with simulated data for Lewitt's filter with different epsilon values.

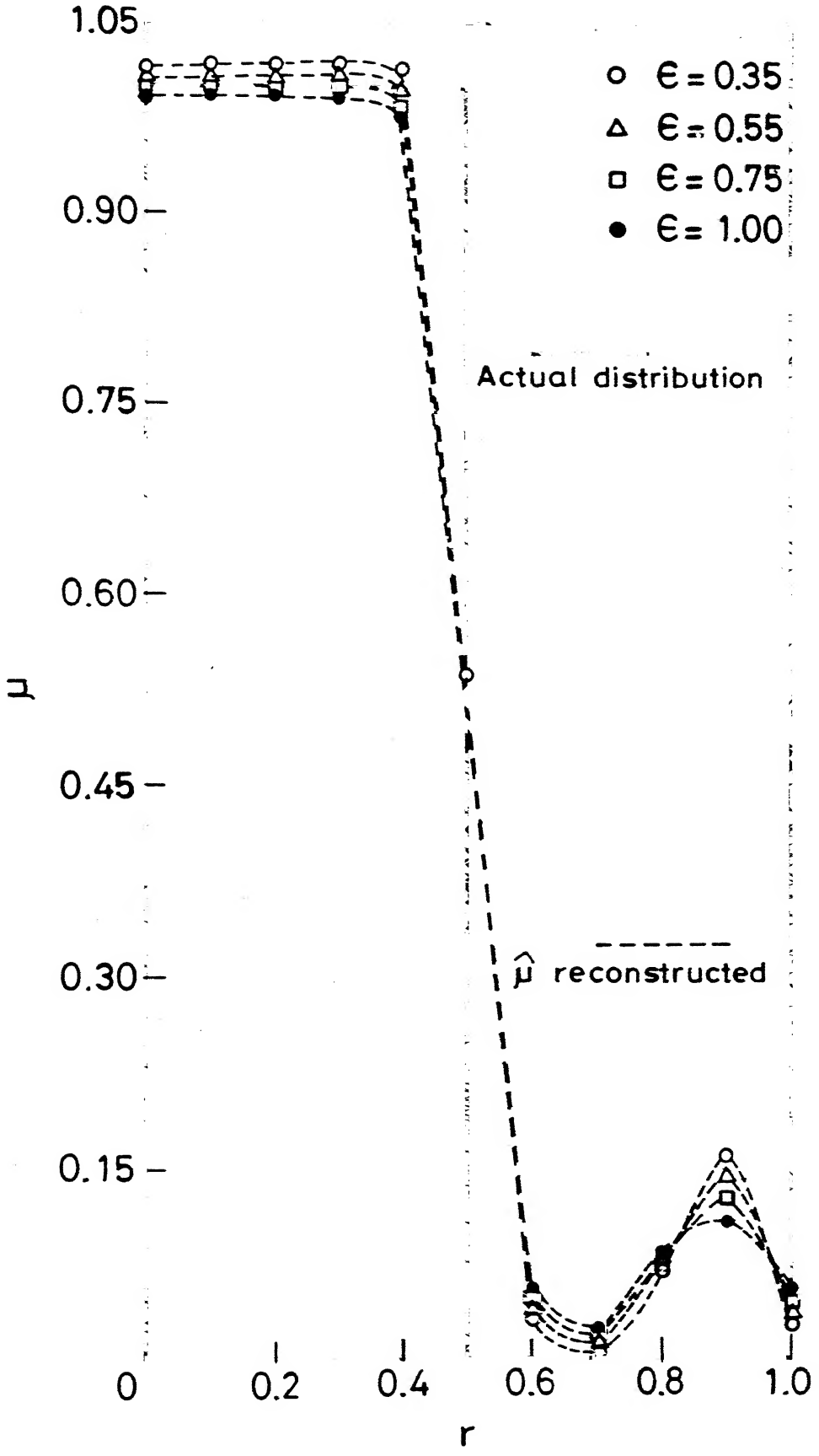

Fig. 3.2(b) Results with simulated data for Lewitt's filter with different epsilon values.

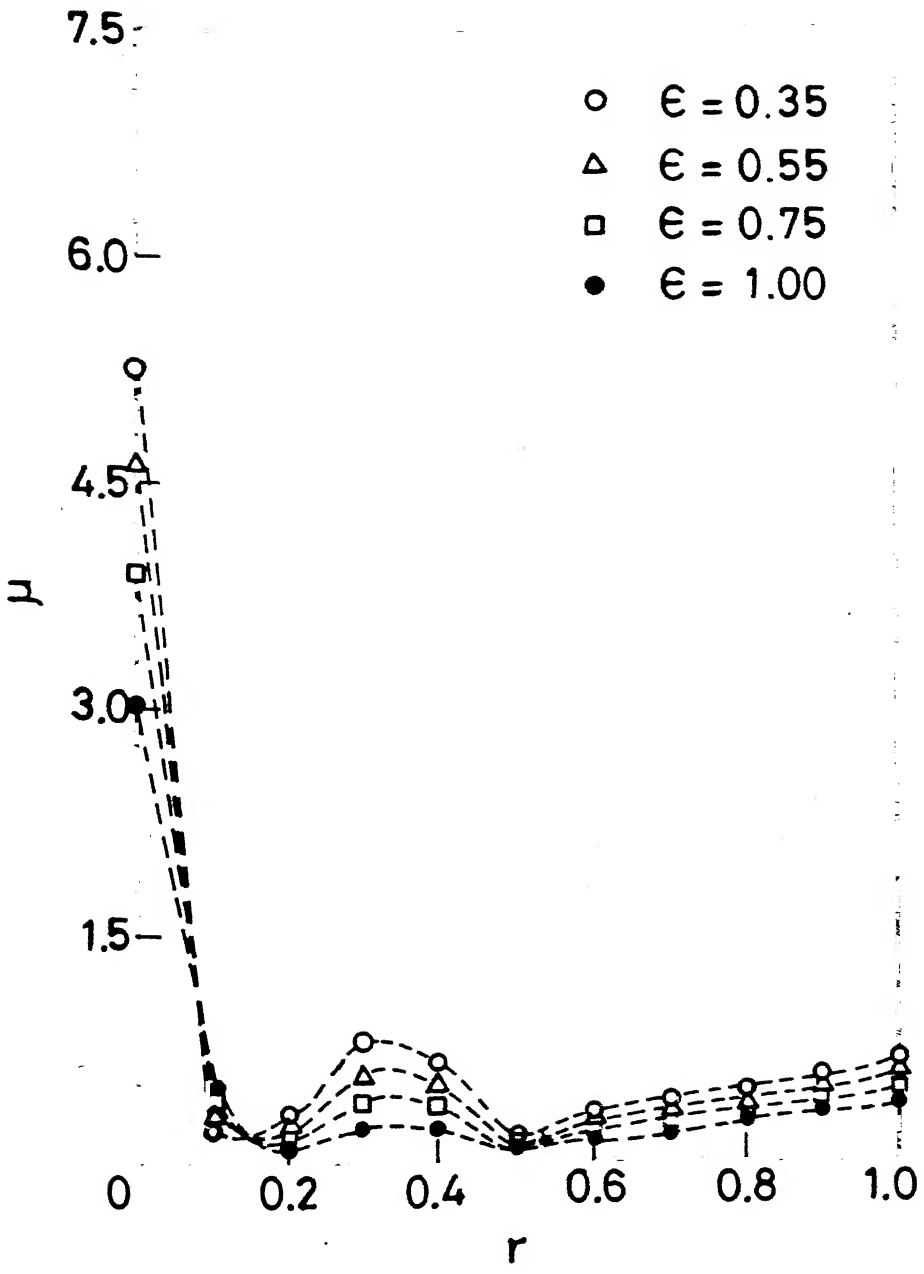

Fig. 3.3 Results with simulated data for $\mu(r) = \delta(0)$ for Lewitts filter with different epsilon

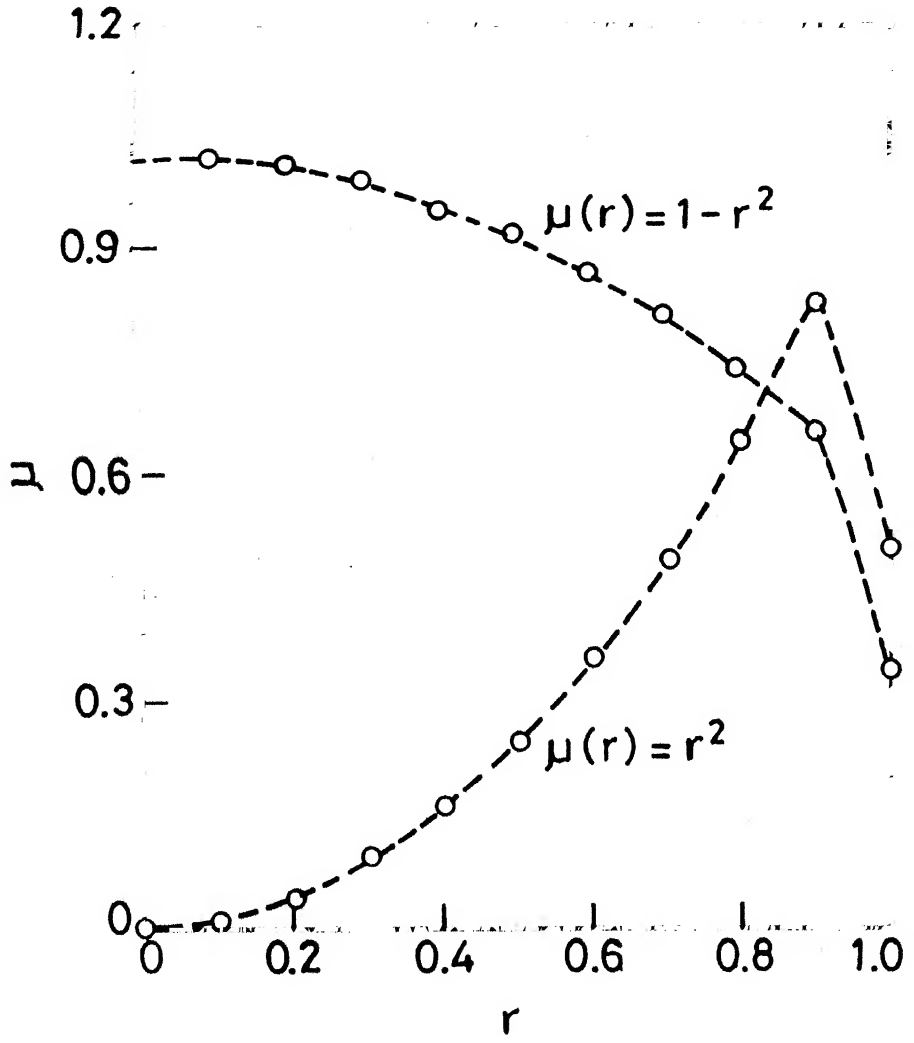

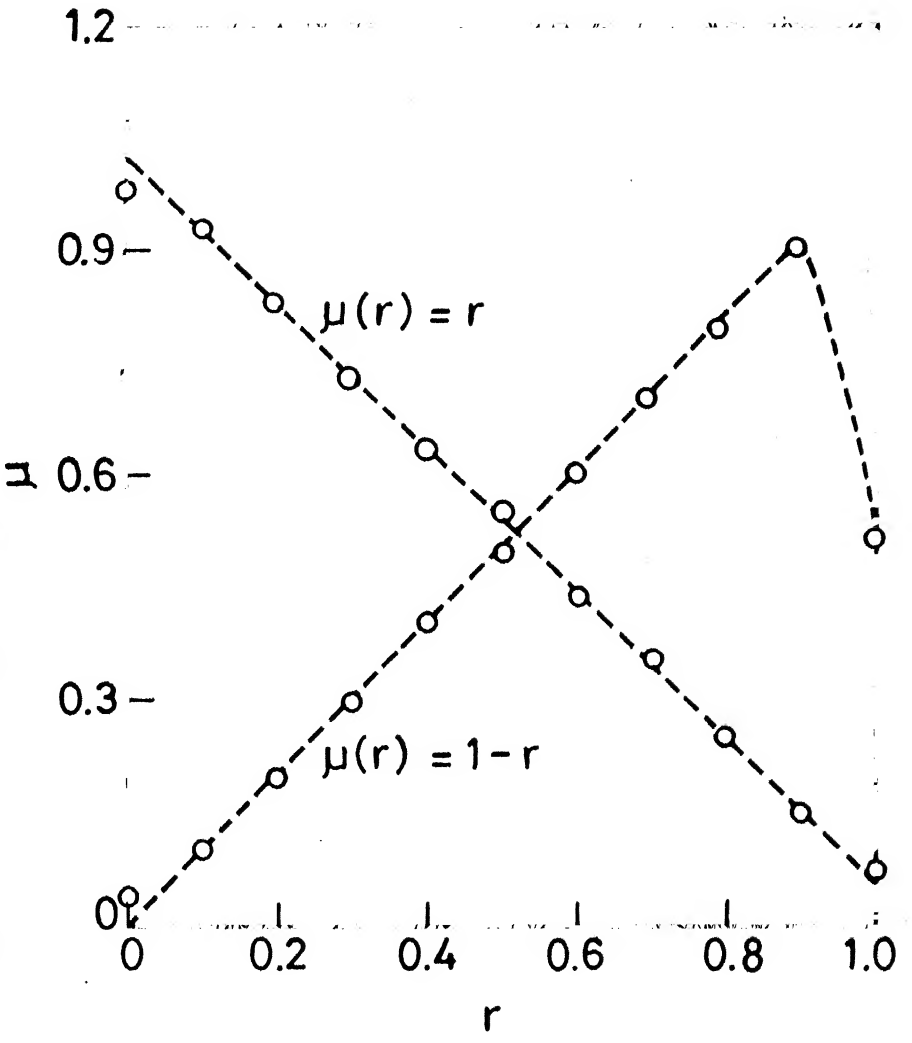

Fig. 3.4 Results with simulated data.

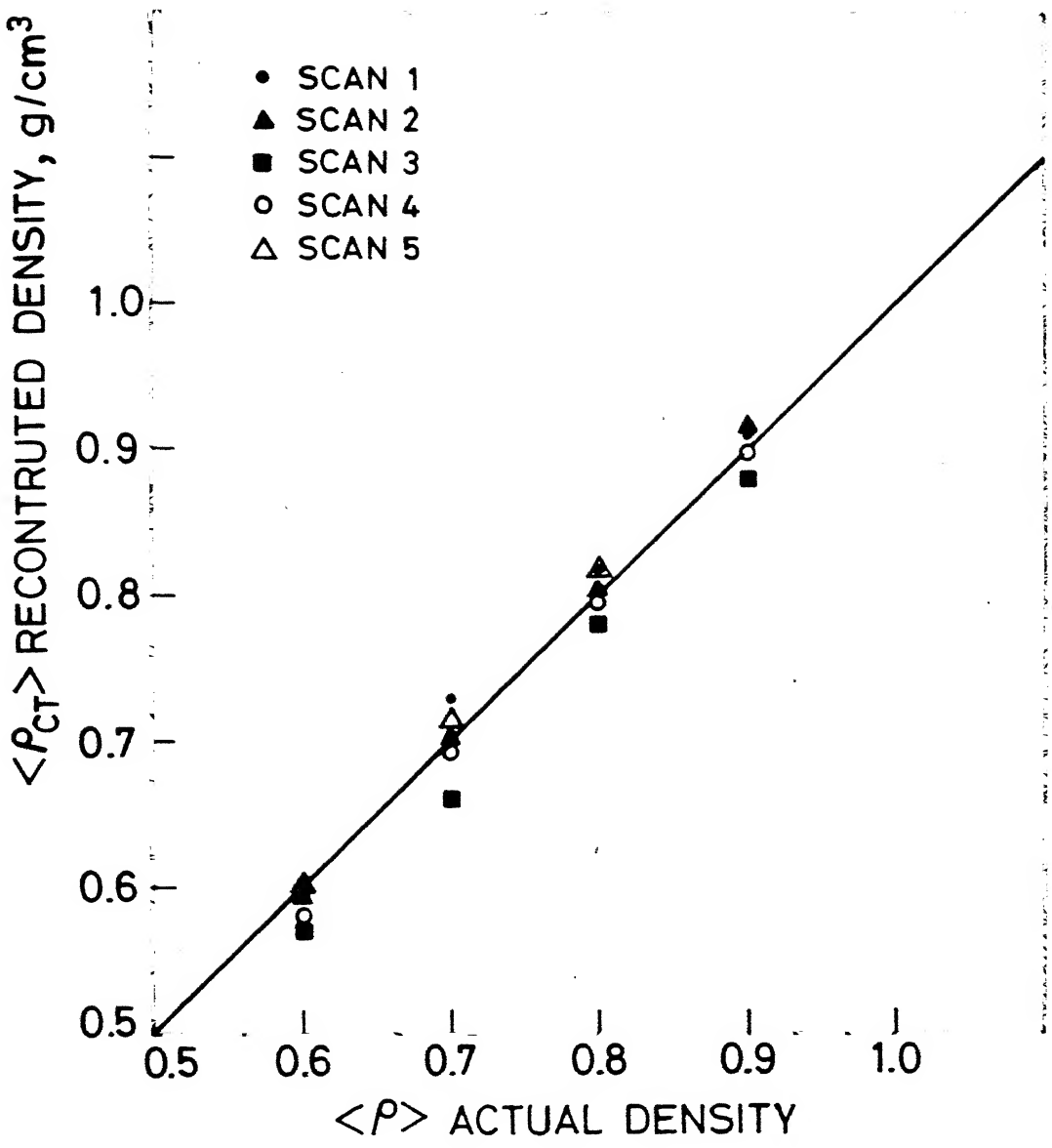

Fig. 3.6 RESULTS FOR VARIOUS DATA-SETS.
(CROSS-SECTIONALLY AVERAGED DENSITY)

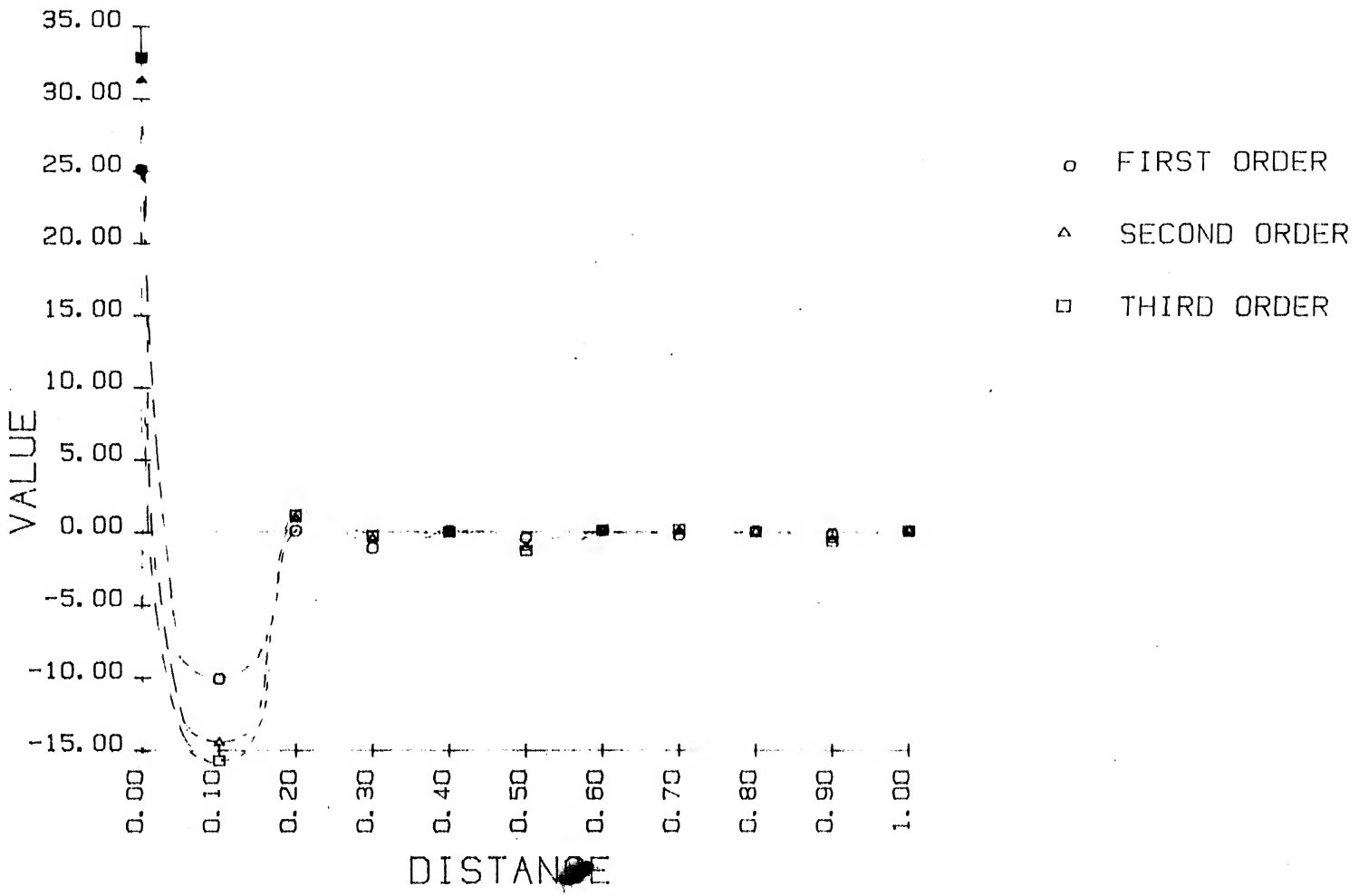

FIG 3.7 THE SPATIAL DOMAIN REPRESENTATION OF THE CONVOLVING FUNCTION WITH LEWITT'S FILTER (ε=0.0)

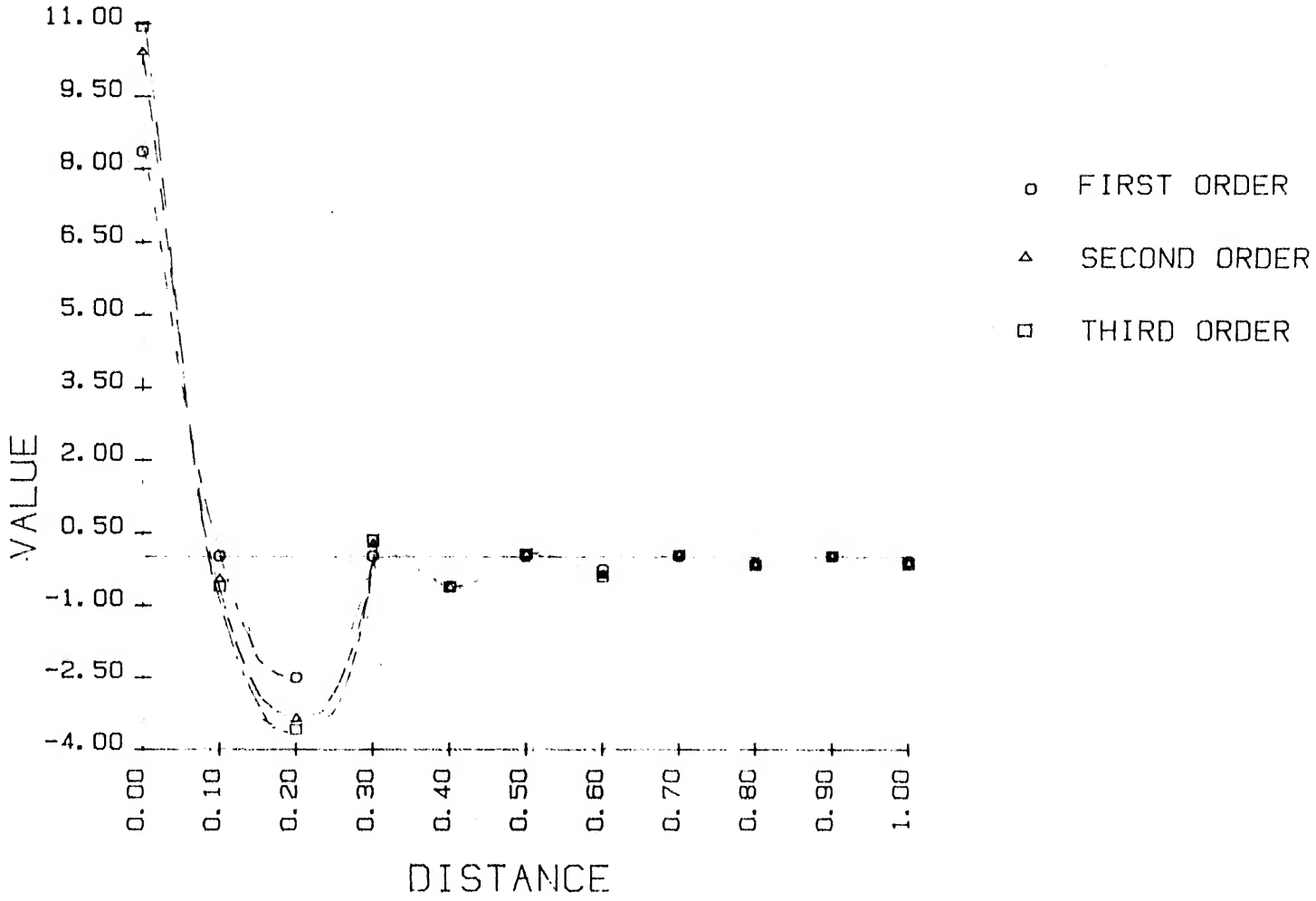

FIG 3.8 THE SPATIAL DOMAIN REPRESENTATION OF THE CONVOLVING FUNCTION WITH LEWITT'S FILTER (ε=1.0)

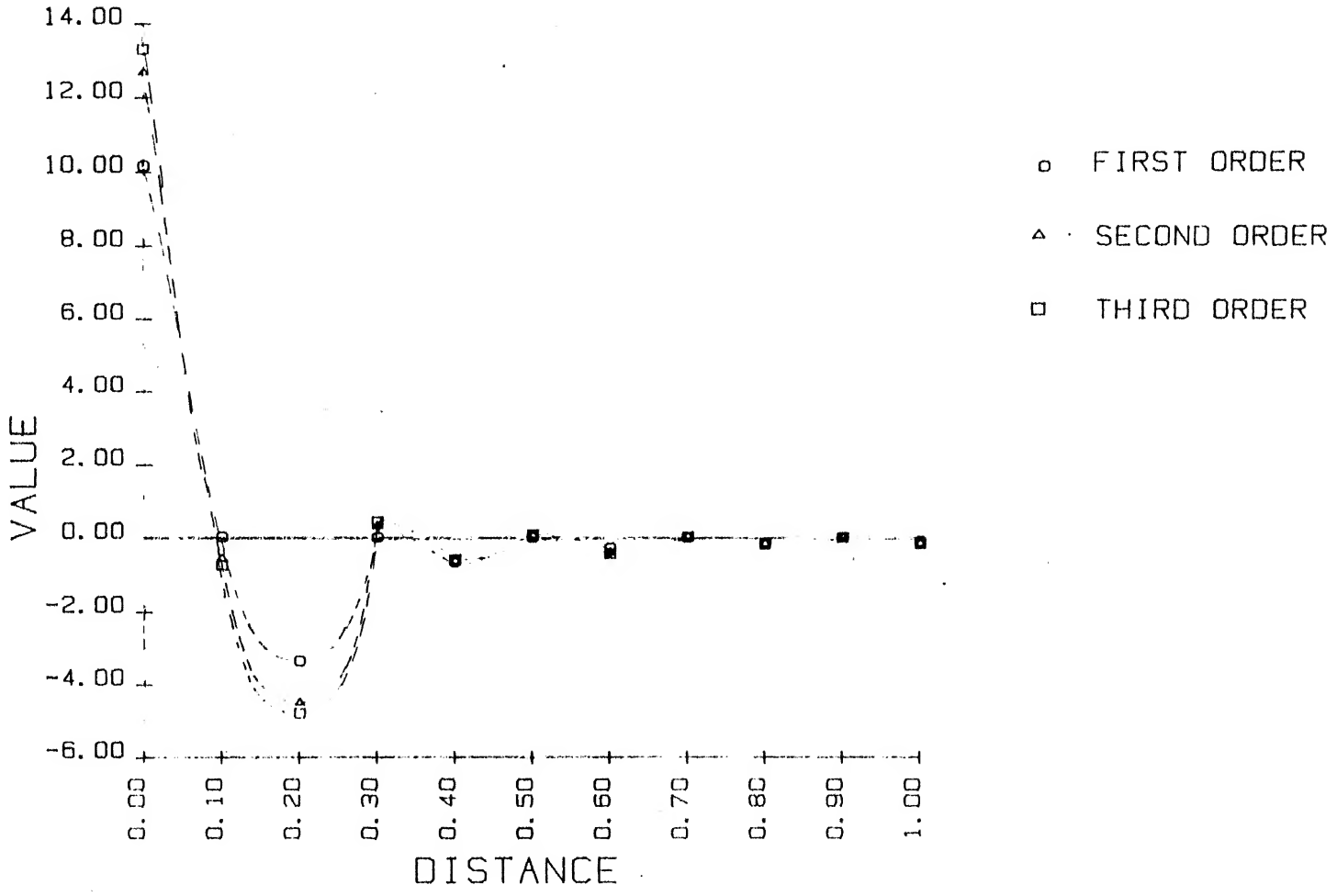

FIG 3.9 THE SPATIAL DOMAIN REPRESENTATION OF THE CONVOLVING FUNCTION WITH SINC FILTER

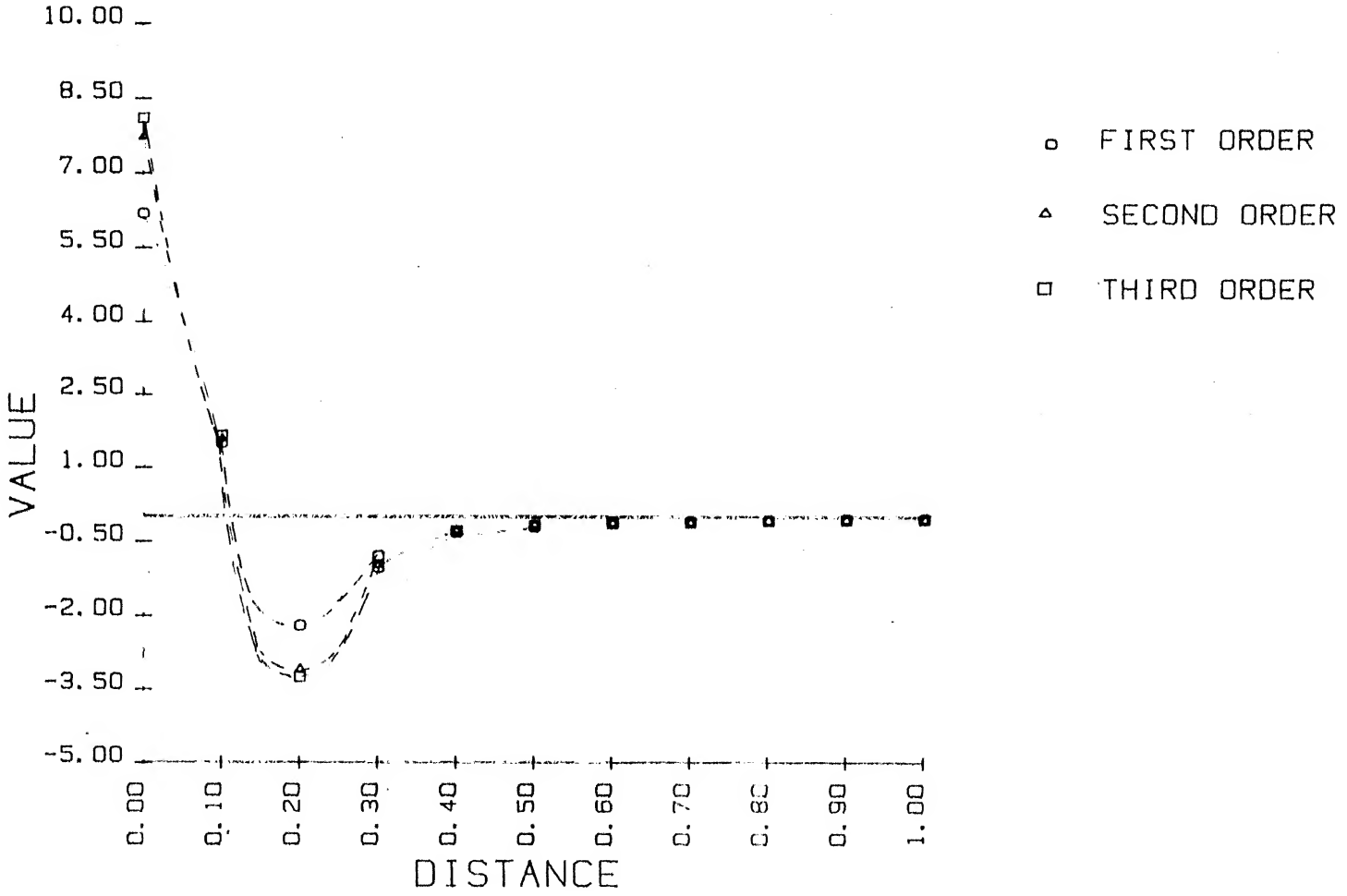

FIG 3.10 THE SPATIAL DOMAIN REPRESENTATION OF THE CONVOLVING FUNCTION WITH SINCSQUARE FILTER

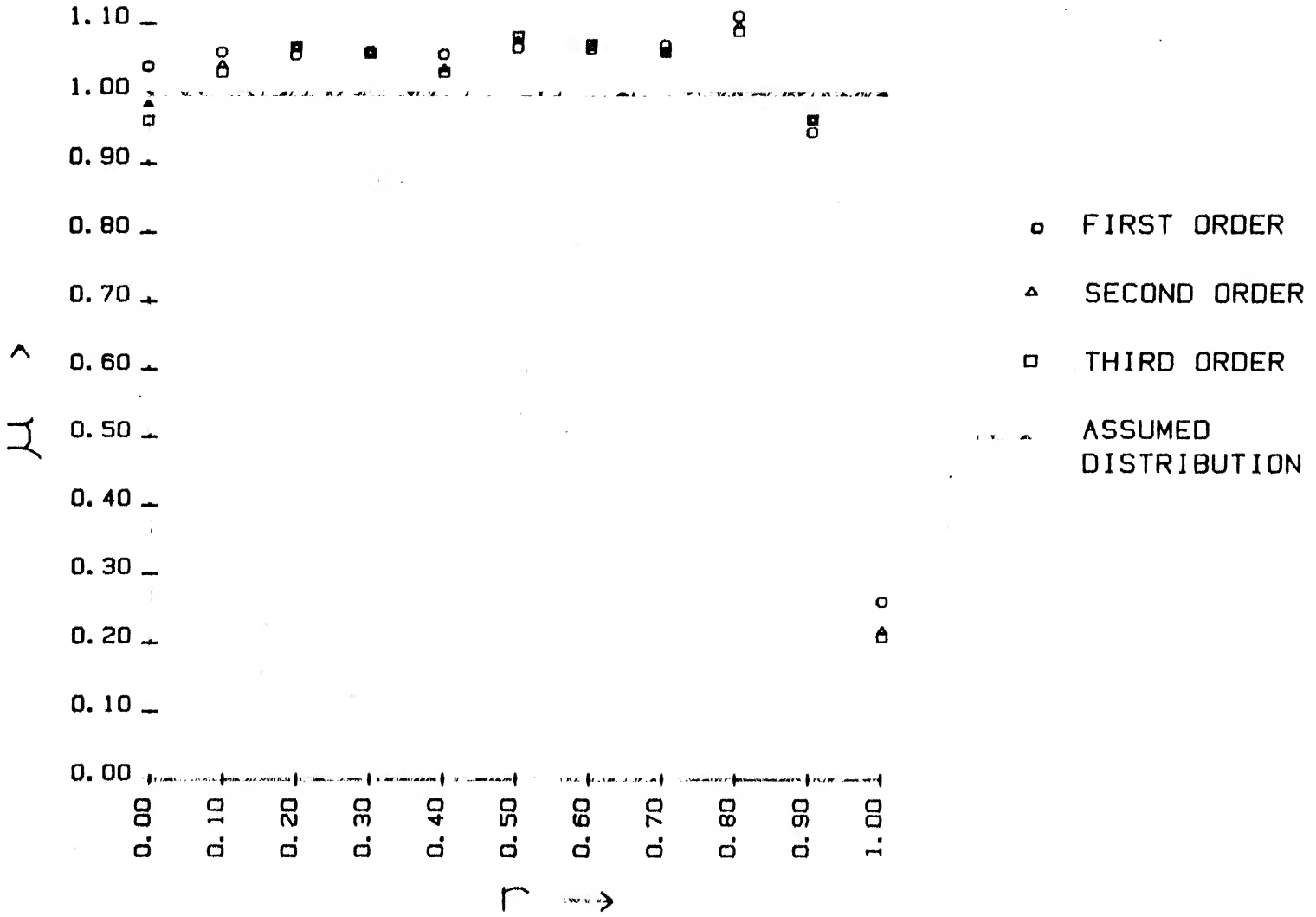

FIG 3.11 RESULTS WITH SIMULATED DATA FOR $\mu(r)=1.0$ FOR LEWITT'S I, II, AND III ORDER FILTERS ($\varepsilon=0.0$)

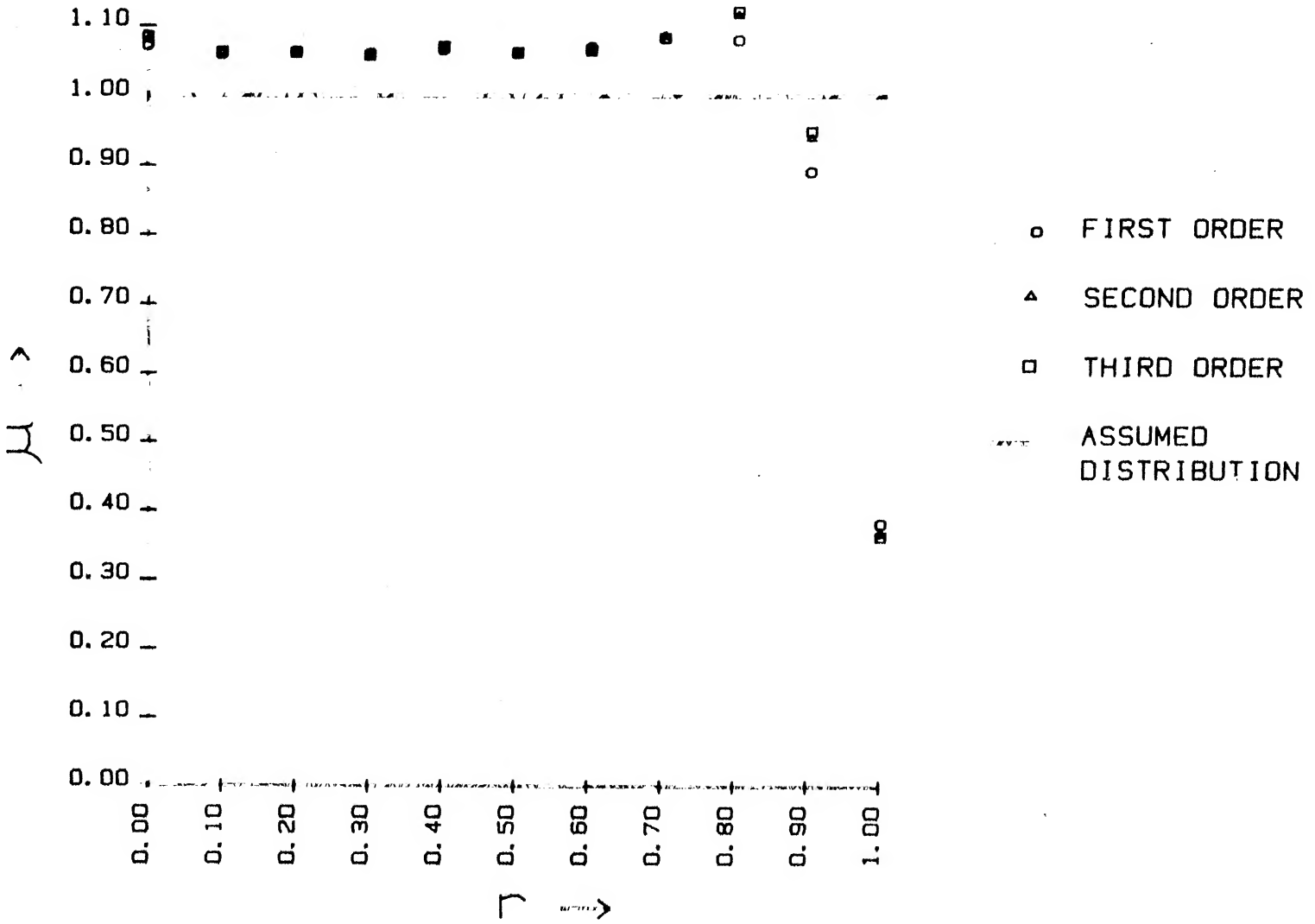

FIG 3.12 RESULTS WITH SIMULATED DATA FOR $\mu(r)=1.0$ FOR SINC I, II, AND III ORDER FILTERS

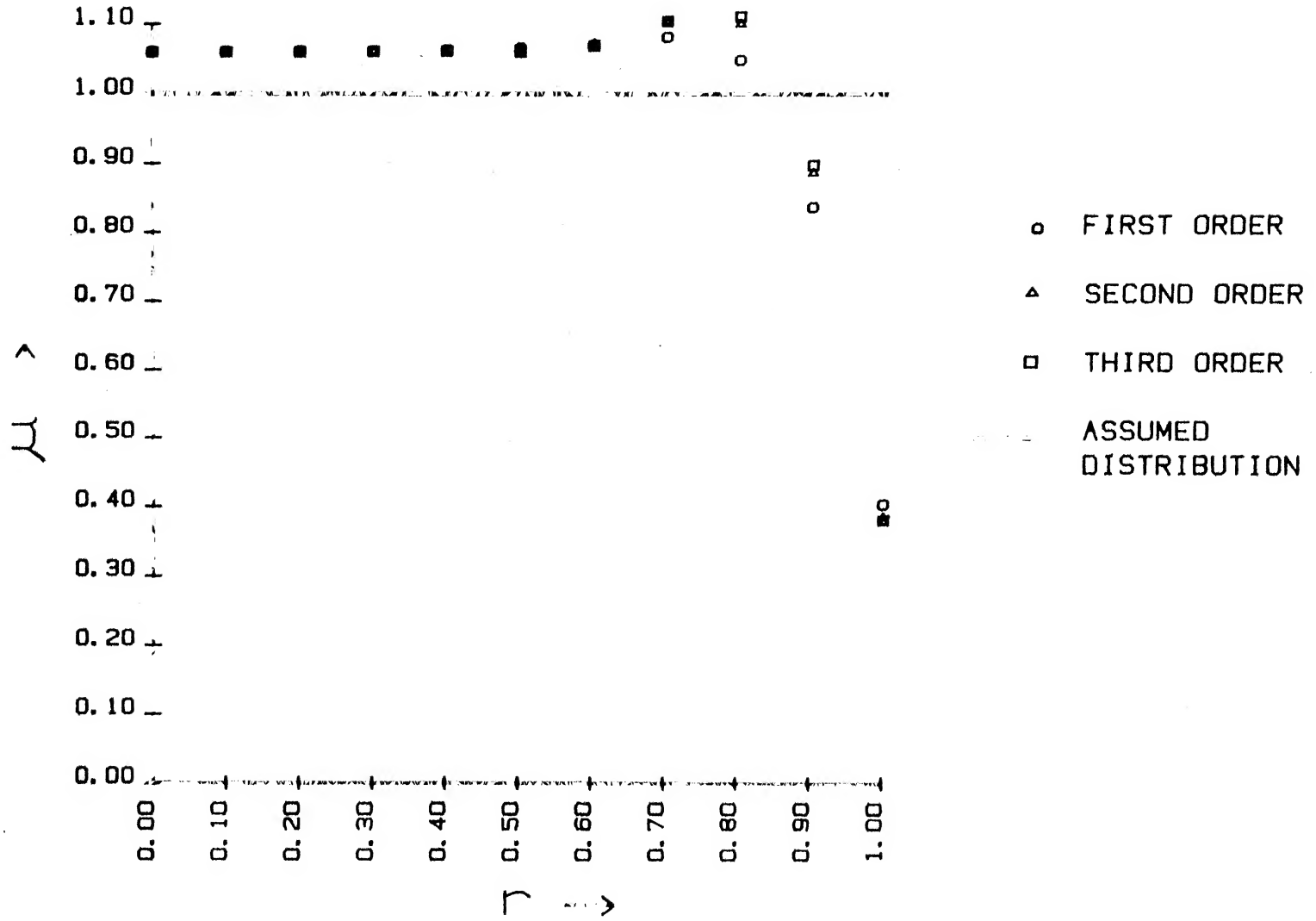

FIG 3.13 RESULTS WITH SIMULATED DATA FOR $\mu(r)=1.0$ FOR SINCSQUARE I, II, AND III ORDER FILTERS

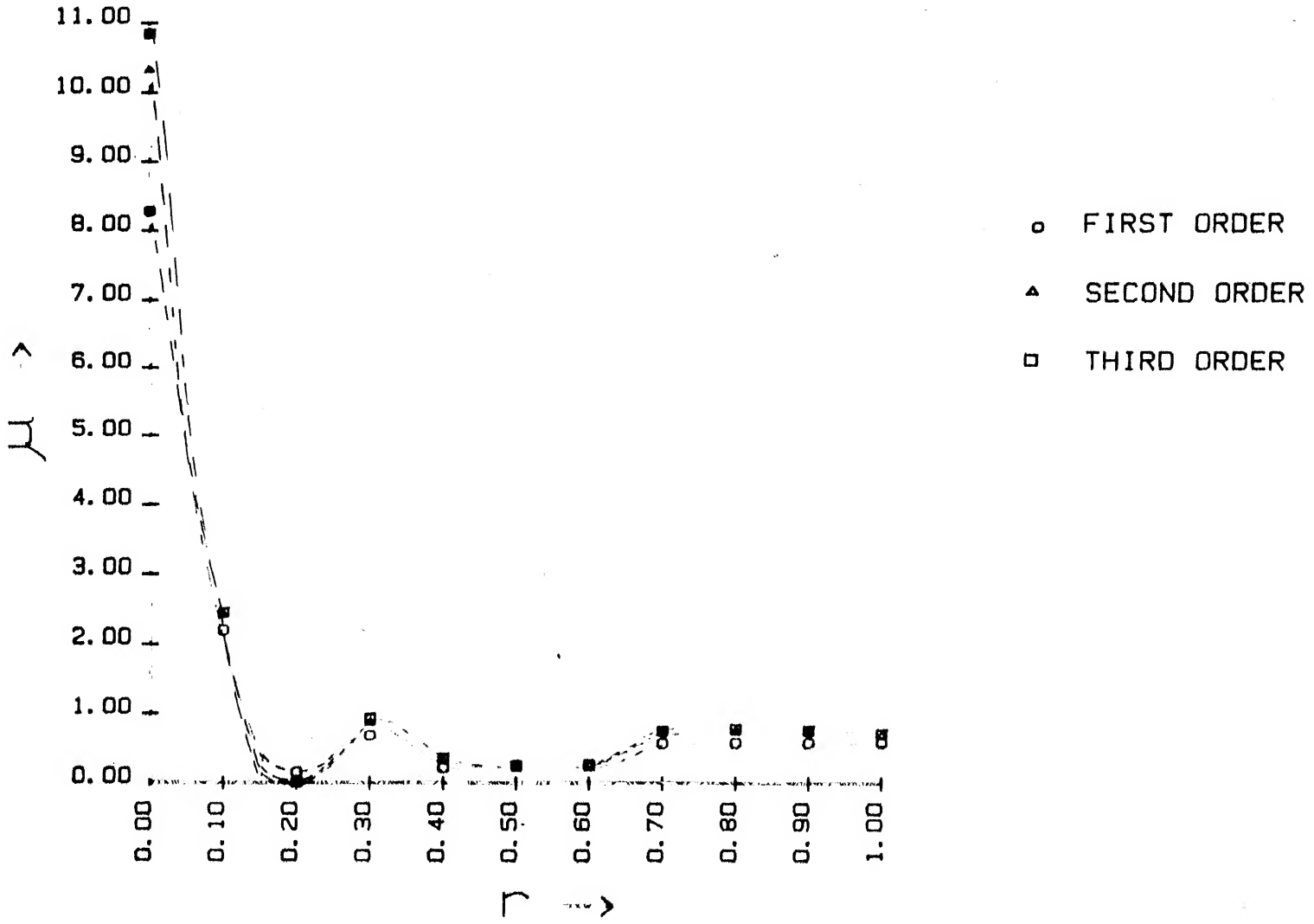

FIG 3.14 RESULTS WITH SIMULATED DATA FOR $\mu(r) = \delta(0)$ FOR LEWITT'S I, II, AND III ORDER FILTERS WITH $\epsilon = 0.0$

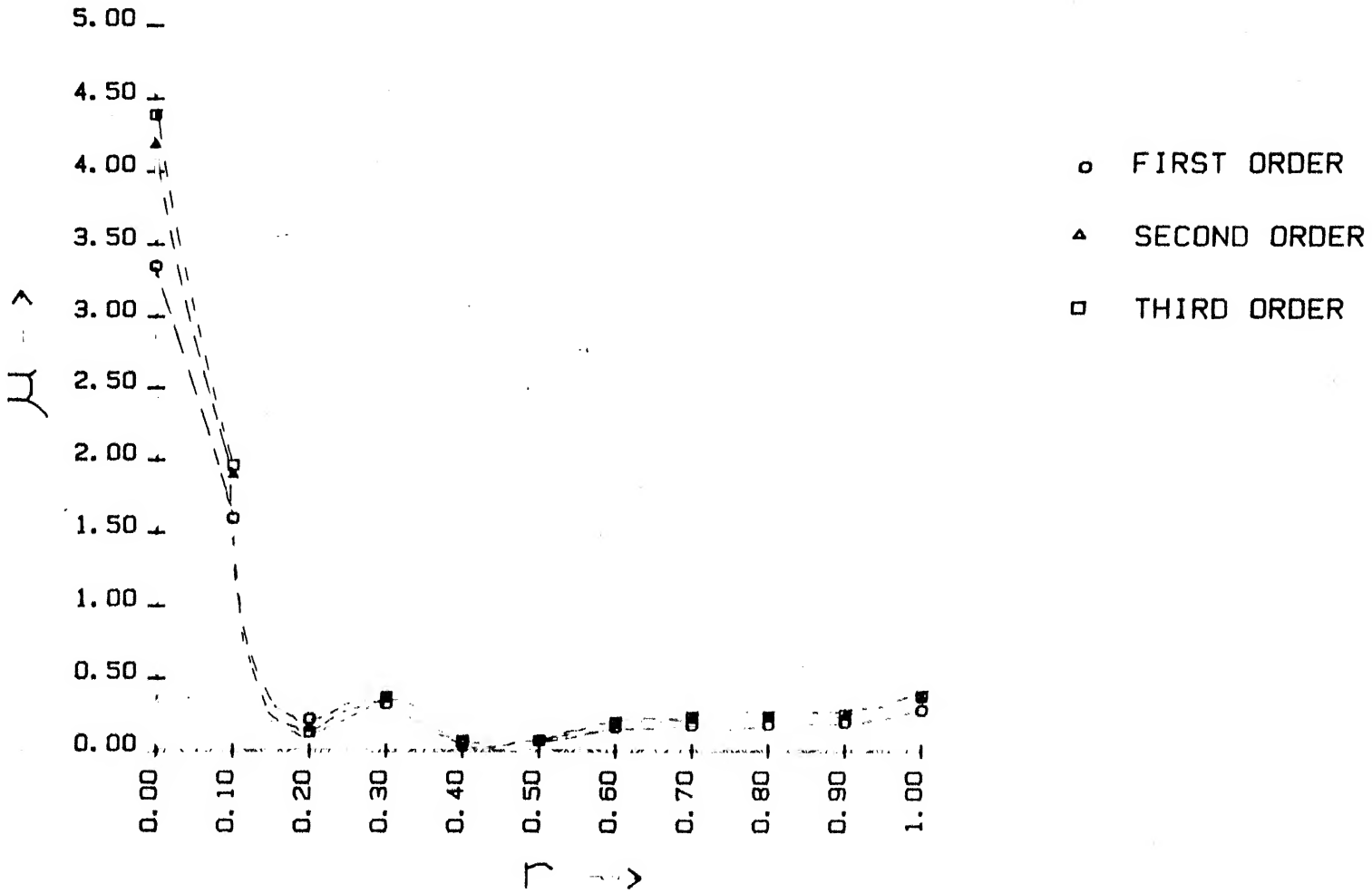

FIG 3.15 RESULTS WITH SIMULATED DATA FOR $\mu(r)=\delta(0)$ FOR SINC I, II, AND III ORDER FILTERS

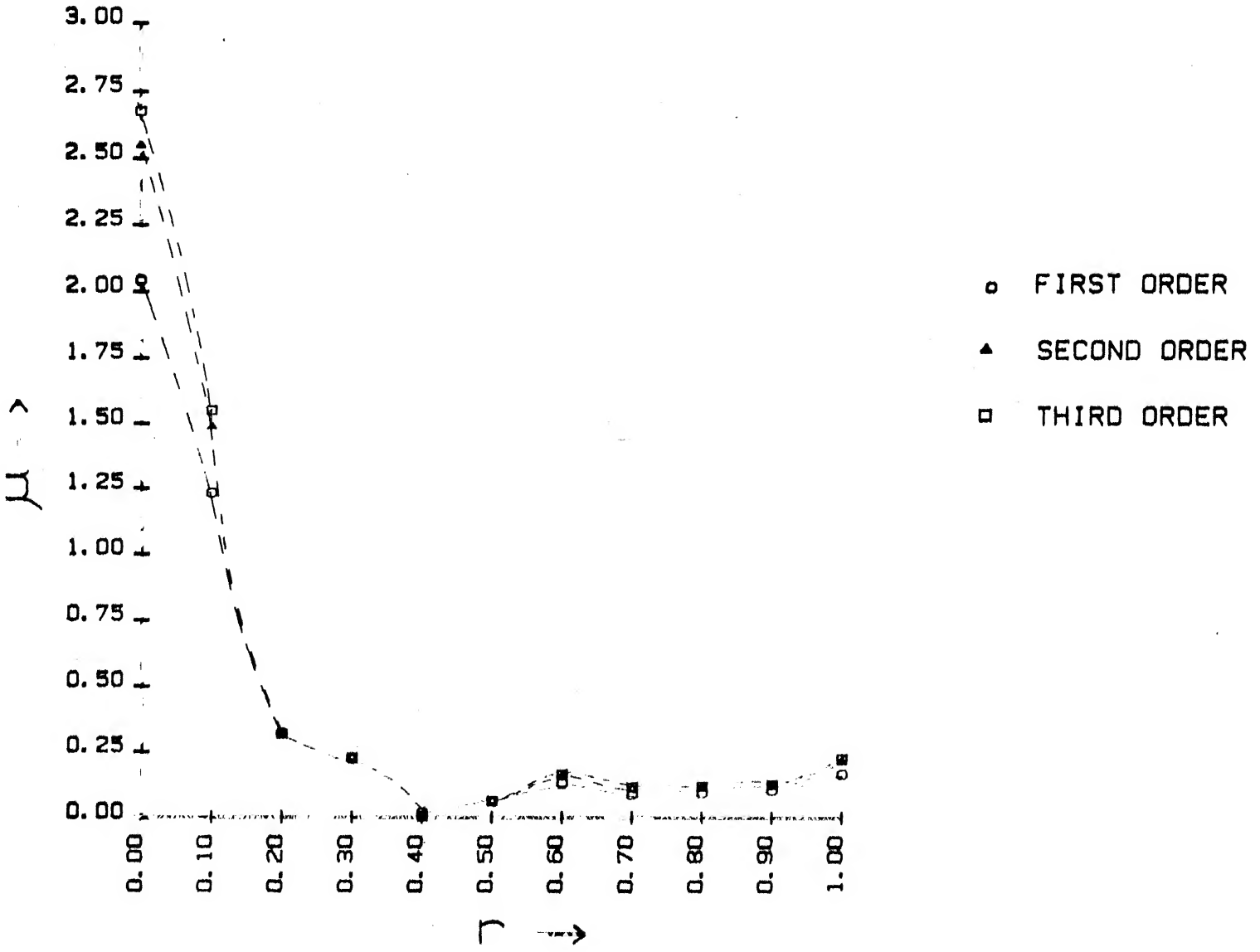

FIG 3.16 RESULTS WITH SIMULATED DATA FOR $\mu(r) = \delta(0)$ FOR SINCSQUARE I, II, AND III ORDER FILTERS

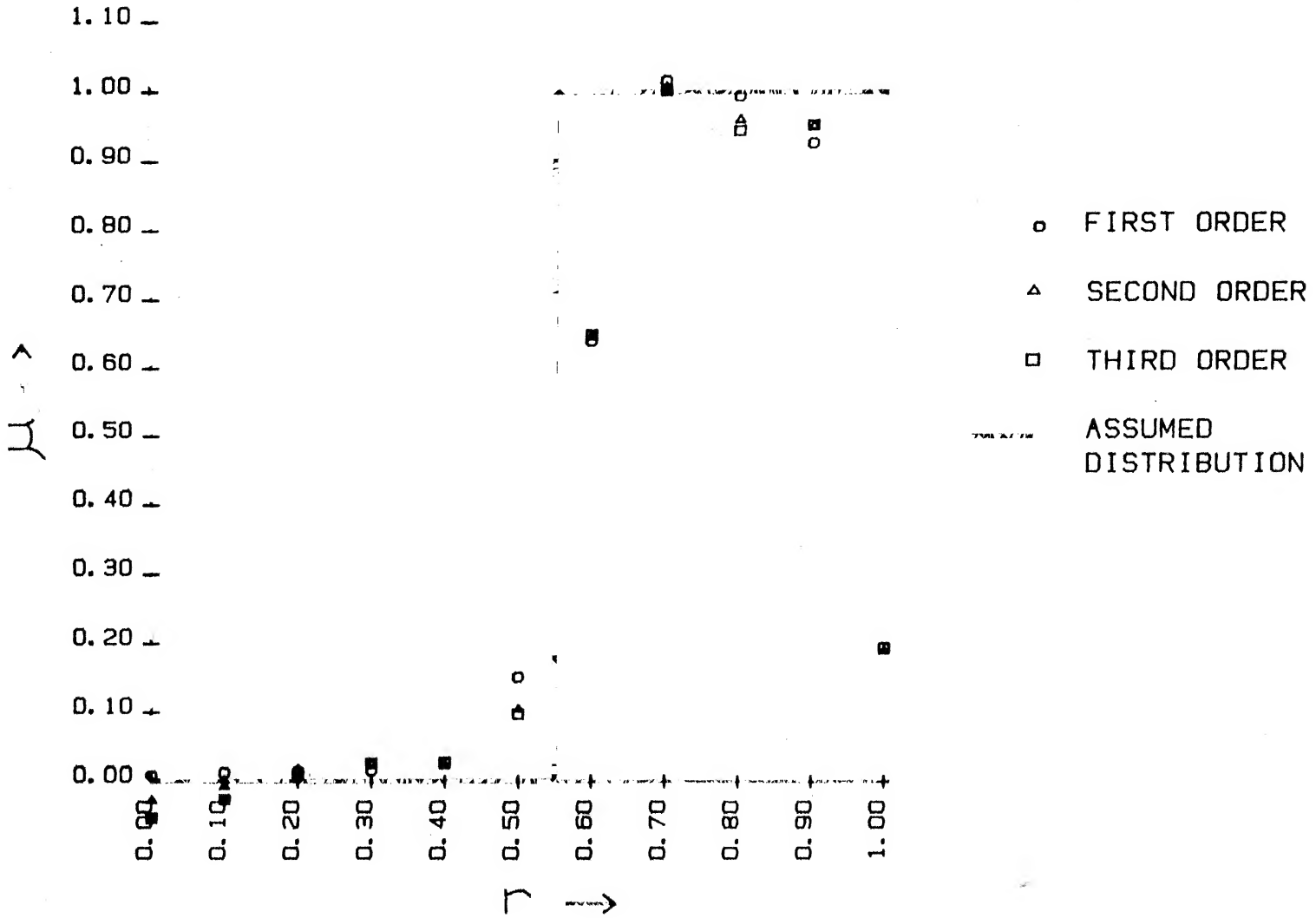

FIG 3.17 RESULTS WITH SIMULATED DATA FOR LEWITT'S I, II, AND III ORDER FILTERS WITH ϵ =0.0

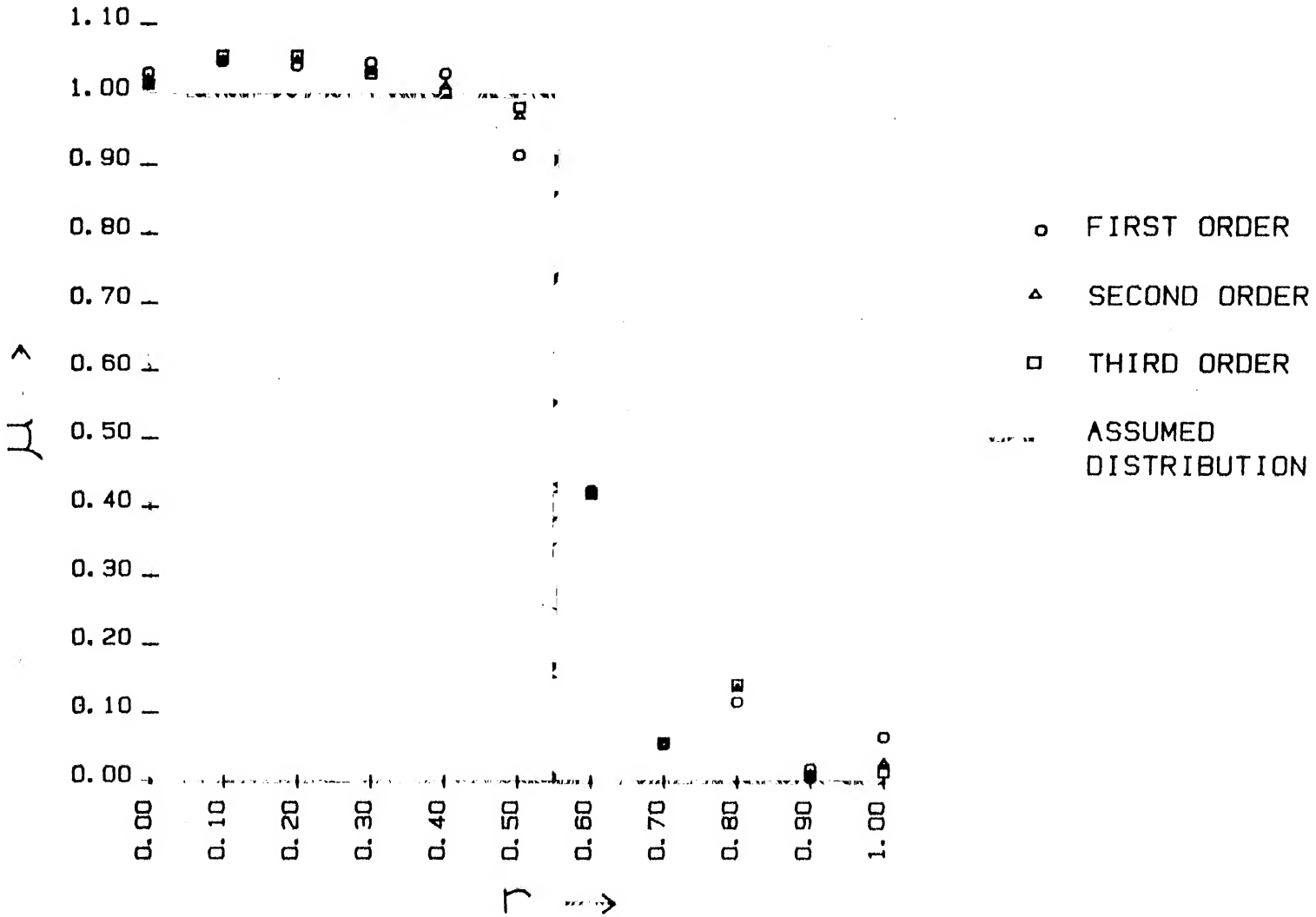

FIG 3.18 RESULTS WITH SIMULATED DATA FOR LEWITT'S I, II, AND III ORDER FILTERS WITH $\epsilon = 0.0$

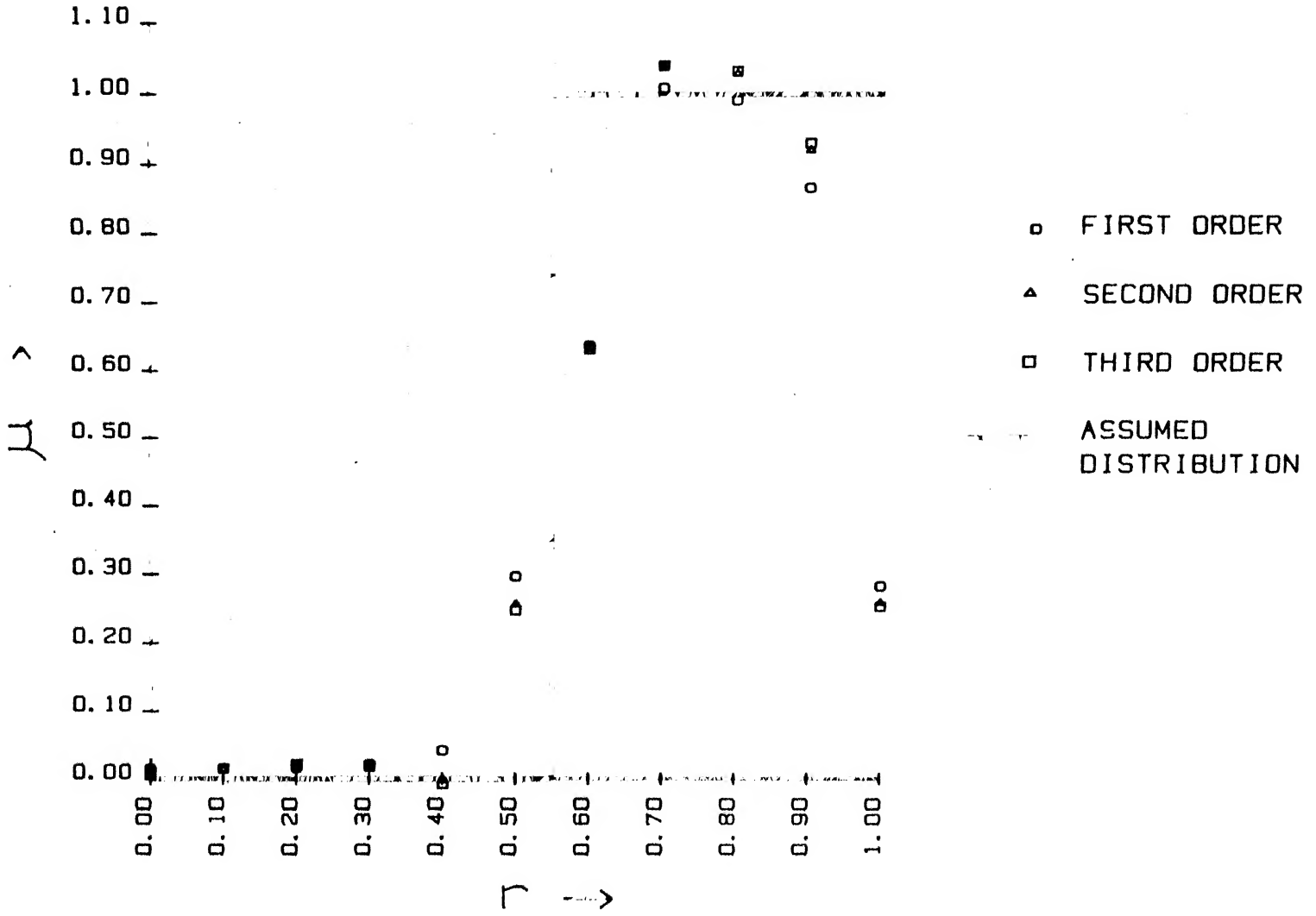

FIG 3.19 RESULTS WITH SIMULATED DATA FOR SINC I, II, AND III ORDER FILTERS

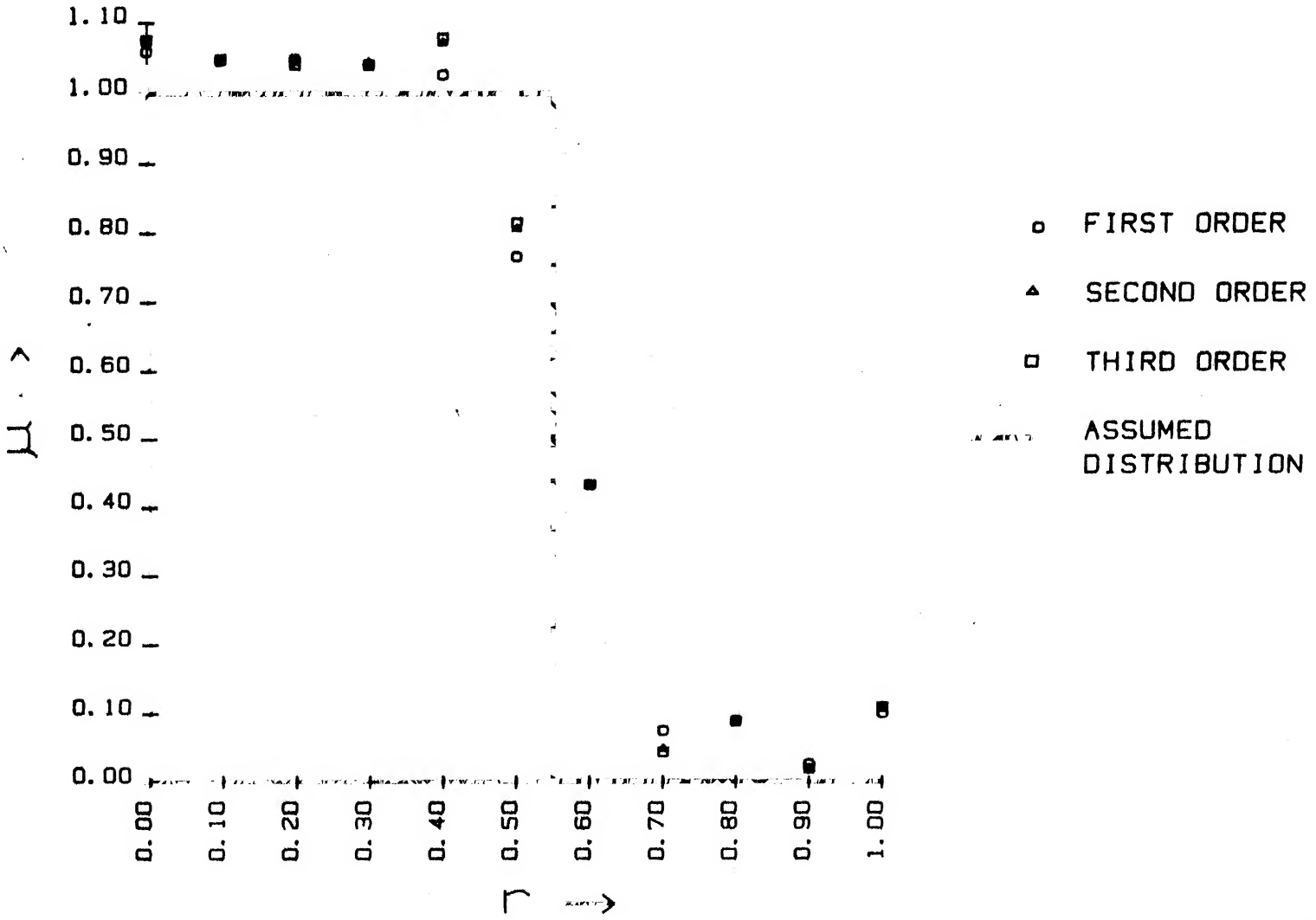

FIG 3.20 RESULTS WITH SIMULATED DATA FOR SINC I, II, AND III ORDER FILTERS

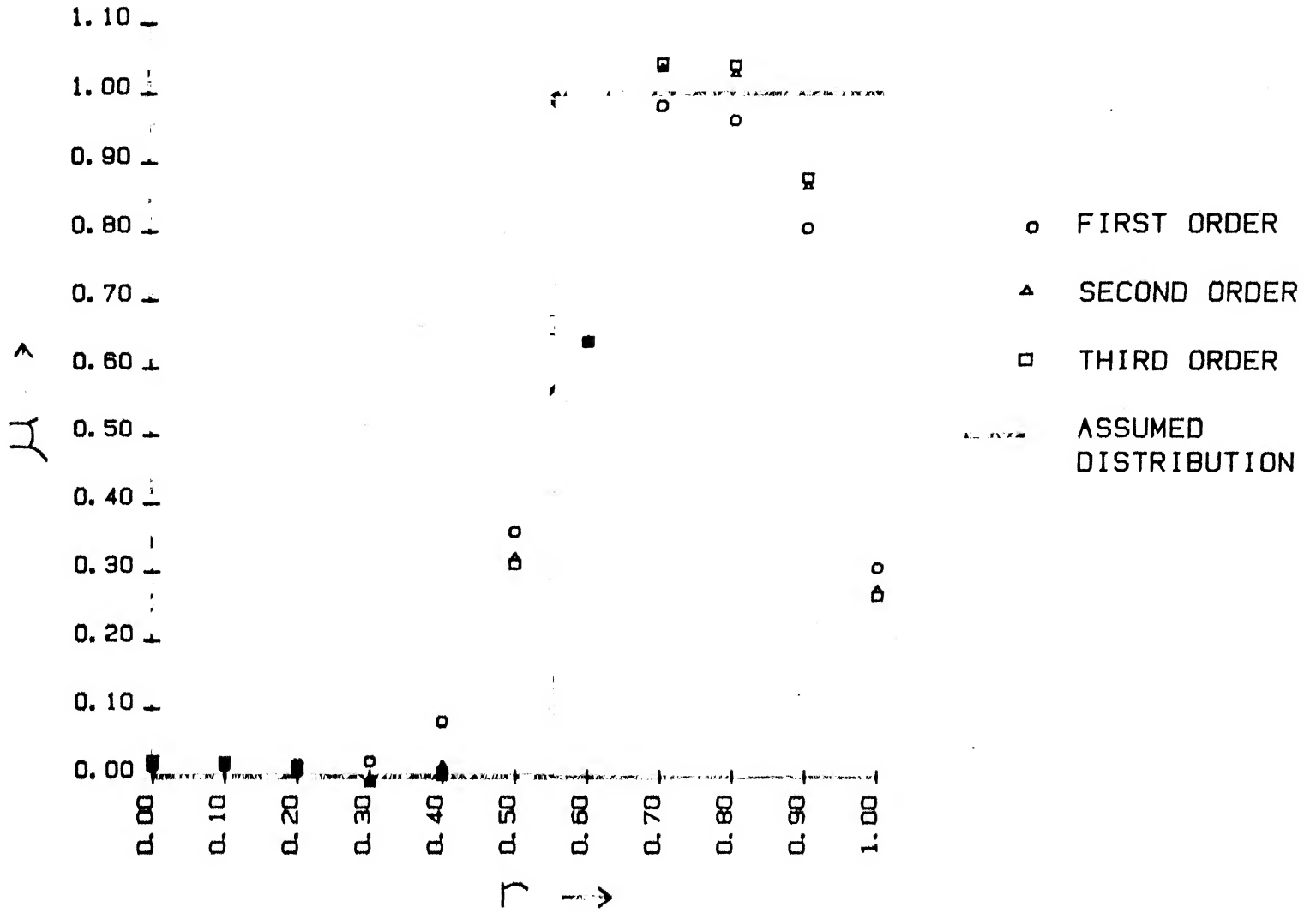

FIG 3.21 RESULTS WITH SIMULATED DATA FOR SINCSQUARE I, II, AND III ORDER FILTERS

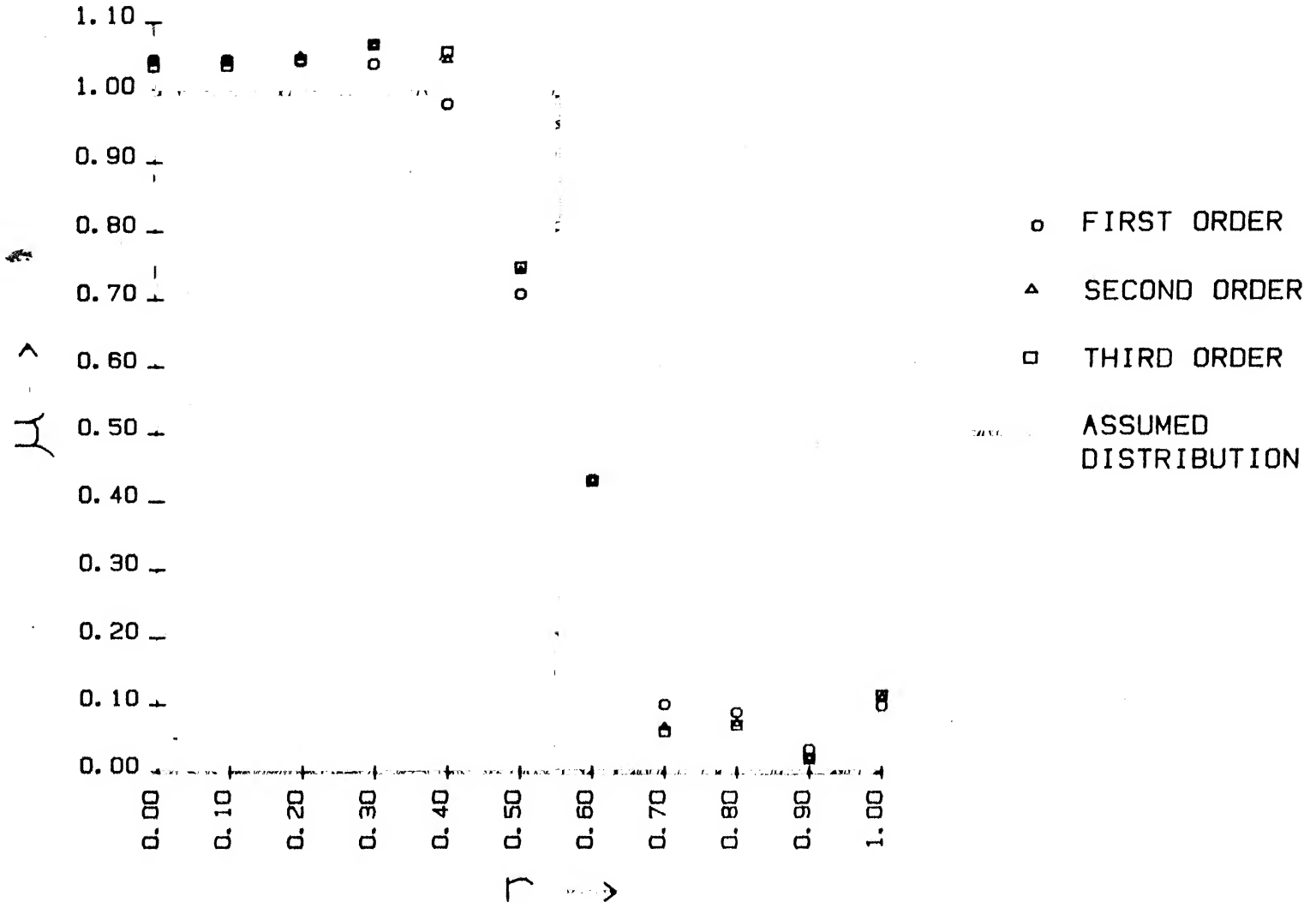

FIG 3.22 RESULTS WITH SIMULATED DATA FOR SINCSQUARE I, II, AND III ORDER FILTERS

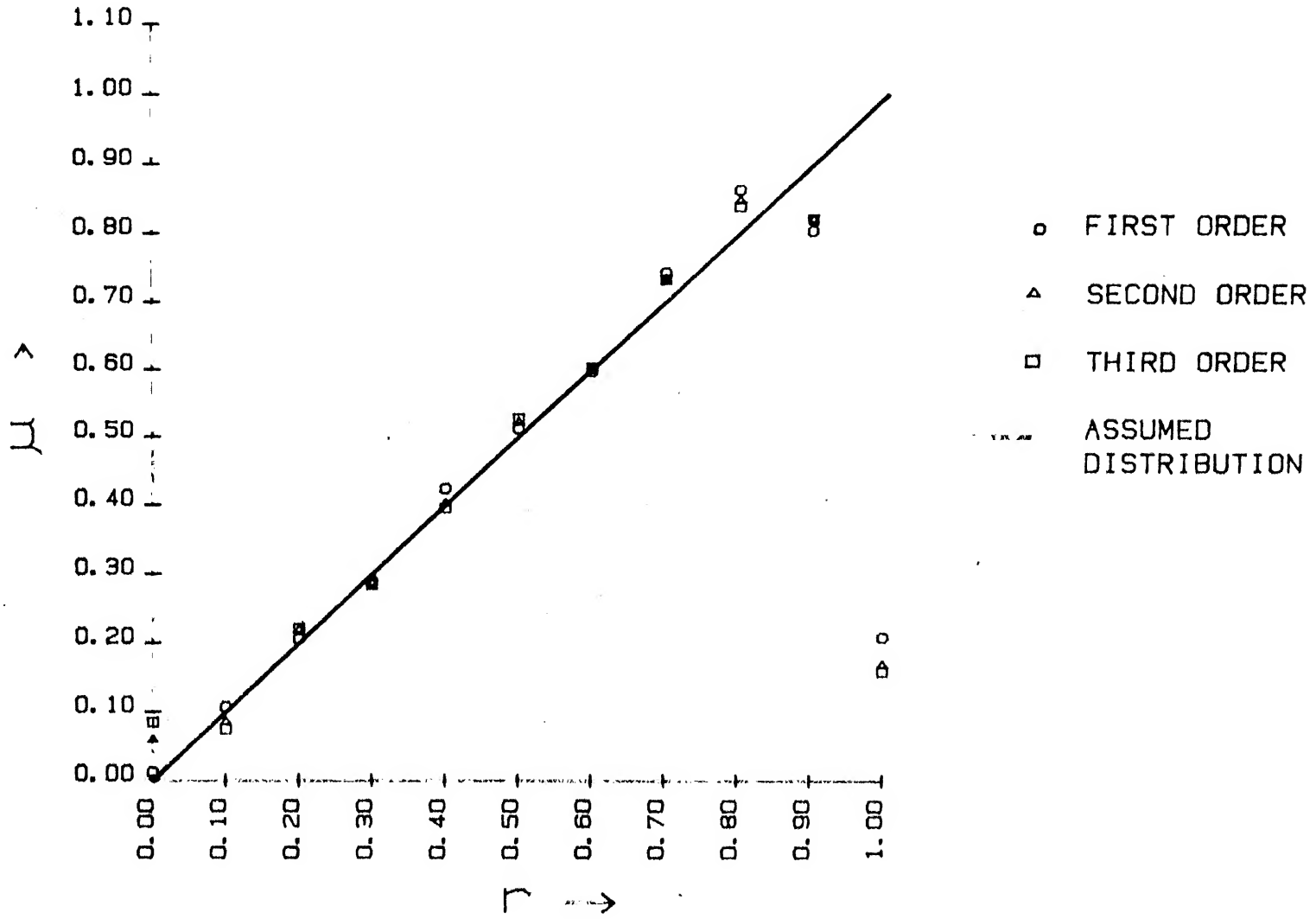

FIG 3.23 RESULTS WITH SIMULATED DATA FOR $\mu(r)=r$ FOR LEWITT'S I, II, AND III ORDER FILTERS WITH $\epsilon=0.0$

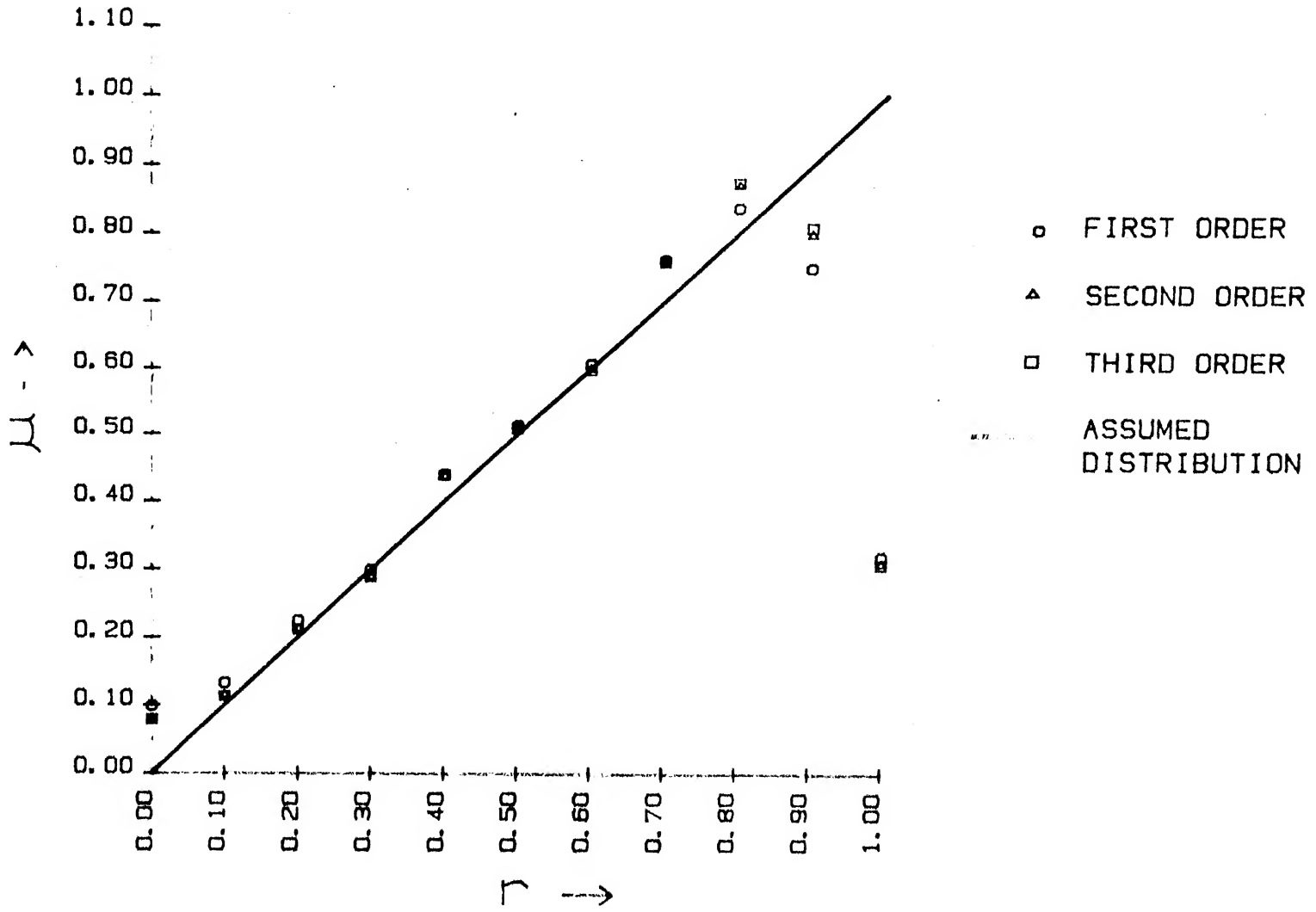

FIG 3.24 RESULTS WITH SIMULATED DATA FOR $\mu(r) = r$ FOR SINC I, II, AND III ORDER FILTERS

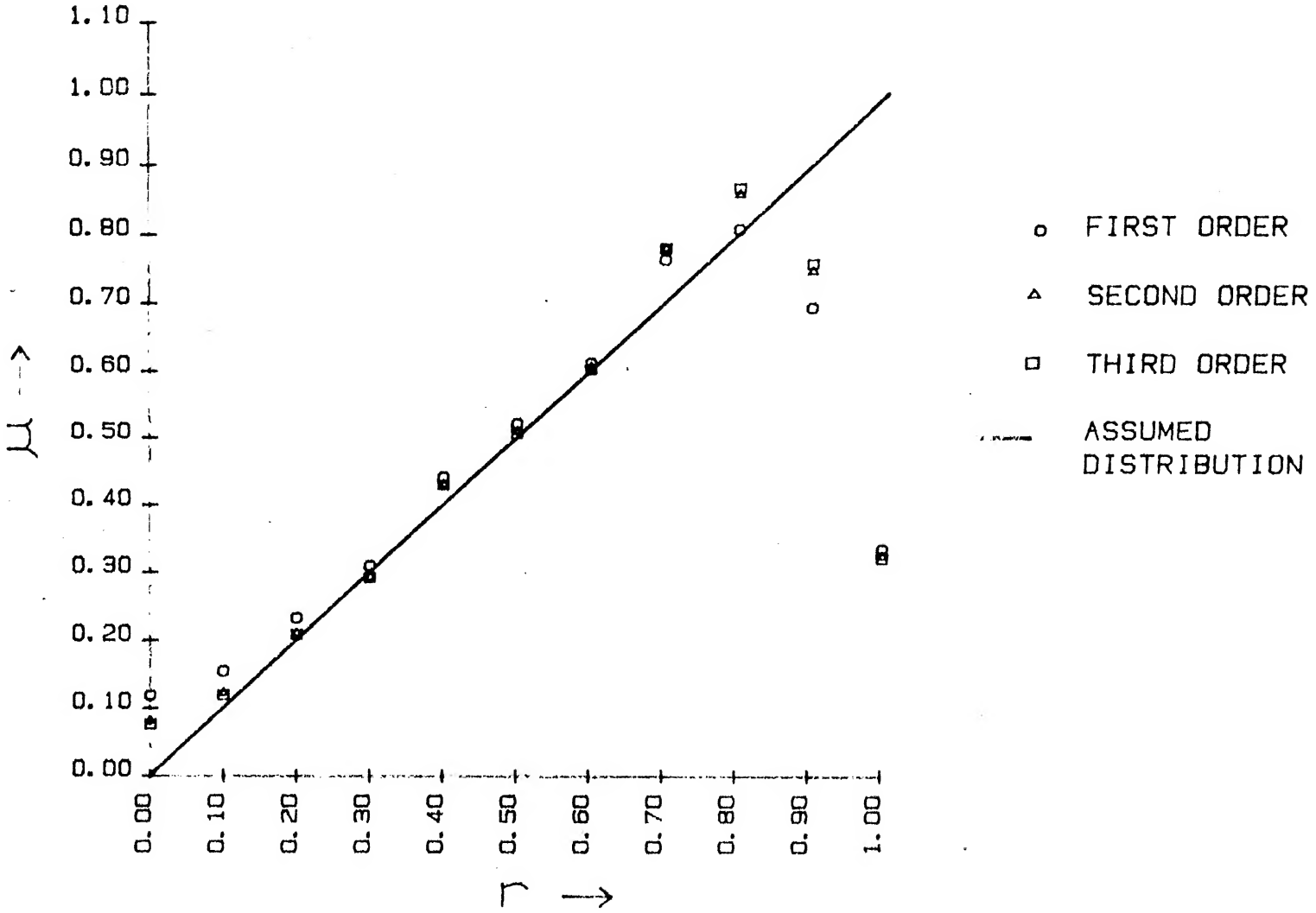

FIG 3.25 RESULTS WITH SIMULATED DATA FOR $\mu(r) = r$ FOR SINCSQUARE I, II, AND III ORDER FILTERS

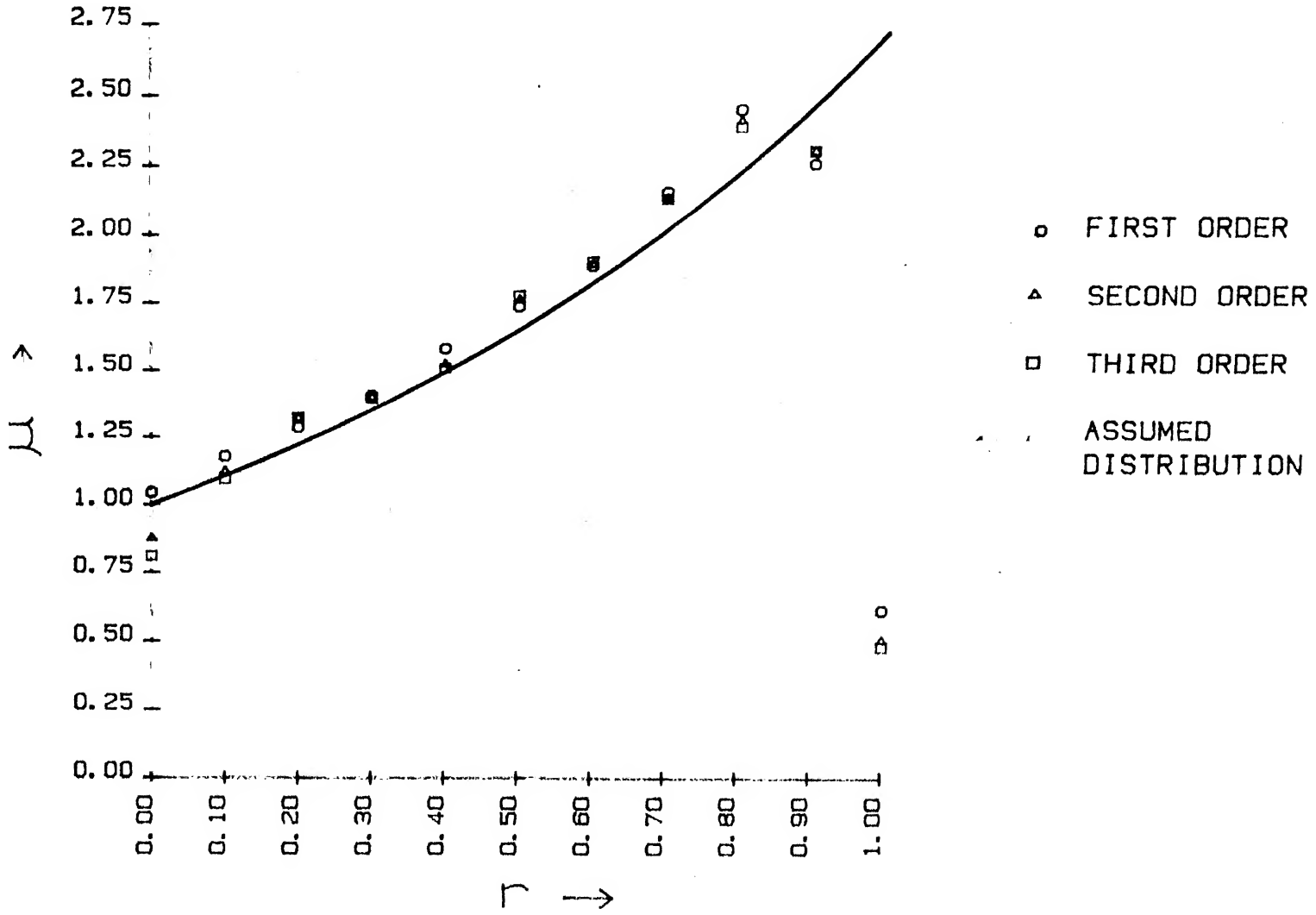

FIG 3.26 RESULTS WITH SIMULATED DATA FOR $\mu(r)=\exp(r)$ FOR LEWITT'S I, II, AND III ORDER FILTERS WITH $\epsilon=0.0$

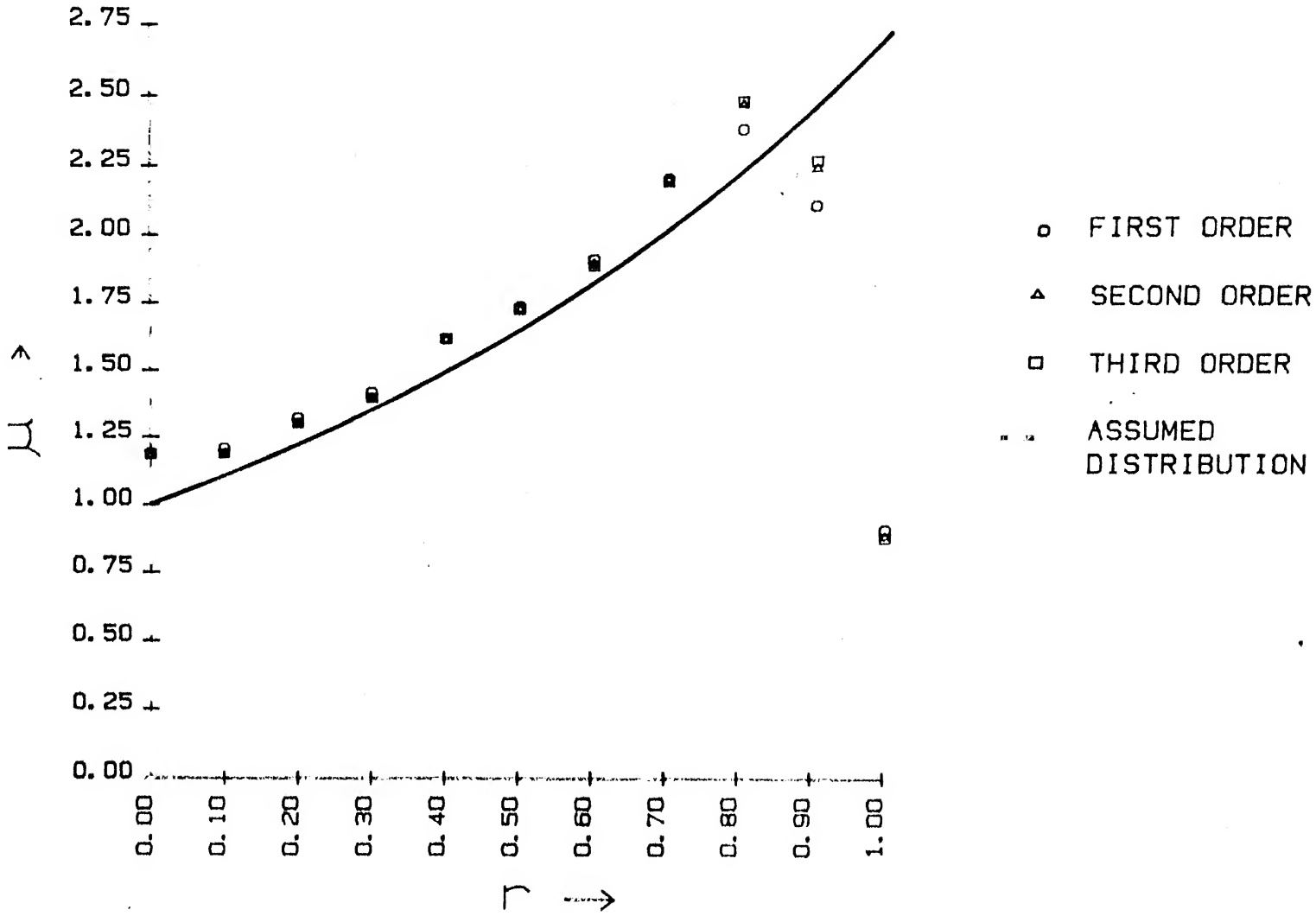

FIG 3.27 RESULTS WITH SIMULATED DATA FOR $\mu(r) = \exp(r)$ FOR SINC I, II, AND III ORDER FILTERS

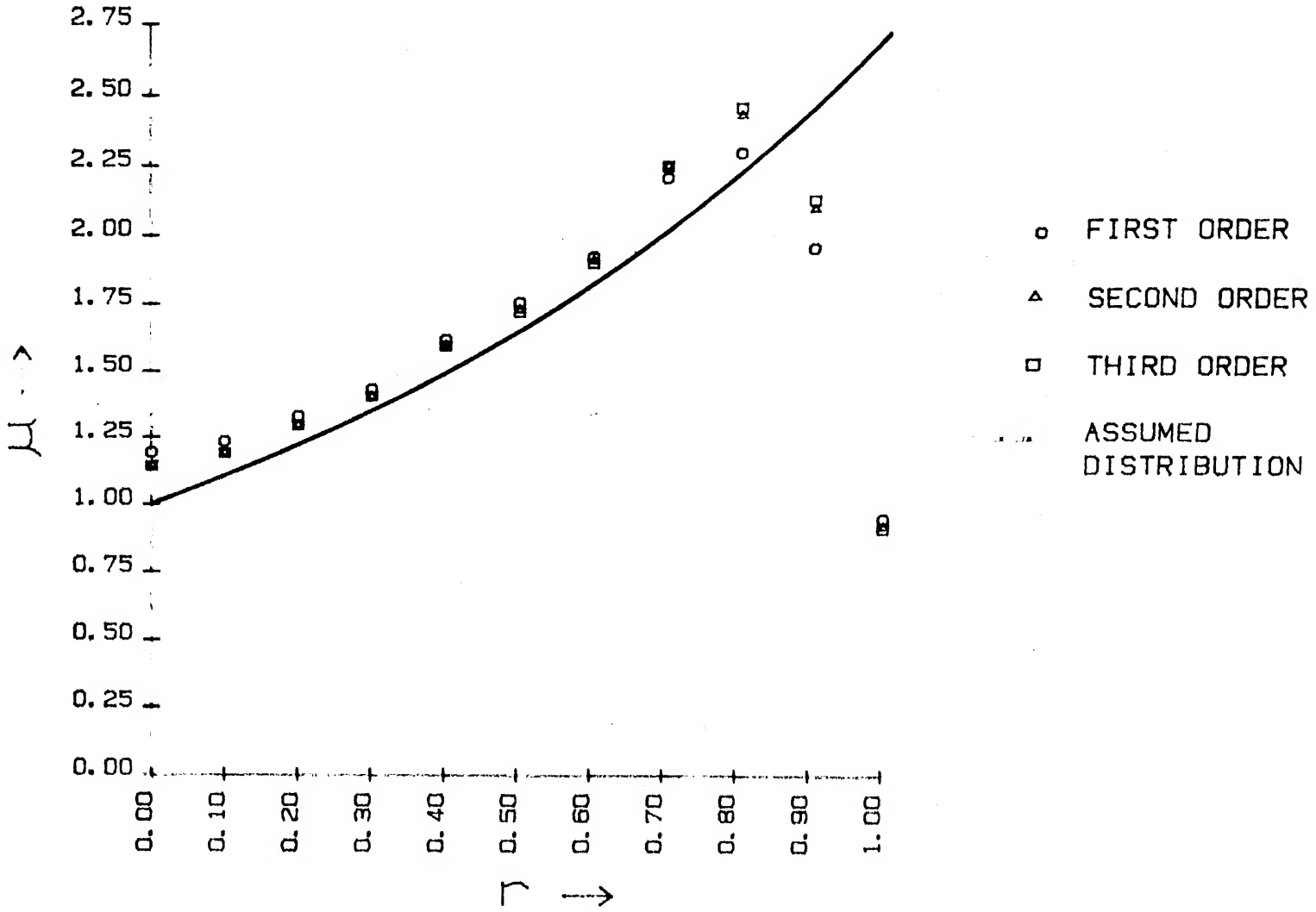

FIG 3.28 RESULTS WITH SIMULATED DATA FOR $\mu(r) = \exp(r)$ FOR SINCSQUARE I, II, AND III ORDER FILTERS

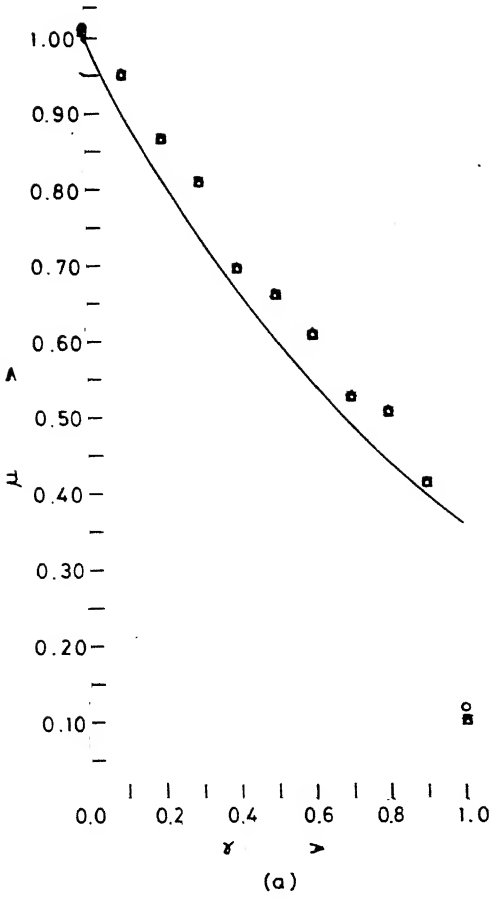

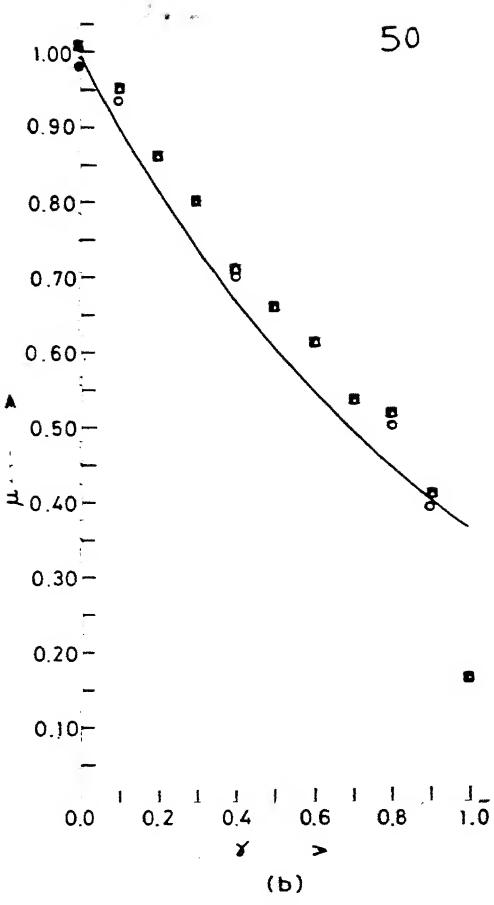

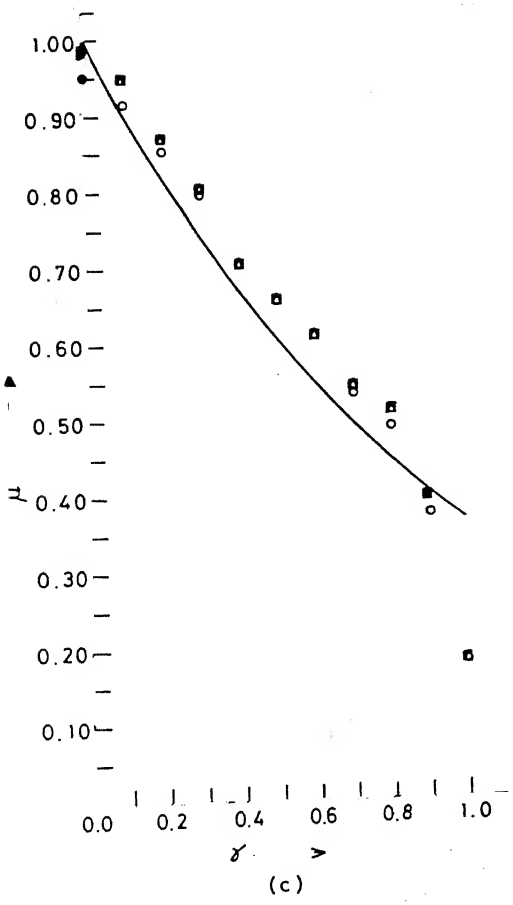

FIG. 3.29 RESULTS WITH SIMULATED DATA FOR $\mu(\gamma) = \exp(-\gamma)$ FOR (a) LEWITT'S FILTER, $\epsilon = 0.0$ (b) SINC FILTER (c) SINC SQUARE FILTER

- o I ORDER
- △ II ORDER
- □ III ORDER

98979

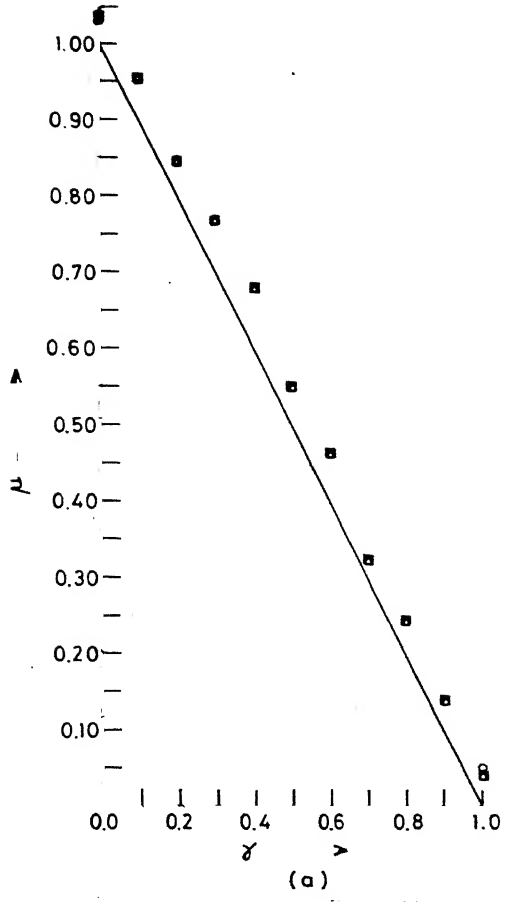

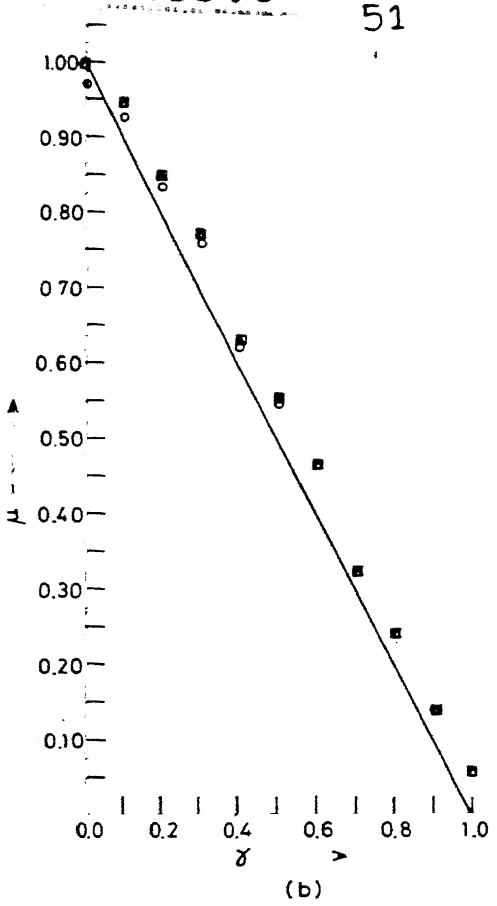

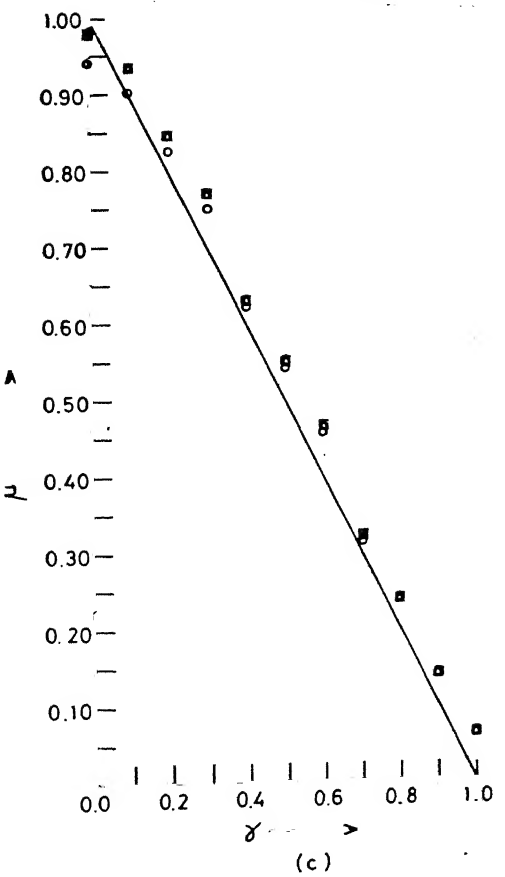

FIG.3.30 RESULTS WITH SIMULATED DATA FOR $\mu(\gamma) = 1-\gamma$ FOR (a) LEWITT'S FILTER, $\epsilon = 0.0$ (b) SINC FILTER (c) SINC SQUARE FILTER

- ○ I ORDER
- △ II ORDER
- □ III ORDER

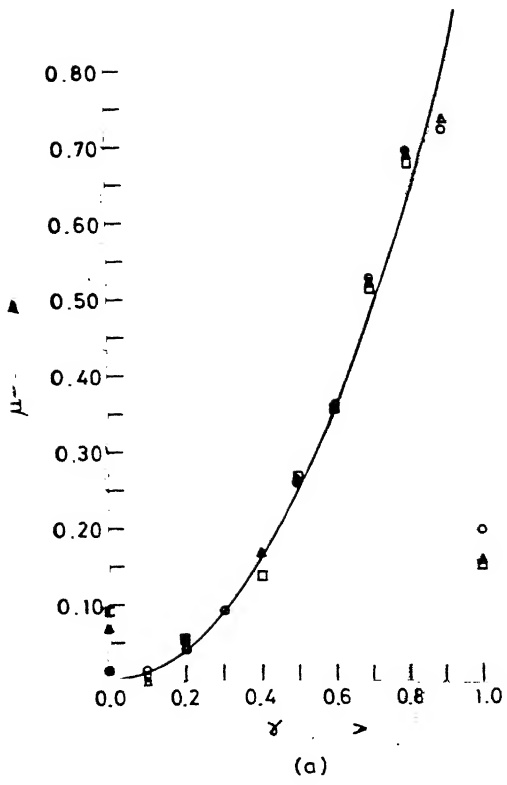

(a)

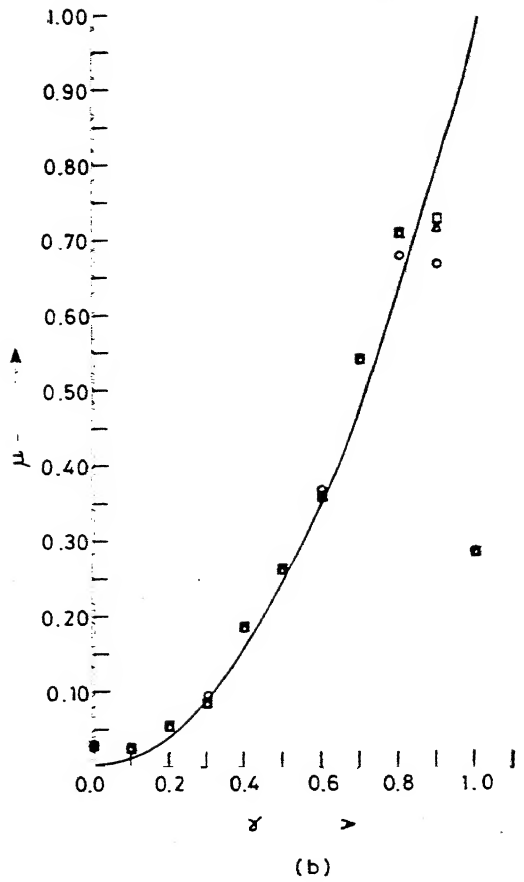

(b)

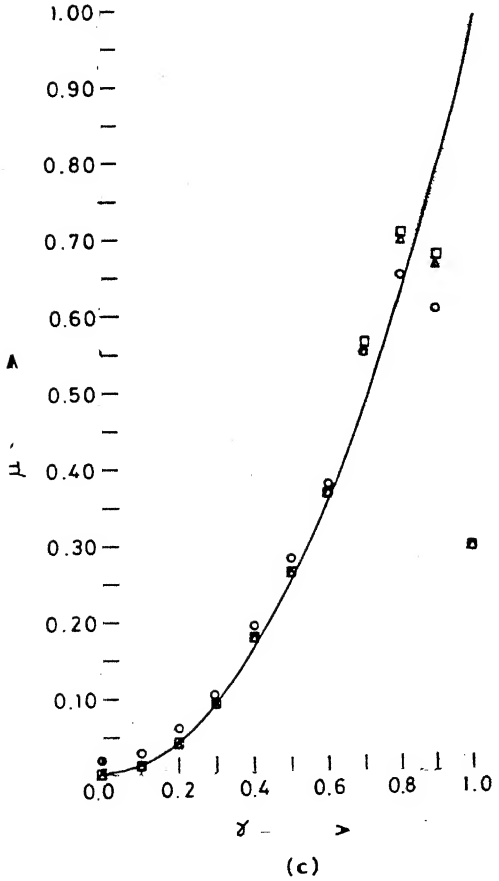

(c)

FIG.3.31 RESULTS WITH SIMULATED DATA FOR $\mu(\gamma) = \gamma^2$ FOR (a) LEWITT'S FILTER, $\epsilon = 0.0$ (b) SINC FILTER (c) SINC SQUARE FILTER

- ○ I ORDER
- △ II ORDER
- □ III ORDER

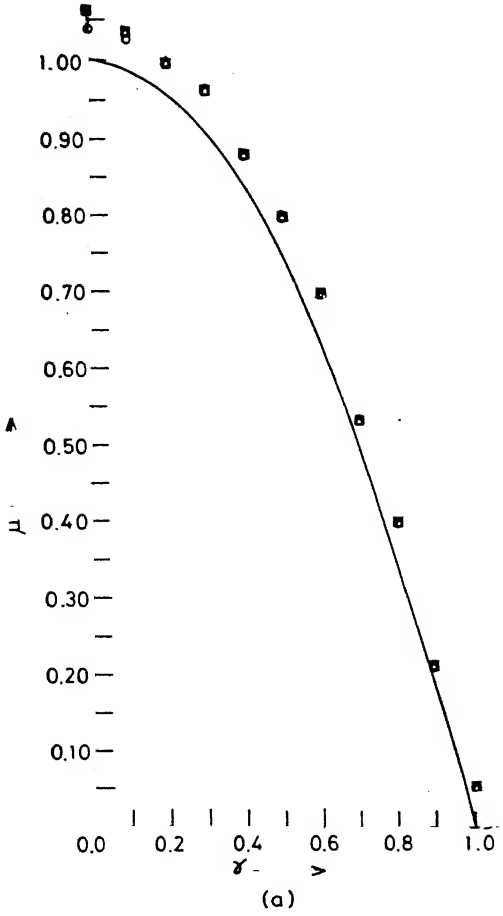

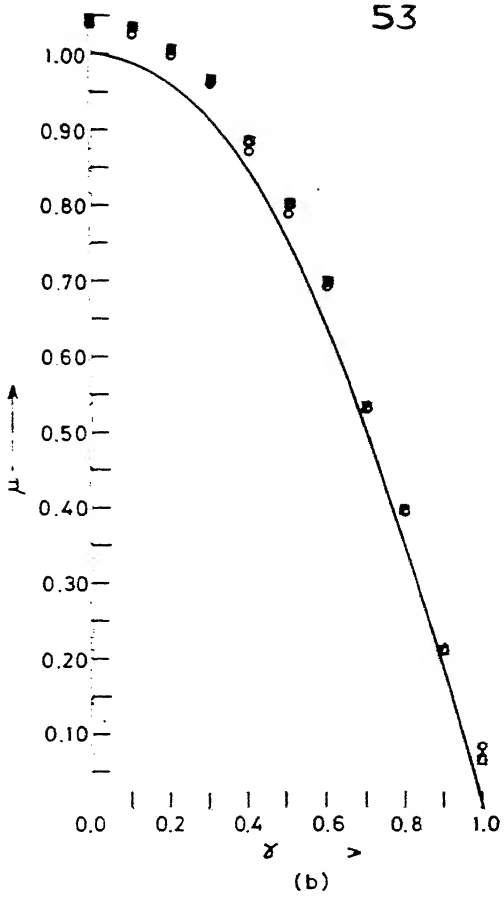

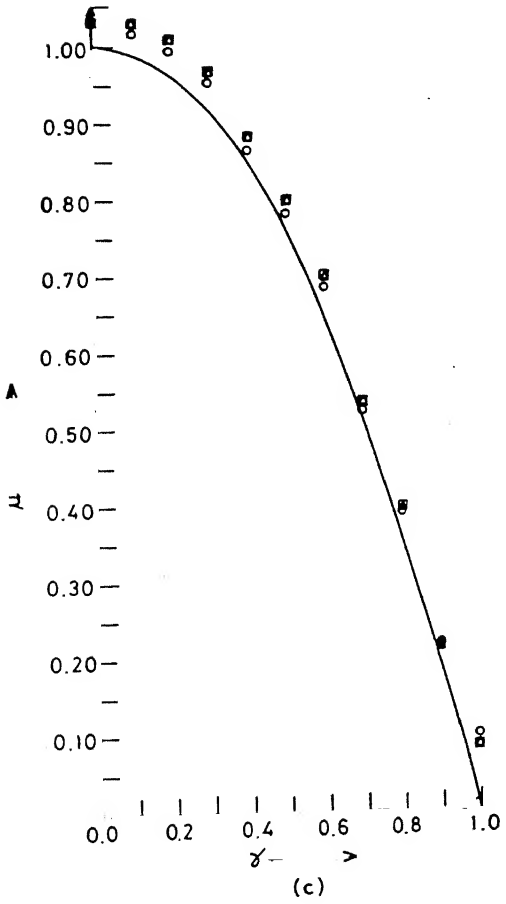

FIG.3.32 RESULTS WITH SIMULATED DATA FOR $\mu(\gamma) = 1-\gamma^2$ FOR (a) LEWITT'S FILTER, $\epsilon = 0.0$ (b) SINC FILTER (c) SINC SQUARE FILTER

- ○ I ORDER
- △ II ORDER
- □ III ORDER

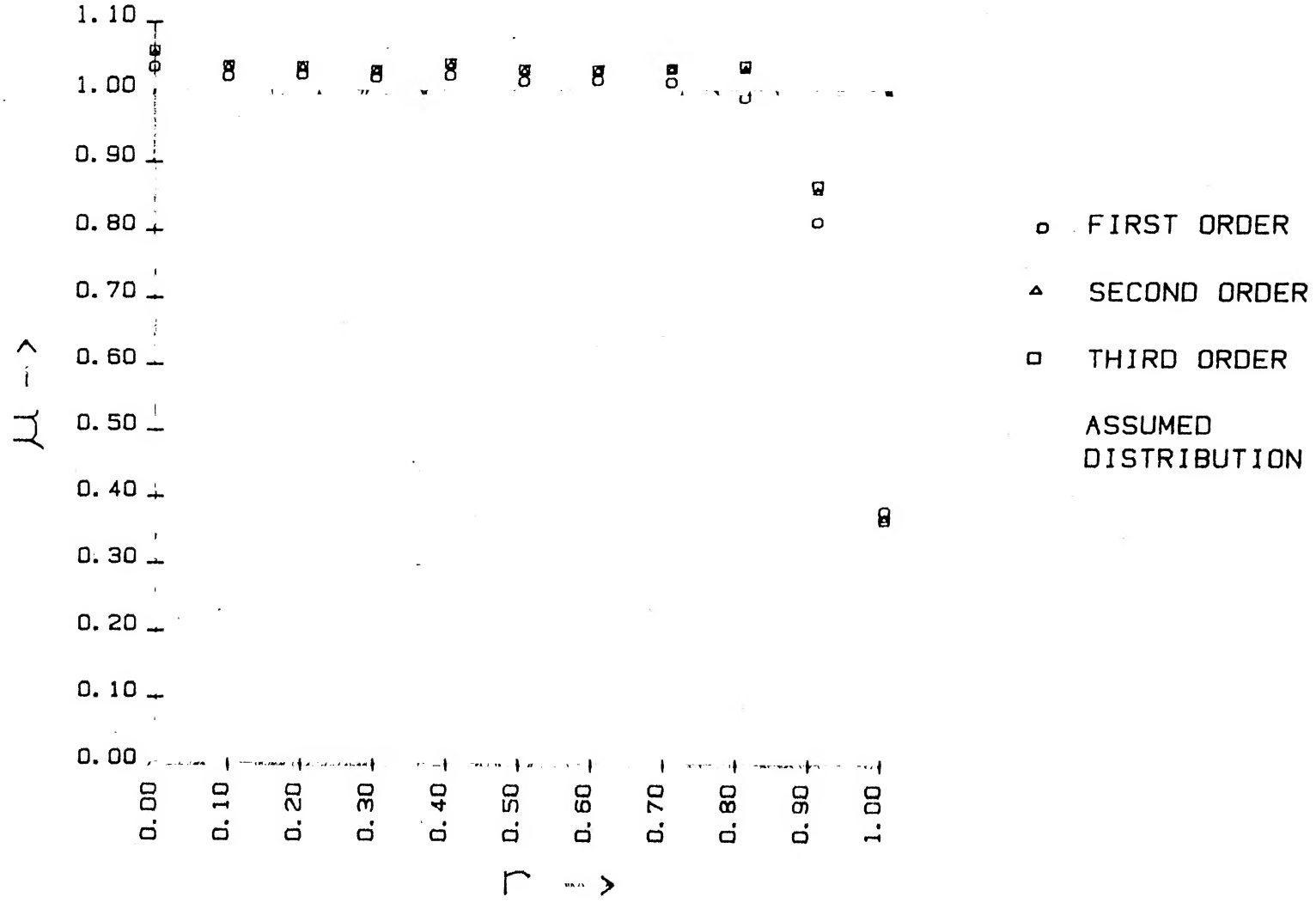

FIG 3.33 RESULTS WITH SIMULATED DATA FOR $\mu(r)=1.0$ FOR LEWITT'S I, II, AND III ORDER FILTERS WITH $\epsilon=1.0$

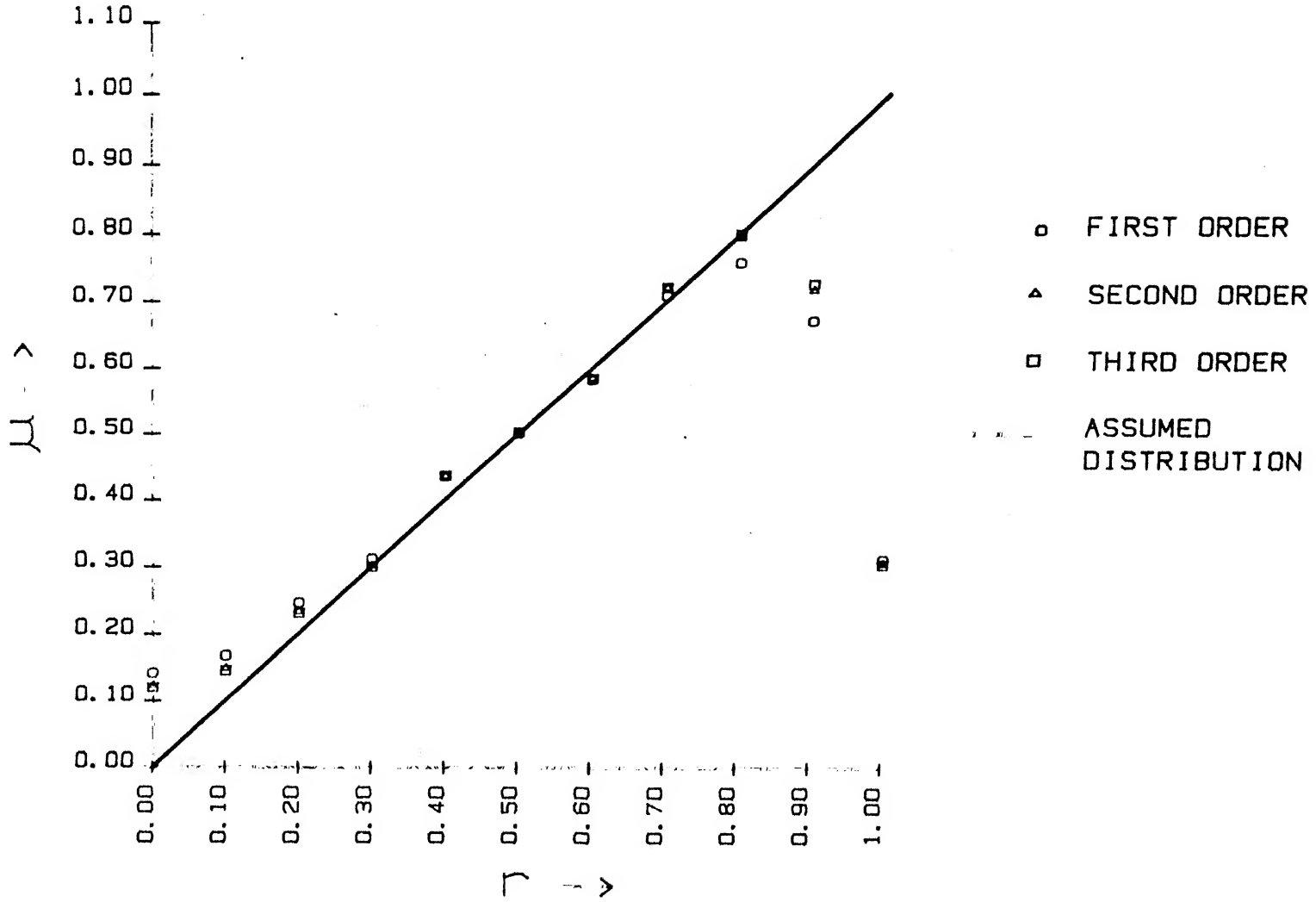

FIG 3.34 RESULTS WITH SIMULATED DATA FOR $\mu(r) = r$ FOR LEWITT'S I, II, AND III ORDER FILTERS WITH $\epsilon = 1.0$

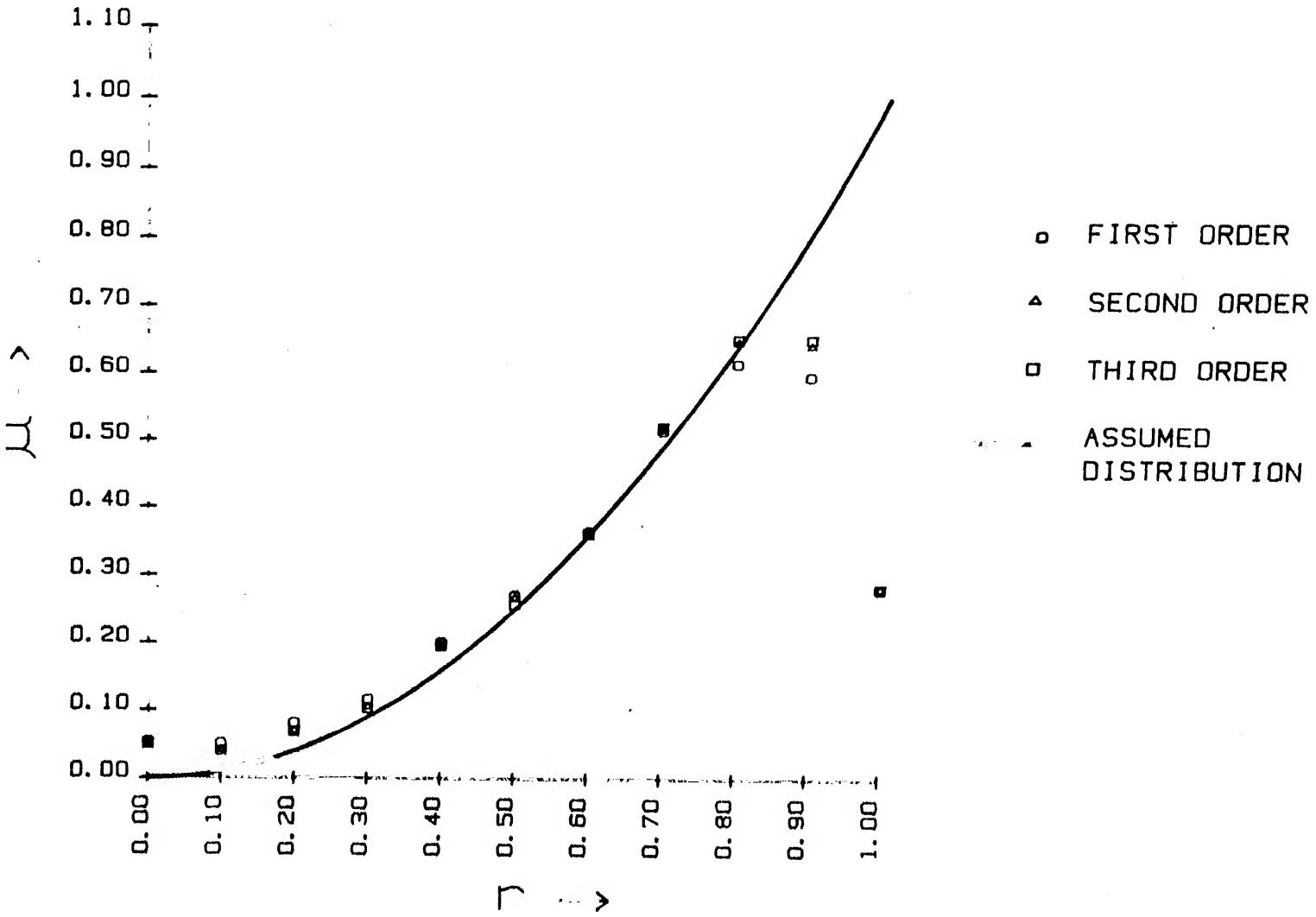

FIG 3.35 RESULTS WITH SIMULATED DATA FOR $\mu(r)=r^2$ FOR LEWITT'S I, II, AND III ORDER FILTERS WITH $\epsilon=1.0$

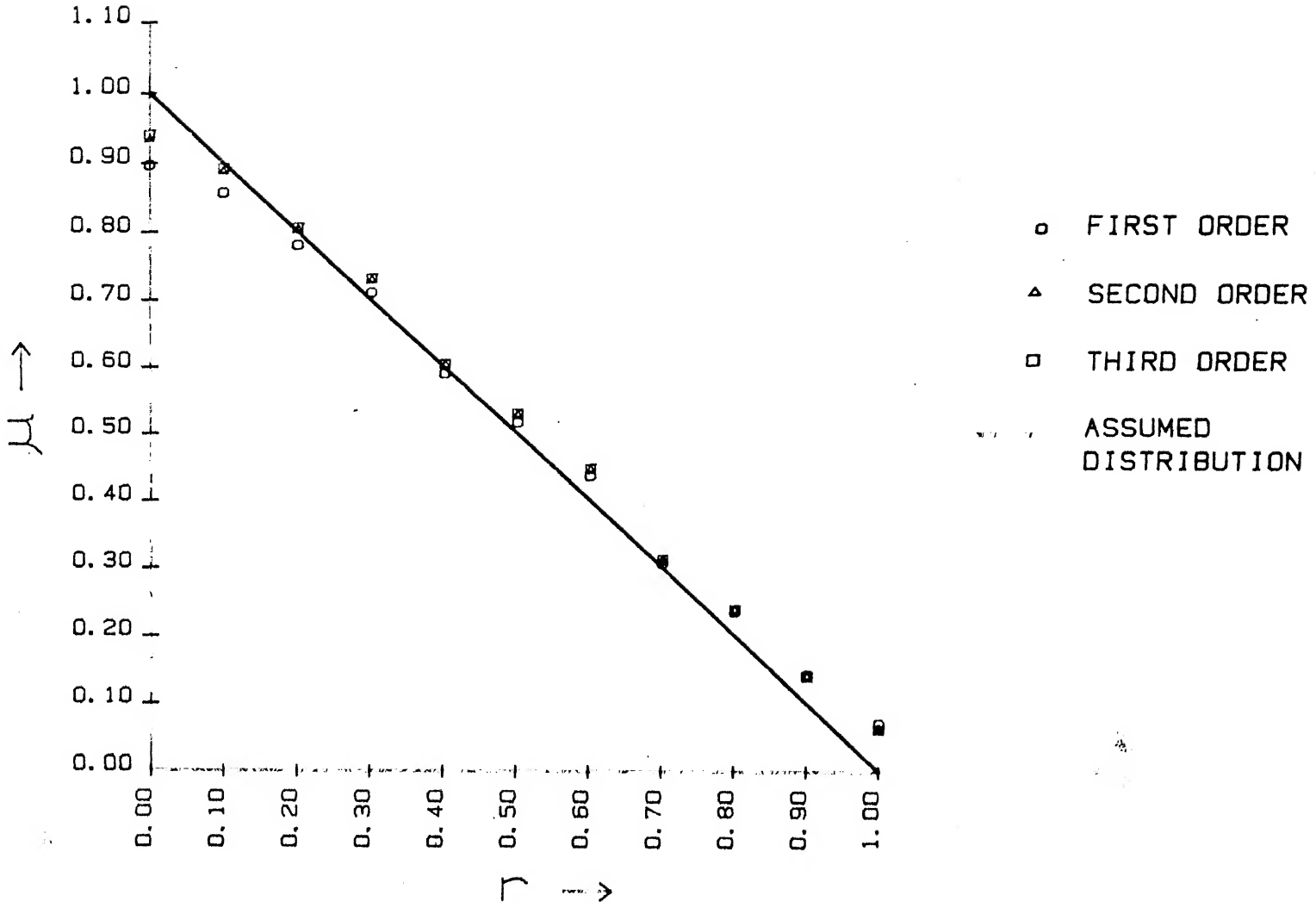

FIG 3.36 RESULTS WITH SIMULATED DATA FOR $\mu(r)=1-r$ FOR LEWITT'S I, II, AND III ORDER FILTERS WITH $\epsilon=1.0$

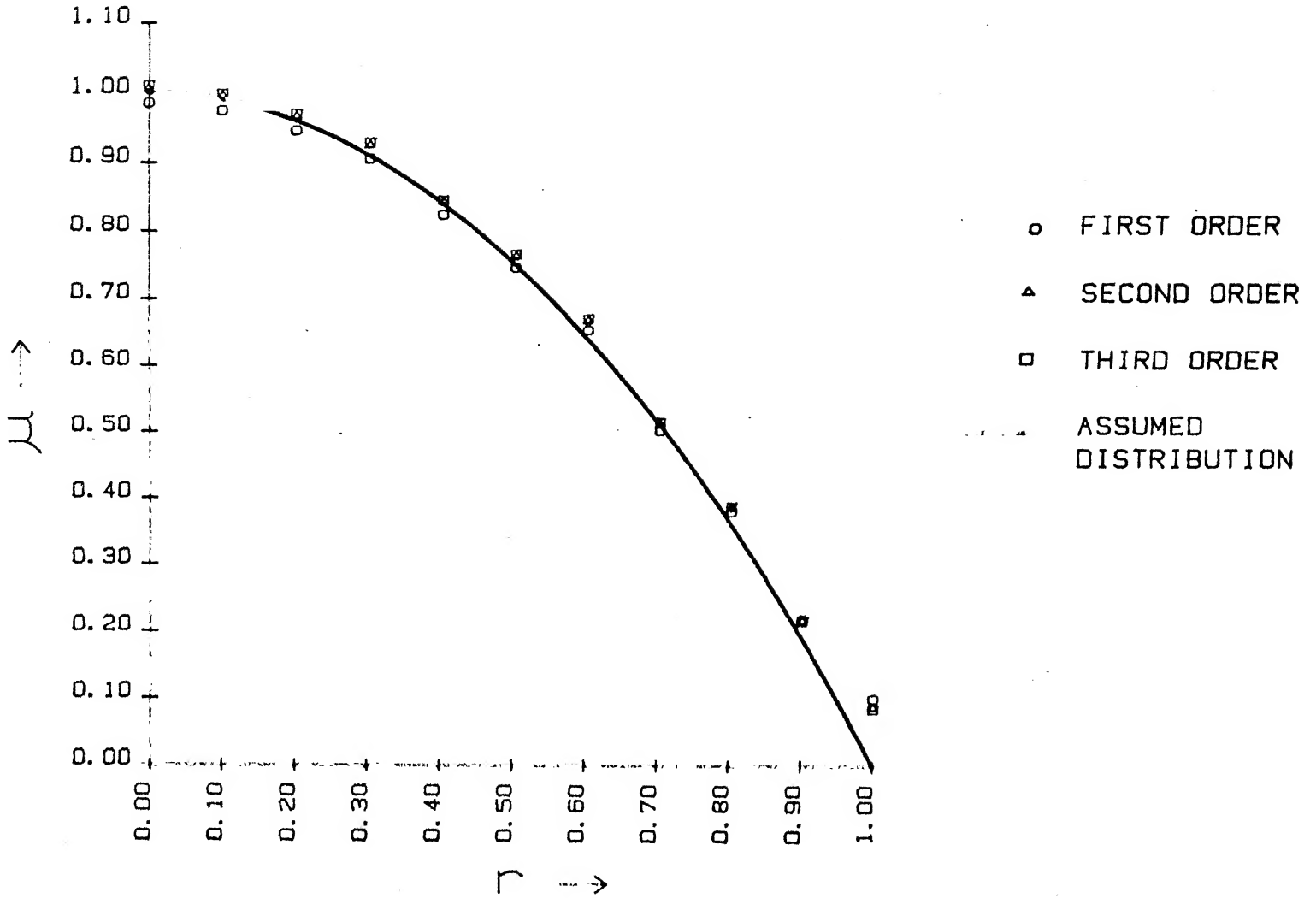

FIG 3.37 RESULTS WITH SIMULATED DATA FOR $\mu(r)=1-r^2$ FOR LEWITT'S I, II, AND III ORDER FILTERS WITH $\epsilon=1.0$

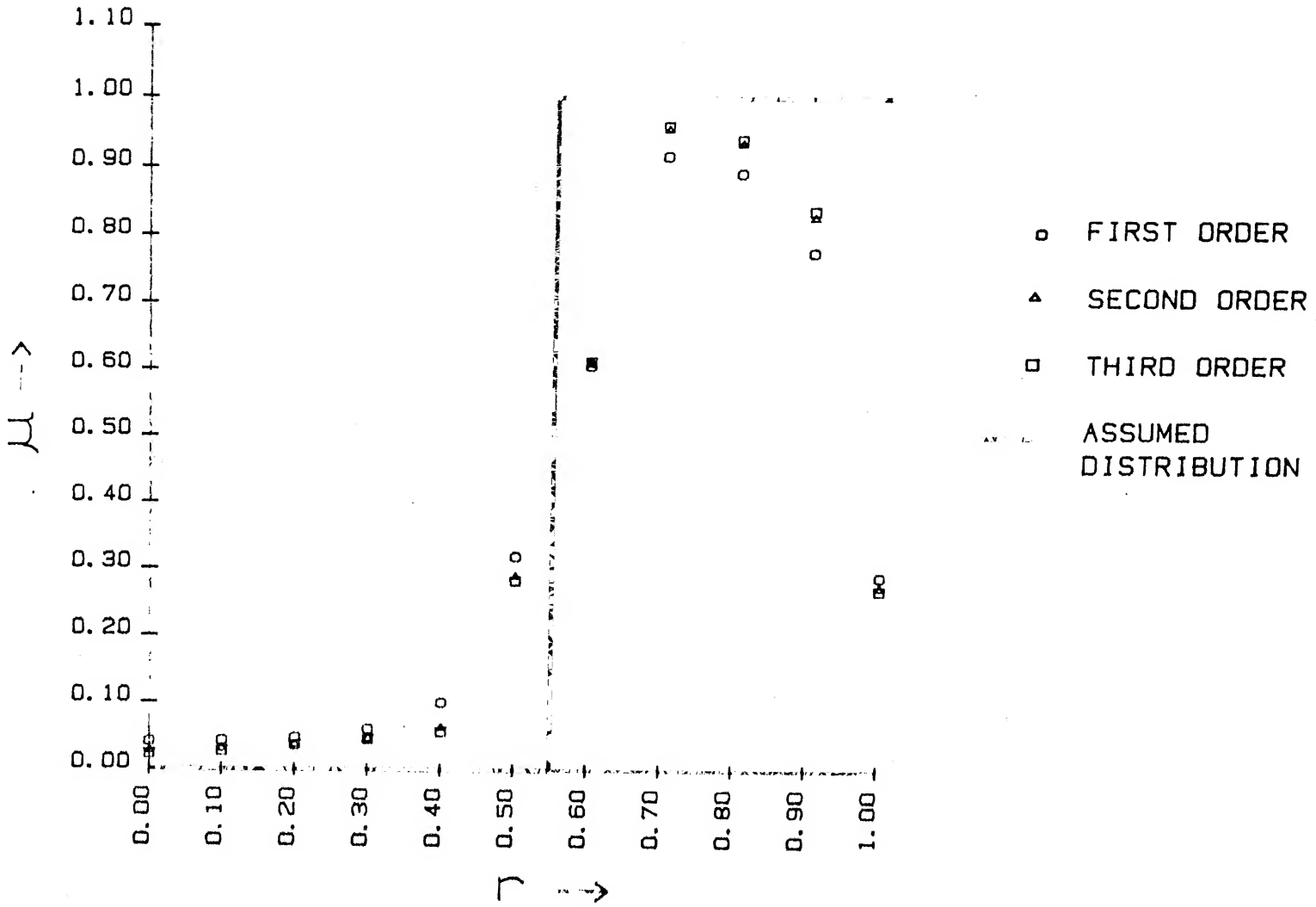

FIG 3.38 RESULTS WITH SIMULATED DATA FOR LEWITT'S I, II, AND III ORDER FILTERS WITH ϵ=1.0

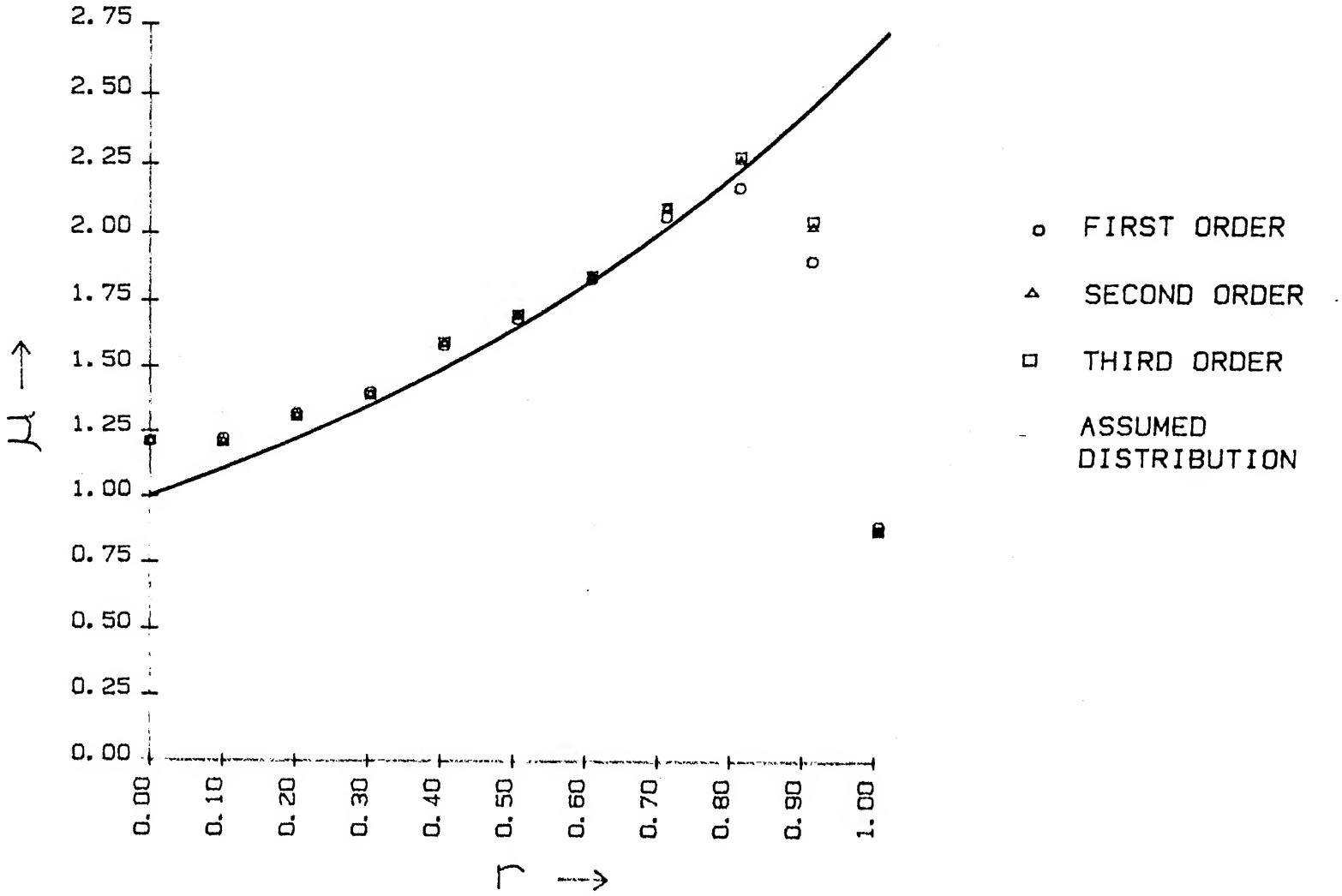

FIG 3.40 RESULTS WITH SIMULATED DATA FOR $\mu(r) = \exp(r)$ FOR LEWITT'S I, II, AND III ORDER FILTERS WITH $\epsilon = 1.0$

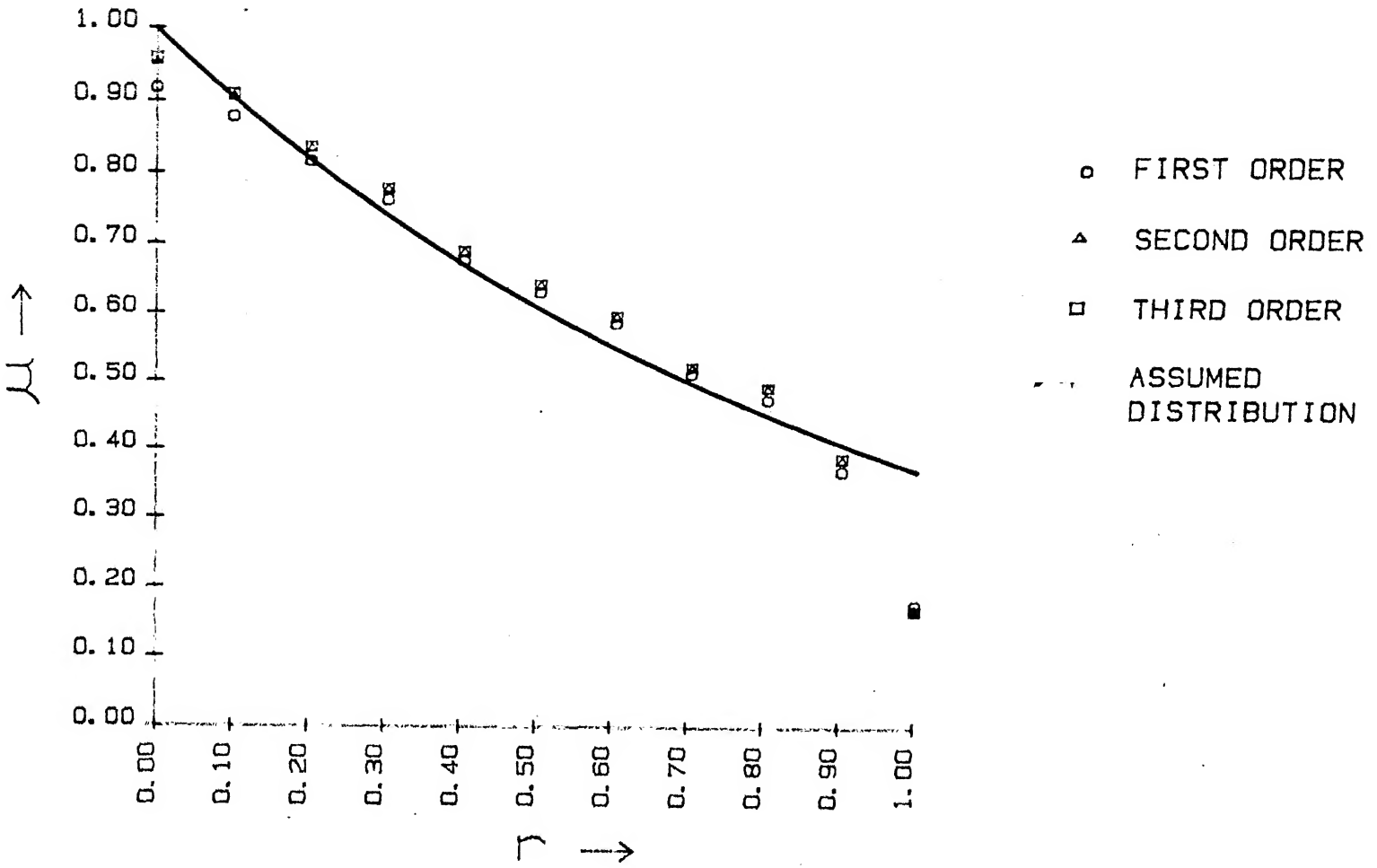

FIG 3.41 RESULTS WITH SIMULATED DATA FOR $\mu(r) = \exp(-r)$ FOR LEWITT'S I, II, AND III ORDER FILTERS WITH $\epsilon = 1.0$

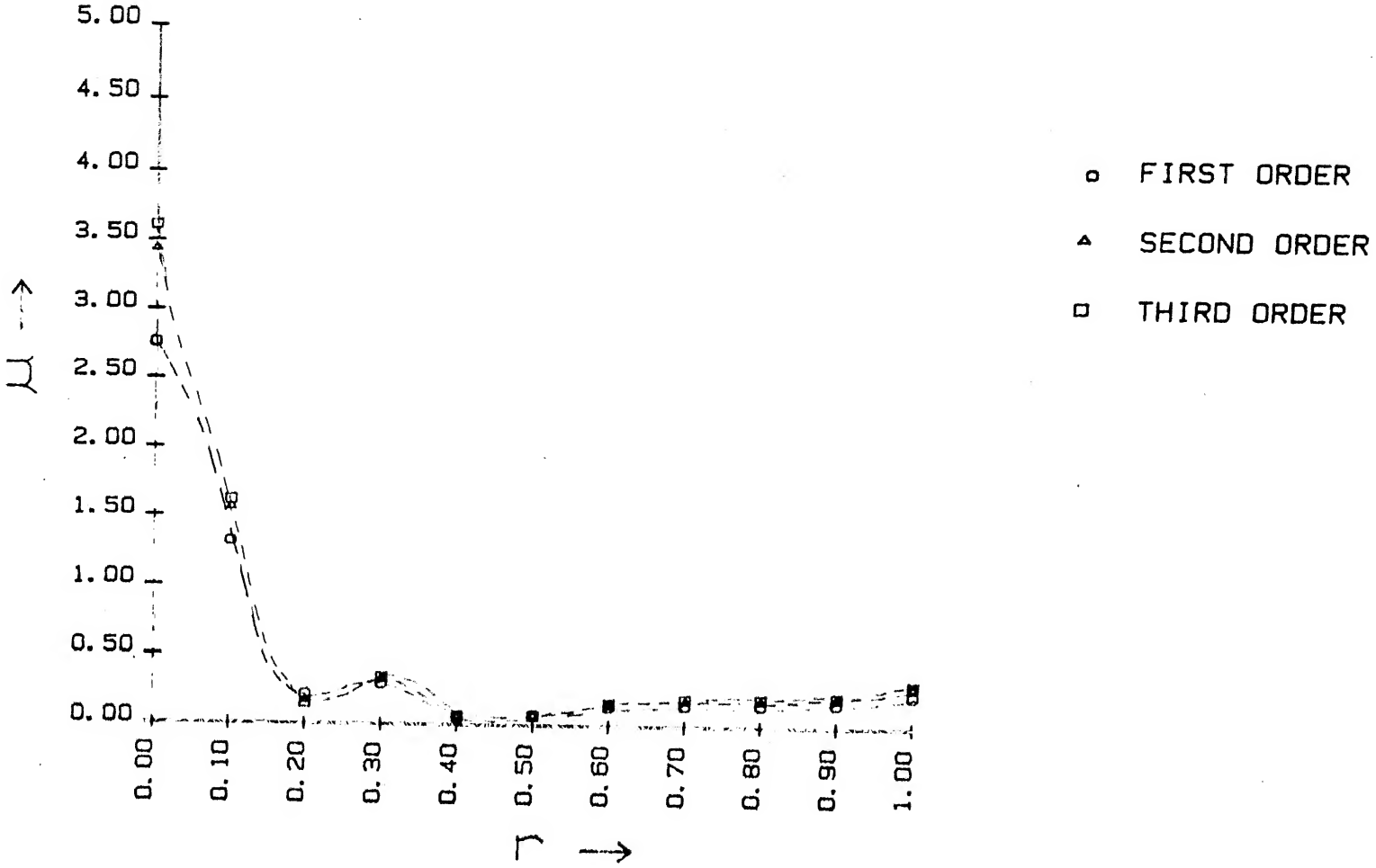

FIG 3.42 RESULTS WITH SIMULATED DATA FOR $\mu(r) = \delta(0)$ FOR LEWITT'S I, II, AND III ORDER FILTERS WITH $\epsilon = 1.0$

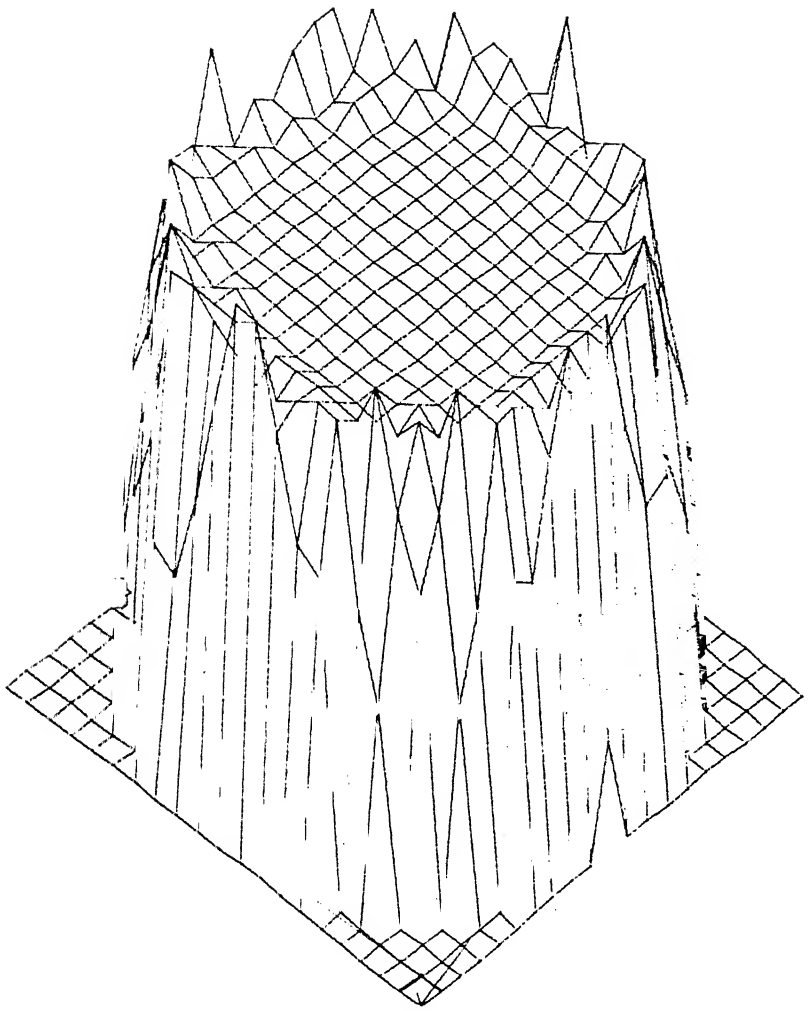

FIG. 3.43 HIDDEN LINE 3-DIMENSIONAL REPRESENTATION OF RECONSTRUCTED FUNCTION $\mu(r) = 1.0$ WITH LEWITT'S FILTER ($\epsilon = 0.0$)

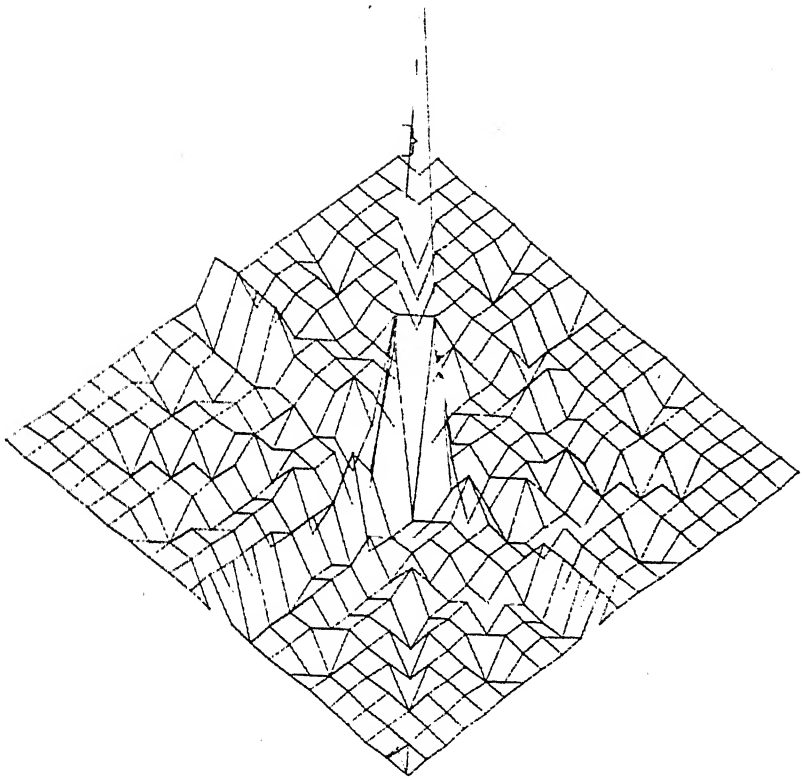

FIG. 3.44 HIDDEN LINE 3-DIMENSIONAL REPRESENTATION OF RECONSTRUCTED FUNCTION $\mu(r) = \delta(0)$ WITH LEWITT'S FILTER ($\epsilon = 0.0$)

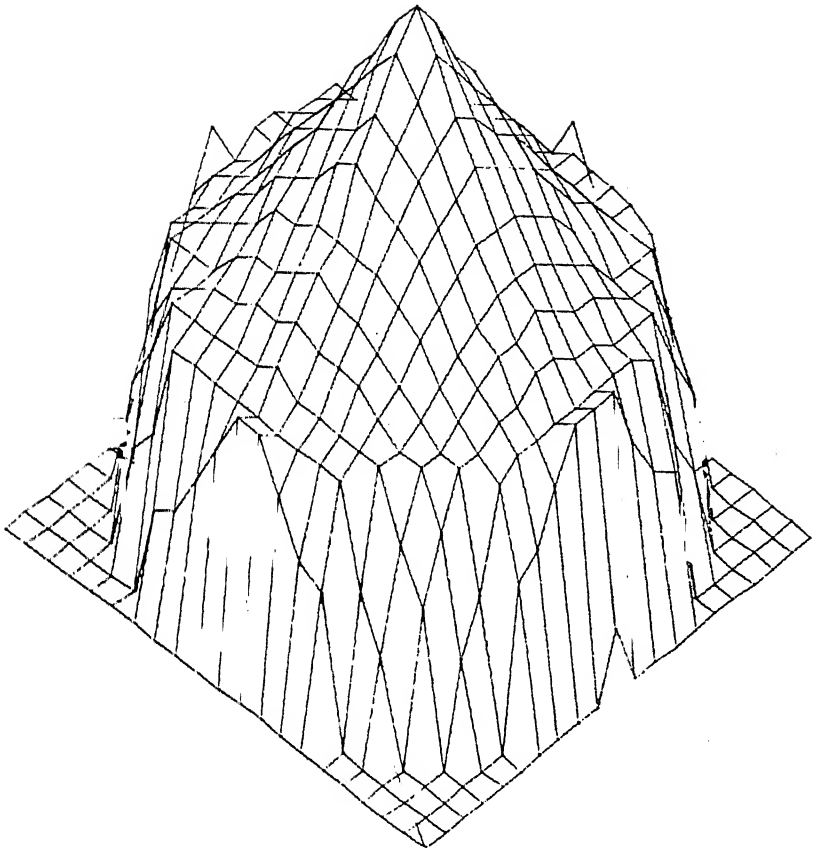

5. 3.45 HIDDEN LINE 3-DIMENSIONAL REPRESENTATION OF RECONSTRUCTED FUNCTION $\mu(r) = \exp(+r)$ WITH LEWITT'S FILTER (ϵ=0.0)

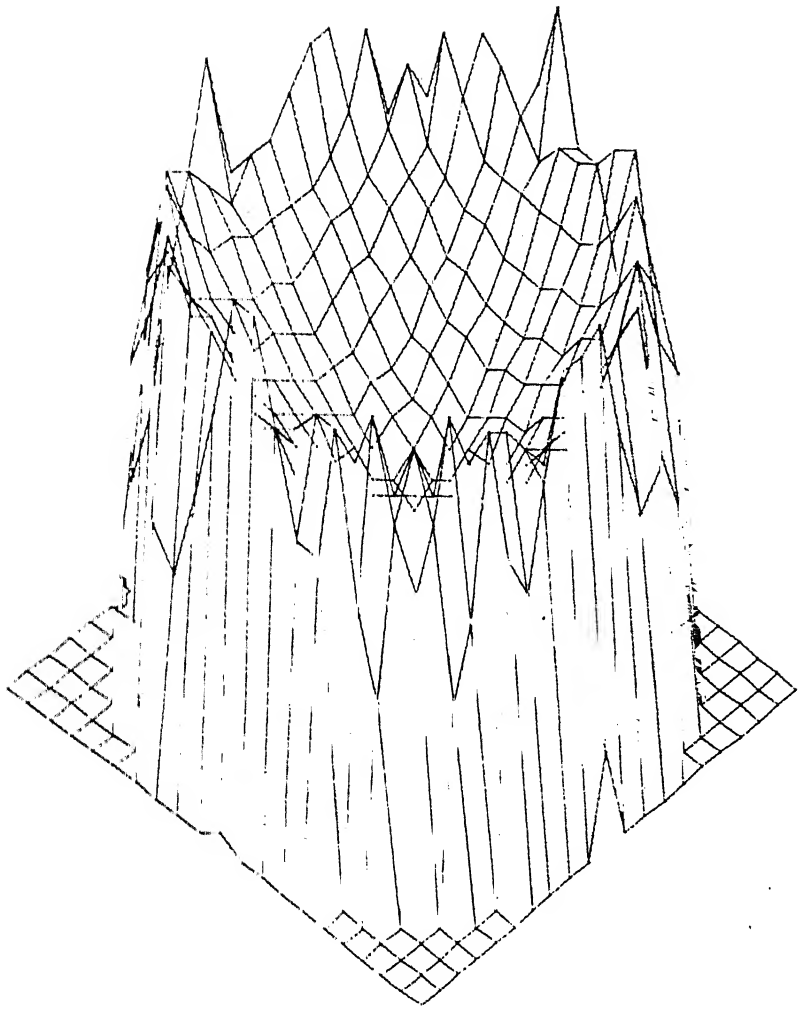

FIG. 3.46 HIDDEN LINE 3-DIMENSIONAL REPRESENTATION OF RECONSTRUCTED FUNCTION $\mu(r) = \exp(-r)$ WITH LEWITT'S FILTER ($\epsilon = 0.0$)

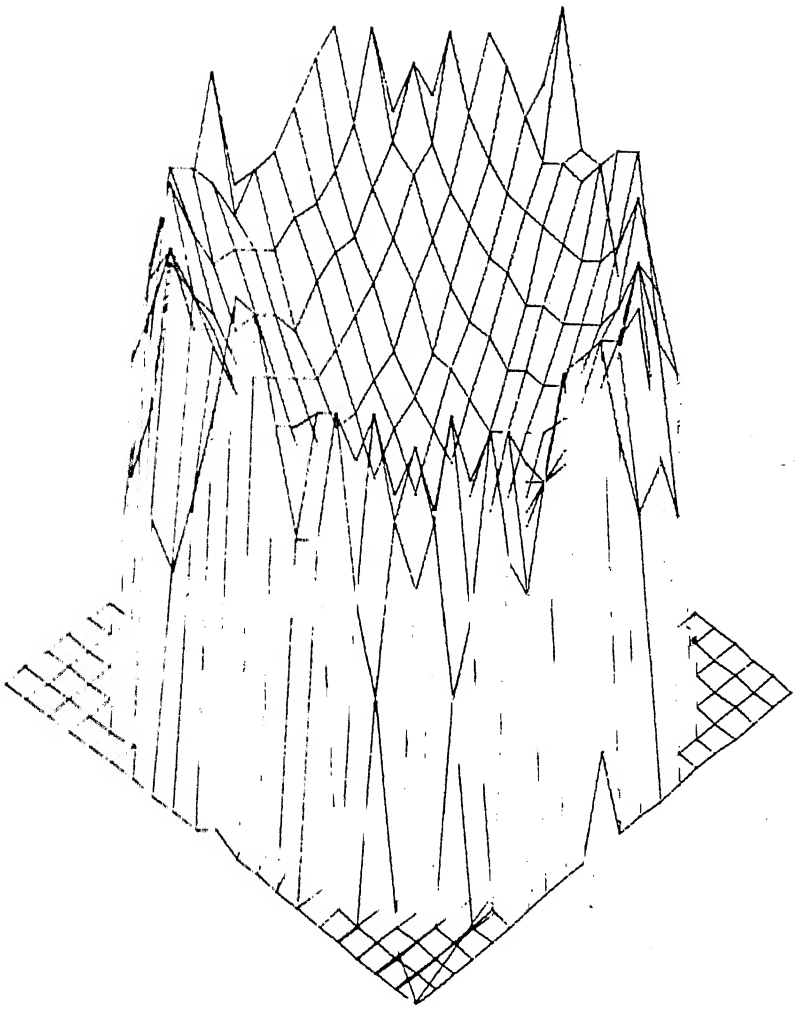

FIG. 3.47 HIDDEN LINE 3-DIMENSIONAL REPRESENTATION OF RECONSTRUCTED FUNCTION $\mu(r) = r$ WITH LEWITT'S FILTER ($\epsilon = 0.0$)

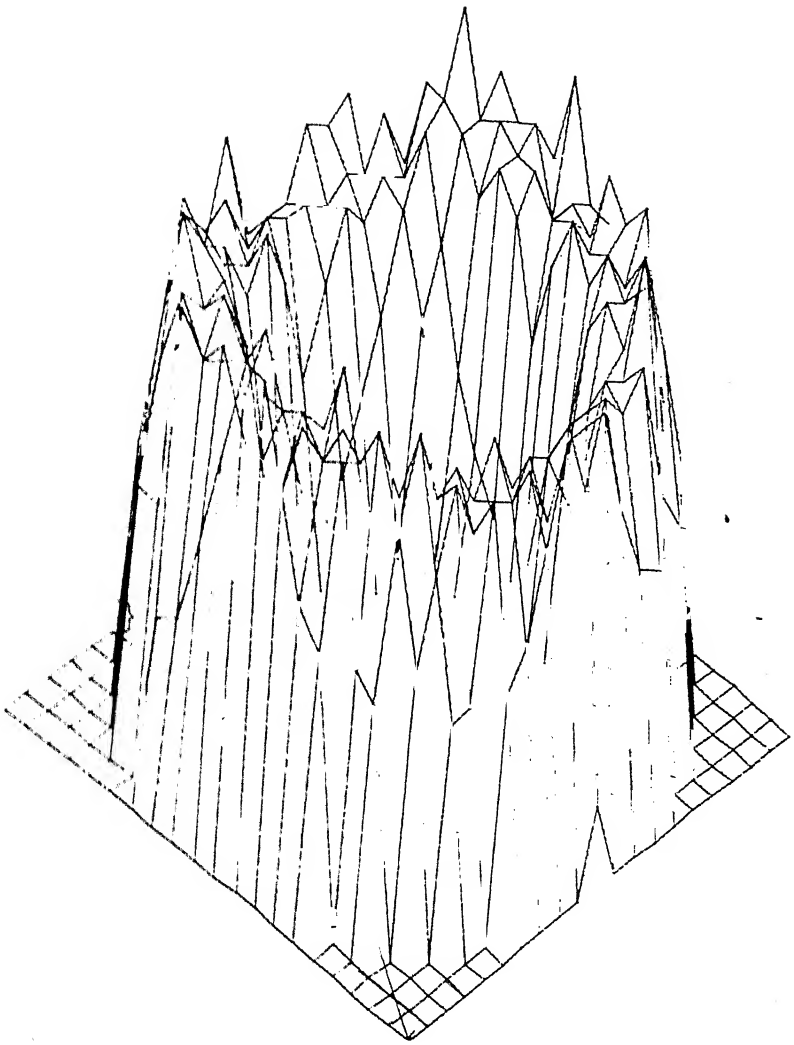

FIG. 3.48 HIDDEN LINE 3-DIMENSIONAL REPRESENTATION OF RECONSTRUCTED FUNCTION $\mu(r) = \begin{bmatrix} 0 & 0 \leq r < 0.55 \\ 1 & 0.55 \leq r \leq 1.0 \end{bmatrix}$ WITH LIWITT'S FILTER.

CHAPTER 4

DISCUSSION AND SUGGESTIONS

The linear filters suggested by Lewitt [2] appear to give a reasonably good reconstruction of the test-functions and of the radial density profile for the two-phase air-water flow data [3,6]. The error in the reconstruction of the average density, $\langle\rho\rangle$, is approximately, $\pm$ 0.03 g/cm^3, which is comparable with various other existing techniques of two-phase density measurement.

The higher-order filters show an improvement in the performance of the Convolution-backprojection algorithm for test-functions of various types. The experimental data was not processed with the higher-order filters because their relative performance could not be judged in the absence of point-wise density measurement by any alternate method.

The following suggestions are expected to improve the performance/efficiency of the Convolution Backprojection algorithm:

(1) Incorporating better integration schemes for the evaluation of convolving functions.

(b) Implementing still higher order filters, i.e. taking $q^{[k+1]}$ with $k > 2$.

(c) Investigating filters other than the linear filters used in the present work.

REFERENCES

1. G.N. Ramachandran and A.V. Lakshminaryanan, "Three-dimensional reconstruction from radiographs and electron micrographs : Application of convolutions instead of Fourier transforms", Proc. Nat. Acad. Sci., USA, Vol. 68, 1970, pp. 2236-2240.

2. Robert M. Lewitt, "Reconstruction Algorithms : Transform Methods", Proc. IEEE, Vol. 71, No.3, March 1983, pp. 390-408.

3. P. Munshi, "Void fraction measurements in the bubbly flow regime using a scanning Gamma-Ray densitometer", M.S. Thesis, Ohio State University, 1979 .

4. P.A. Schlosser, A.C. De Vuono, F.A. Kulacki, P. Munshi, "Analysis of high-speed CT scanners for non-medical applications", IEEE Trans. Nucl. Sci., NS-27, 1, 1980, pp. 788-794.

5. F.A. Kulacki, P.A. Schlosser, A.C. De Vuono, P. Munshi, "A preliminary study of the application of reconstruction tomography to void-fraction measurements in two-phase flow", Proc. ANS/ASME/NRC Topical Meeting on Nuclear Reactor Thermal Hydraulics, Saratoga Springs, New York, 1980, NUREG/CP-0014, pp. 904-922.

6. G.T. Herman, Image reconstruction from projections : The fundamentals of computerized tomography, Academic Press, NY, 1980.

7. R.K.S. Rathore, P. Munshi, "Higher order filters for computerized tomography", Tech. Report, Nuclear Engineering Programme, IIT Kanpur, 1987.

8. R.K.S. Rathore, P. Munshi, R.K. Jarwal, "Measurement of void-fraction distribution using a tomographic chord-segment inversion technique", To be presented at the ASME Spring Meeting, Cincinnati, USA, June 1987.

9. R.K.S. Rathore, P. Munshi, V.K. Bhatia, S. Pandimani, "Point-density measurements in Radially symmetric flows using Bessel functions", To be presented at the ANS Annual Meeting, Dallas, USA, June 1987.

APPENDIX B

TABLE 1 RESULTS WITH LEWITT'S I, II, AND III ORDER FILTERS (ε=0.0)

NCTION	I ORDER	II ORDER	III ORDER	ACTUAL AVERAG DENSITY
1.0	1.01669	1.02075	1.02078	1.00000
r	0.66861	0.67263	0.67269	0.66666
1−r	0.34807	0.34812	0.34809	0.33333
r^2	0.49622	0.50027	0.50033	0.50000
$1-r^2$	0.52047	0.52048	0.52045	0.50000
xp(+r)	2.01505	2.02603	2.02617	2.00000
xp(−r)	0.54222	0.54376	0.54375	0.52848
(0)	0.06613	0.07284	0.07423	
0,1	0.70468	0.71030	0.71056	0.75000
1,0	0.31201	0.31045	0.31022	0.25000

APPENDIX B

TABLE 2 RESULTS WITH LEWITT'S I, II, AND III ORDER FILTERS (ε=1.0)

:TION	I ORDER	II ORDER	III ORDER	ACTUAL AVERAGE DENSITY
.0	0.93573	0.96098	0.96485	1.00000
-	0.60544	0.62479	0.62786	0.66666
-r	0.33029	0.33619	0.33698	0.33333
-2	0.44313	0.45911	0.46174	0.50000
$-r^2$	0.49259	0.50185	0.50311	0.50000
p(+r)	1.83467	1.89012	1.89887	2.00000
p(-r)	0.50412	0.51616	0.51796	0.52848
(0)	0.04457	0.04823	0.049092	
0,1	0.63211	0.65401	0.65741	0.75000
1,0	0.30362	0.30696	0.30744	0.25000

APPENDIX B

TABLE 3 RESULTS WITH SINC I, II, AND III ORDER FILTERS

FUNCTION	I ORDER	II ORDER	III ORDER	ACTUAL AVERAGE DENSITY
1.0	0.9975	1.01476	1.01709	1.00000
r	0.64993	0.66581	0.66718	0.66666
1−r	0.34756	0.34975	0.3499	0.33333
r^2	0.47808	0.49157	0.49365	0.50000
$1-r^2$	0.51942	0.52319	0.52344	0.50000
exp(+r)	1.96439	2.0060	2.01200	2.00000
exp(−r)	0.53495	0.54225	0.54318	0.52848
(0)	0.04866	0.05278	0.0538	
0.1	0.68206	0.69971	0.70209	0.75000
1.0	0.31543	0.31504	0.31500	0.25000

APPENDIX B

TABLE 4 RESULTS WITH SINCSQUARE I, II, AND III ORDER FILTERS

INCTION	I ORDER	II ORDER	III ORDER	ACTUAL AVERA DENSITY
1.0	0.98053	1.00460	1.00800	1.00000
r	0.63471	0.65506	0.65821	0.66666
1−r	0.34581	0.34961	0.34981	0.33333
r^2	0.46418	0.48174	0.48457	0.50000
$1-r^2$	0.51635	0.52293	0.52336	0.50000
exp(+r)	1.92256	1.97904	1.98757	2.00000
exp(−r)	0.52796	0.53846	0.53977	0.52848
(0)	0.04284	0.04555	0.04625	
0,1	0.66393	0.68858	0.69245	0.75000
1,0	0.31660	0.31609	0.31557	0.25000

APPENDIX B

TABLE 5 RESULTS WITH LEWITT'S FILTER FOR DIFFERENT EPSILON VALUES

FUNCTION	C=0.0	C=0.35	C=0.55	C=0.75	C=1.0	ACTUAL AVERAGE
1.0	1.01099	0.99568	0.98694	0.97821	0.96727	1.00000
r	0.66823	0.65577	0.64864	0.64152	0.63261	0.66666
exp(+r)	2.01025	1.97506	1.95494	1.93483	1.90969	2.00000
exp(-r)	0.53725	0.53032	0.52636	0.52241	0.51745	0.52848
0,1	0.75578	0.74143	0.73324	0.72504	0.71479	0.75000
1,0	0.25521	0.25425	0.25371	0.25315	0.25217	0.25000
1,0,1	0.79586	0.78141	0.77313	0.76487	0.75454	0.79000

TH
621.3815324
Ar67S
Date Slip 98979
This book is to be returned on the date last stamped.

NETP-1987-M-ARO-SEN